THE UNIVERSITY OF WARWICK

AUTHOR: **Reza Ghaffari** DEGREE: **Ph.D.**

TITLE: **Non-destructive Detection of Diseases Using Plant Emitted Volatiles**

DATE OF DEPOSIT: .....

I agree that this thesis shall be available in accordance with the regulations governing the University of Warwick theses.
I agree that the summary of this thesis may be submitted for publication.
I **agree** that the thesis may be photocopied (single copies for study purposes only).
Theses with no restriction on photocopying will also be made available to the British Library for microfilming. The British Library may supply copies to individuals or libraries. subject to a statement from them that the copy is supplied for non-publishing purposes. All copies supplied by the British Library will carry the following statement:

> "Attention is drawn to the fact that the copyright of this thesis rests with its author. This copy of the thesis has been supplied on the condition that anyone who consults it is understood to recognise that its copyright rests with its author and that no quotation from the thesis and no information derived from it may be published without the author's written consent."

AUTHOR'S SIGNATURE: .....

USER'S DECLARATION

1. I undertake not to quote or make use of any information from this thesis without making acknowledgement to the author.
2. I further undertake to allow no-one else to use this thesis while it is in my care.

DATE SIGNATURE ADDRESS

.....

.....

.....

.....

.....

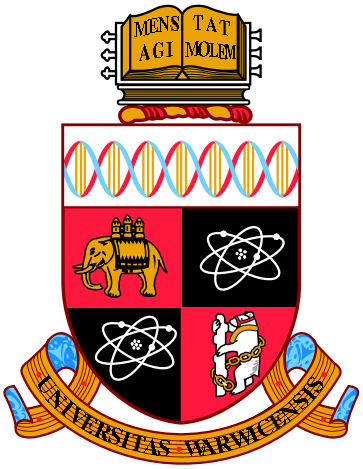

Non-destructive Detection of Diseases Using Plant Emitted Volatiles

by

Reza Ghaffari

Thesis

Submitted to the University of Warwick

for the degree of

Doctor of Philosophy

School of Engineering

November 2013

THE UNIVERSITY OF WARWICK

To my Father, Mohammadreza

Mother, Mahnaz

and brother, Sina.

Contents

List of Tables

List of Figures

Acknowledgments

First and foremost I want to thank my supervisors, Dr. Daciana D. Iliescu, Prof. Evor L. Hines and Dr. Mark Leeson for their guidance and support.

I would like to extend my sincerest thanks and appreciation to Dr Igor Khovanov for his generous support and priceless help. He is a true academic with real passion for spreading knowledge. He has not only guided me patiently but also has been a true inspiration.

My sincere gratitude is reserved for Prof. Richard Napier and Dr. Mark Pharaoh for their invaluable insights, kind assistance and extremely helpful suggestions.

I gratefully acknowledge the funding sources that made my PhD work possible. The work was funded by the European Commission, Directorate General for Research, within the 7th Framework Programme of RTD.

Thanks also go to my colleagues at Intelligent Systems Lab, School Of Engineering, Dr. Jianhua Yang, Dr. Harsimrat Singh, Dr. Huseyin Kusetogullari, Dr. Li XuQin, Dr. Fu Zhang and Dr. Wei Ren for their fruitful discussion and support.

I also would like to thank a dear friend, Dr. Behrouz Zafari, who has generously helped me throughout the process. One should feel privileged to have such a friend who poses vast knowledge, insights, passion for life and incredible sense of humor.

Last but not least, my deepest gratitude goes to my beloved parents and also to my brother, Sina, for their endless love and encouragement. Without the vision and sacrifices of my father, I would simply be no where near where I am right now.

Declarations

This thesis is presented in accordance with the regulations for the degree of doctor of philosophy. The work described in this thesis is entirely original and my own, except where otherwise indicated.

Reza Ghaffari
November 2013

Publications and Presentations

Ghaffari, R., Iliescu, D., Hines, E., Leeson, M., Grosu, I. (2013), *Dimensionality Reduction For Sensory Datasets Based On Master-Slave Synchronization Of Lorenz System*, International Journal of Bifurcation and Chaos, 23, 05, doi:10.1142/S0218127413300139.

Ghaffari, R., Laothawornkitkul, J., Iliescu, D., Hines, E., Leeson, M., Napier, R., Moore, J., Tayloer, J., Paul, N. (2012), *Plant Pest and Disease Diagnosis: Electronic Nose and Support Vector Machine Approach*, Journal of Plant Diseases and Protection, 119, 200 - 207.

Ghaffari, R., Zhang, F., Iliescu, D., Hines, E., Leeson, M., and Napier, R. (2011). *Detection of Diseases and Volatile Discrimination of Plants: An Electronic Nose and Self-Organizing Maps Approach.* Intelligent Systems for Machine Olfaction: Tools and Methodologies, IGI Global, 214 - 230, doi: 10.4018/978-1-61520-915-6.ch008.

Ghaffari, R., Zhang, F., Iliescu, D., Hines, E., Leeson, M., and Napier, R. (2011). *The Analysis of Plants Organic Volatiles Compounds with Electronic Nose and Pattern Recognition Techniques.* Applied Signal and Image Processing: Multidisciplinary Advancements, IGI Global, 115-126, doi:10.4018/978-1-60960-477-6.ch007.

Ghaffari, R., Zhang, F., Iliescu, D., Hines, E., Leeson, M., Napier, R., Clarkson, J., *Early detection of diseases in tomato crops: An Electronic Nose and intelligent systems approach*, IEEE Neural Networks (IJCNN), 1 - 6, 18 - 23 July 2010, doi:10.1109/IJCNN.2010.5596535.

Ghaffari, R., Grosu, I., Iliescu, D., Hines, E., Leeson, *Classification of Biomedical Datasets using Master-Slave Synchronisation of Lorenz System* 11th IEEE Conference on Cybernetic Intelligent Systems (CIS), August 2012.

Ghaffari, R., Iliescu, D., Hines, E., Leeson, M., *Intelligent Health Monitoring Tool*, Strictly Engineering, British Science Festival, Royal Academy of Engeneering, Edinburgh, September 2012, Finalist and Presenter.

Ghaffari, R., Iliescu, D., Hines, E., Leeson, M., *Intelligent Action Based Systems*, EPSRC UK ICT Pioneers Competition, Westminister, London, March 2011, Finalist and Presenter.

Ghaffari, R., Iliescu, D., Hines, E., Leeson, M., *Plant Disease Detection: Discriminating VOCs using High-Field Asymmetric Ion Mobility Spectrometry*, 4th Oxford University SIAM Conference, Society for Industrial and Applied Mathematics (SIAM), University of Oxford, UK, February 2011, Presenter.

Ghaffari, R., Iliescu, D., Hines, E., Leeson, M., *Greenhouse Intelligent Monitoring Software*, New Technologies for Early Pest And Disease Detection, Association of Applied Biologists, Linconshire, UK, October 2011, Presenter.

Ghaffari, R., Iliescu, D., Hines, E., Leeson, M., *Plant Disease Detection:*

Discriminating VOCs using High-Field Asymmetric Ion Mobility Spectrometry, Biomedical and Biological Systems Society, University of Warwick, March 2011, Presenter.

Abstract

The detection of plant diseases is an important part of commercial greenhouse crop production and can enable continued disease and pest control which will ultimately lead to the economical benefit as well as the significant reduction in use of chemical and biochemical treatments. A plant subject to infection typically releases exclusive volatile organic compounds (VOCs) which may be detected by appropriate sensors. A set of experiments were designed, constructed and conducted at University of Warwick in which the state-of-the-art gas sensors namely Electronic Nose (EN) and Field Asymmetric Ion Mobility Spectrometry (FAIMS) were employed to sample the VOC profiles in order to detect powdery mildew-infected and spider mite-infested tomato plants in a non-destructive manner. The data acquired from the EN and FAIMS devices was analysed using Principal Component Analysis, Linear Discriminant Analysis, Support Vector Machines and Artificial Neural Networks. Both EN and FAIMS proved to be able to distinguish between healthy and infected tomato plants with desirable accuracy when coupled with an appropriate data analysis technique. A review of the literature on plant diseases, destructive and non-destructive plant's disease detection tools as well as VOC sampling procedures and instrumentation will be given throughout this thesis.

Moreover, the latter part of this thesis presents the master-slave synchroni-

sation of identical chaotic dynamical systems using the open-plus-close-loop (OPCL) control method. The study is mainly concerned with the behaviour of the synchronisation of chaotic dynamical systems in respect to an added bias and in the case of mismatch of parameters of master and slave systems. The link between the external bias and the synchronisation error generated as well as between the value of parameters mismatch and the synchronisation error is examined and discussed. The usability of the newly-proposed approaches is assessed by the aid of two applications. The first application demonstrates that a weak bias acting on Nano-mechanical resonator shows the linear correlation with the synchronisation error and, consequently, the bias can be estimated via this error. The second application is related to the synchronisation of the cantilevers commonly found in ENs and Atomic Force Microscopy (AFM). It is suggested to use a novel scheme of coupled master–slave cantilevers and estimate the difference in cantilever-surface interactions in master oscillator and in slave oscillator via measuring the synchronisation error. The scheme is particularly useful for using the master cantilever as a control and the slave cantilever as a unit device which measures surface properties. The study shows that by calculating the error of synchronisation, a precise measurements can be conducted when two cantilevers leave the synchronous region, that is when they de-synchronise. Thus, this thesis also contributes to the understanding of de-synchronisation of nano-scale chaotic systems (Nano-electromechanical Systems) in respect to the addition of an external bias and/or parameters mismatch by outlining the possible applications.

Abbreviations

AFM	Atomic Force Microscopy
AN	Artificial neuron
ANN	Artificial neural network
CMOS	Complementary metaloxidesemiconductor
CI	Chemical ionization
CP	Conducting polymer sensors
CV	Compensation voltage
CVES	Cross-validated early stopping
DF	Dispersion field
DNA	Deoxyribonucleic acid
DPI	Day post infection
DS	Dynamical Systems
ELISA	Enzyme-linked immunosorbent assay
EN	Electronic nose

ERM	Empirical risk minimization
FAIMS	Field Asymmetric Ion Mobility Spectrometry
FAO	Food and Agriculture Organization
FFNN	Feed forward neural network
FISH	Fluoresence in-situ hybridization
GCMS	Gas chromatography-mass spectrometry
IFAS	Immunofluorescence antibody staining
IFCS	Immunofluorescence colony staining
IMS	Ion mobility spectrometry
IS	Intelligent systems
JA	Jasmonic acid
LCE	Lyapunov characteristic exponents spectrum
LDA	Linear discriminant analysis
LSVM	Linear Support Vector Machine
MEMS	Microelectromechanical systems
MOS	Metal oxide sensor
MSE	Mean squared error
NEMS	Nanoelectromechanical systems
NIR	Near infrared

NMR	Nuclear magnetic resonance
ODE	Ordinary differential equation
OPCL	Open-plus-closed-loop
PC	Principal component
PCA	Principal component analysis
PCR	Polymerase chain reaction
PR	Pattern recognition
PTFE	Polytetrafluoroethylene
QDA	Quadratic discriminant analysis
QP	Quadratic programming
RBF	Radial Basis Function
RNA	Ribonucleic acid
RMSE	Root-mean-square error
RSD	Relative standard deviation
SMO	Sequential minimal optimization
SRM	Structural risk minimization
SVM	Support vector machine
VOC	Volatile organic compound

Chapter 1

INTRODUCTION

1.1 Chapter Overview

This chapter presents a comprehensive introduction to the research that is going to be reported in this thesis. Firstly, a background of the problem will be given. The issues and challenges concerned with world's food security and crop production specifically greenhouse (protected) crop production will be covered in this chapter. Additionally, the motives, aim and objectives of the research will be specified, clearly indicating the tasks and deliverables. Finally, the chapter closes by presenting the summary of each chapter of this thesis.

1.2 Background

Inevitably, much of the evolutionary success of our species can be attributed to our ability to procure, process, and consume a wide range of foods [1] using the prodigious intelligence [2]. The world's progression through huntergatherer, agricultural, and industrial stages to provider of modern food products have

accelerated the development of a multi-disciplinary crop production industry, which has contributed immensely to the basis for a healthy and prosperous human civilisation [3].

Modern crop production with the aid of science and technology have provided enormous benefits including: reduction in nutrient deficiency-related diseases [4], harvests protection, enhanced food safety [5], consistent food quality [6], decreased food-preparation time [7], reduced food waste [8], lower household food costs [9], specifically formulated products for specific subpopulations [10] and efficient global food distribution [11] to deal with the ever growing world population. Food and Agriculture Organisation of the United Nations (FAO) recently [12] announced that the world population is projected to grow by 31% from 7.1 billion today to 9.20 billion in 2050 (Fig. 1.1).

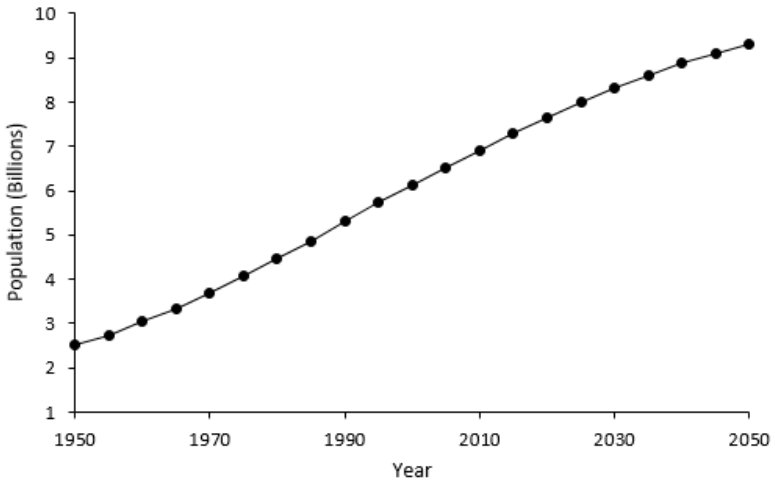

Figure 1.1: World's population 1950-2050 (FAO).

Contrariwise, 4 billion metric tonnes of fruit and vegetable is being produced

per annum [13]. Yet due to poor practices in production, harvesting, storage and transportation, as well as market and consumer wastage, it is estimated that 30–50% (1.22 billion tonnes) of all productions never reaches a consumer. Subsequently, large amounts of land, energy, fertilisers and water have also been lost in the production of crops which end up as waste. A complex, linked and collaborative global strategy is needed to ensure efficient and equitable crop production which will safeguard a sustainable food security [14]. Such strategies require innovative, scientific and technological foundations covering all aspects of the crop production including farmlands and *greenhouses*.

1.3 Greenhouses

In order to feed the world's more urban population, food production must increase by 70% [12]. Thus, the global greenhouse industry is attaining ever greater importance since it offers the following tangible benefits: **a)** throughout the year crops can be grown due to the availability of required environmental conditions (i.e. temperature and humidity), **b)** the long-term productivity of the crop is increased considerably, **c)** superior quality produce can be obtained as they are grown under suitably controlled environment, **d)** automated systems for efficient use of various inputs like water, fertilisers, seeds and crop protection chemicals can be precisely maintained in a greenhouse, **e)** products can grow in large quantities on a relatively small surface area, and **f)** crop production schedules can be planned effectively to take advantage of the market needs [12].

Across the world and especially in Asia and Europe, greenhouses are consid-

ered to play a significant role in the horticultural industry. An approximation of greenhouse production areas world-wide is presented in figure 1.2.

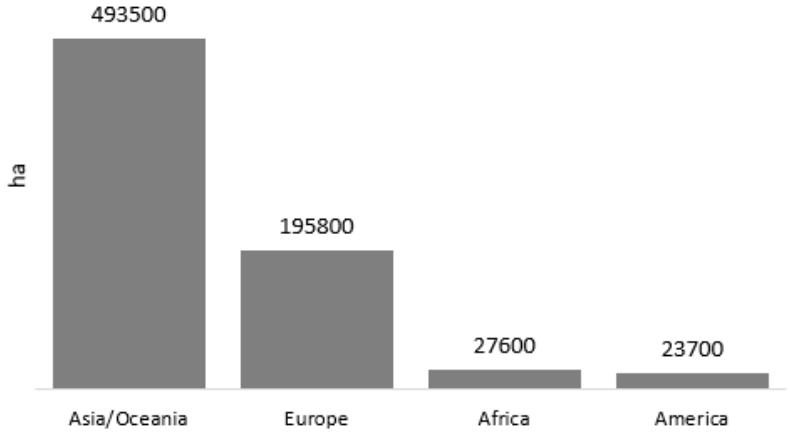

Figure 1.2: Greenhouse production areas world-wide [12].

The gross income from greenhouses may reach values of £30,000-£60,000/ha, up to £300,000/ha in case of potted or ornamental crops [15]. For example, the greenhouse industry in Holland, generated a total added value of £4 billion in 2005 [16]. Analogously, other countries around the globe such as Mexico and Spain have substantial greenhouse crop export trade as illustrated in table 1.1.

	Tomatoes		Cucumbers		Peppers	
	Export €	%	Export €	%	Export €	%
Netherlands	1,331,119,143	24	422,078,439	25	924,016,890	32
Mexico	1,119,341,215	20	380,719,319	24	583,503,608	21
Spain	1,009,908,150	18	407,353,639	22	581,899,463	21
Others	2,169,659,836	38	498,509,372	29	734,117,983	26

Table 1.1: Global protected (greenhouse) production [23]

Although greenhouses offer exceptional benefits, they do present some crucial challenges. Elevating productivity [17, 18], optimising energy consumption [19, 20], minimising environmental impacts [21, 22], avoiding chemicals [23, 24] and preventing/controlling diseases [25-28] are some of the problems that both scientists and growers face in regards to commercial greenhouse crop production. This thesis attempts to propose a prototype methodology to deal with the latter problem using non-destructive and non-invasive methods in a small scale.

1.4 Problem Description and Motivations

The greenhouse controlled environment is known to be very conducive to several diseases which may cause economic losses up to 100% in a single season [29]. In reality, any crop or fruit that cannot be sold due to disease, infection, insect damage, overall appearance, or poor market timing can greatly hinder a greenhouse operation's ability to be economically profitable [30]. Plant diseases may be caused by viral, fungal, bacterial and pest sources [31]. A complete survey of greenhouse plant diseases and their sources will be given in chapter 2.

Plant and crop protection in European greenhouses became strongly chemically oriented shortly after the Second World War in the 1950s [32]. This was mainly due to the fast reproduction of pests and diseases which demanded high chemical spray frequencies. There are several pesticides (e.g. *Abamectin*, *Bifenazate*, *Chlorfenapyr*, *Malathion*, *Pyriproxyfen* and *Sulfur*), fungicides (e.g. *Azoxystrobin*, *Carbendazim*, *Enilconazole*, *Mancozeb*, *Thiram* and *Vinclozolin*)

and bio-control products (e.g. *Bacillus thuringiensis*, *Encarsia formosa* and *Lecanicillium*) available, most of which are targeted for greenhouse crops but have high costs, environmental impacts and are toxic to human beings [33]. Reduction in using chemicals in greenhouses is not only economically beneficial but also prevents the rapid development of plant resistance against them [34].

Additionally, environmental and health concerns have increased public attention and pressure to reduce chemical use in agriculture and greenhouse production [20]. The European Commission (EC) strongly encourages agricultural practices to reduce or eliminate pesticide use. In response, the parliament recommended a 50% reduction in the use of these chemicals over 10 years (Resolution of the European Parliament 2002/2277). Hence, chemical control in greenhouse environment is gaining ever more importance in both local and global scale.

Moreover, currently plant inspection, disease blockage and infection prevention procedures are routinely and manually conducted by humans due to the constant danger of disease and infection spread within a greenhouse environment [23]. The assessment and appraisal of greenhouse's healthiness need to be accurate and meticulous as incorrect diagnosis may promote infection to scatter instantaneously throughout a greenhouse which again result in hefty economic losses. Such accurate, regular, on-site inspections of plants are not only acutely inefficient and in some cases futile but also requires skilled personnel which leads to high costs.

The motives mentioned above have urged the industry to find alternative methods to control pest and diseases for sustainable and profitable greenhouse production. A major challenge is to detect and quantify diseases within a plant population before they spread throughout a greenhouse to allow agile control within a short timeframe since this would reduce cost, resource use and environmental pressure. A unique niche is now created for the innovative tools for predicting and controlling the diseases within the greenhouse [35].

1.5 Research Aim and Objectives

There are many systems which employ various sensors to monitor the environmental conditions of a plant. The complete overview of such systems will be given in the next chapter. However, the available sensors hardly monitor the internal state of the crop and may require the use of exhaustive laboratory testing for diagnosis. Such laboratory procedures are often time consuming, involve destructive methods and most are not feasible for daily practice. Laboratories and instruments are indeed expensive making them unsuitable. Furthermore, advanced scientific skills are required to carry out laboratory based diagnosis taking control away from growers.

This thesis propose a methodology for non-destructive, rapid, cost-effective, easy to deploy disease detection system. The unique contribution of this thesis comes from two directions:

a) Designing and executing of an experimental procedure in which the state-of-the-art gas sensors (i.e. Electronic Nose and Field Asymmetric Ion Mobility

Spectrometry) are employed to analyse the Organic Volatile Compounds emitted from tomato plants in order to construct a rapid and non-destructive plant disease detection tool.

b) The subordinate objective of this work, presented in chapter 6, is to develop a method based on the master-slave synchronisation of chaotic dynamical systems for signal processing and measurements. The usability of the newly-proposed method is assessed by considerations of two distinct applications: **first**: the synchronisation of multiple Nano-mechanical Resonators using the open-close control loop approach to demonstrate the relationship between the synchronisation error and an added bias and, **second**: the synchronisation of identical cantilevers (NEMS) typically found in ultra-sensitive Electronic Noses and Atomic Force Microscopes in the case of mismatch of cantilever parameters. The schema predominantly investigates the estimation of parameters change (i.e. cantilever mass or cantilever-surface interaction) in such high precision instruments based on the error of synchronisation.

1.6 Scope and Delimitation

This study is solely focused on the detection of the powdery mildew infection (*Oidium neolycopersici*) and spider mites infestation (*Tetranychus urticae*) in commercial tomato plants. Tomato (*Lycopersicon esculentum*) was predominantly used in this study for the following reasons: **a)** Tomato is the second most consumed vegetable in the world [23], **b)** global production of tomato crop and fruit are an economically important industry (Table 1.1), **c)** Universally, tomato production suffers from yield losses caused by various infections

and diseases, **d)** commercial tomato plant is mainly grown under protected (greenhouse) environment and **e)** tomato plant is a biologically recognised model in plant pathogen and disease interactions research and can be applied on other species [23].

Powdery Mildew (*Oidium neolycopersici*) is an infection caused by the fungal family of *B. graminis*. Spider mites (*Tetranychus urticae*) is a plant-feeding mite found across the world, and is considered as a pest. This mite has been reported [36] to be infesting over 200 species of plants around the world. A number of vegetable plants such as tomatoes, squash, eggplant and cucumber are routinely subject to spider mite infestations and damage [37].

The incentive to select powdery mildew and spider mites in this study is based on the two following facts: first, these diseases are two of the most comprehensively studied conditions, and thus extensive body of research and literature are available. Secondly, these diseases are considered as the major cause for substantial damage and loss in a wide range of plant species including tomato plants.

1.7 Thesis Outline

In this section the outline of this thesis is presented.

1.7.1 Chapter Two

Chapter two will provide a brief review of the plants health monitoring methodologies that are widely used in the field of agriculture and protected horti-

culture. It covers both theoretical and practical aspects of plant's disease detection methods using different instruments and procedures.

1.7.2 Chapter Three

Chapter three gives a detailed introduction to the experimental methodology, samples, features and parameters of the proposed disease detection experimental procedures and techniques. The chapter also introduces the gas sensors used in the experiments reported in this thesis.

1.7.3 Chapter Four

Chapter four is concerned about the analysis of data acquired from sensor arrays particularly Electronic Noses (EN). Datasets generated by the ENs will be analysed using clustering and classification methods in order to detect unhealthy samples. The experimental technique will be evaluated and the results will be compared and discussed in details.

1.7.4 Chapter Five

In chapter five the data acquired form a Field Asymmetric Ion Mobility Spectrometry (FAIMS) device will be discussed and analysed. This chapter assesses the performance of FAIMS in categorising the healthy and infected samples.

1.7.5 Chapter Six

Chapter six begins with an in-depth discussion on synchronisation schema of the chaotic dynamical systems focusing on the stability types and specific

parameters needed for full synchronisation. The application of bias and computed synchronisation error in signal processing via a novel approach is also presented in this chapter.

1.7.6 Chapter Seven

Finally, chapter seven summarises the main findings of the research presented throughout this thesis. A brief conclusion will be provided which discusses the overall results. The thesis closes by outlining a framework for further research as well and recommending potential enhancements.

1.8 Summary

The current chapter presented an overview of research conducted at the University of Warwick and reported in this thesis. The aim and objectives of the research were also presented and discussed. The next chapter reviews the plant's diseases and the greenhouse pest and disease detection methodologies.

1.9 References

1. Ungar, P.S. and M.F. Teaford, Human diet: its origin and evolution. 2002: J F Bergin & Garvey.

2. Thompson, N.S. and F. Tonneau, Perspectives in Ethology: Evolution, Culture, and Behavior. 2000: Springer.

3. Floros, J.D., et al., Feeding the World Today and Tomorrow: The Importance of Food Science and Technology. Comprehensive Reviews in Food Science and Food Safety, 2010. 9(5): p. 572-599.

4. Go, V.L.W., et al., Nutrient-Gene Interaction: Metabolic Genotype-Phenotype Relationship. The Journal of Nutrition, 2005. 135(12): p. 3016S-3020S.

5. Patel, P.D., (Bio)sensors for measurement of analytes implicated in food safety: a review. TrAC Trends in Analytical Chemistry, 2002. 21(2): p. 96-115.

6. Gunasekaran, S., Computer vision technology for food quality assurance. Trends in Food Science & Technology, 1996. 7(8): p. 245-256.

7. Bittman, M., J.M. Rice, and J. Wajcman, Appliances and their impact: the ownership of domestic technology and time spent on household work. The British Journal of Sociology, 2004. 55(3): p. 401-423.

8. Parfitt, J., M. Barthel, and S. Macnaughton, Food waste within food supply chains: quantification and potential for change to 2050. Philosophical Transactions of the Royal Society B: Biological Sciences, 2010. 365(1554): p. 3065-3081.

9. Ronteltap, A., et al., Consumer acceptance of technology-based food innovations: Lessons for the future of nutrigenomics. Appetite, 2007. 49(1): p. 1-17.

10. Kreitzman, S.N., et al., Safety and effectiveness of weight reduction using a very-low-calorie formulated food. Archives of internal medicine, 1984. 144(4): p. 747.

11. Popkin, B.M., Technology, transport, globalization and the nutrition transition food policy. Food Policy, 2006. 31(6): p. 554-569.

12. FAO, How to Feed the World in 2050. Food and Agriculture Organisation of the United Nations, 2010.

13. Fox, T., Global Food, Waste Not, Want Not. Institution of Mechanical Engineers, 2013.

14. Misselhorn, A., et al., A vision for attaining food security. Current Opinion in Environmental Sustainability, 2012. 4(1): p. 7-17.

15. Pardossi, A., F. Tognoni, and L. Incrocci, Mediterranean greenhouse technology. Chronica Hort, 2004. 44(2): p. 28-34.

16. Breukers A, H.O., & Ruijs M, The power of Dutch greenhouse vegetable horticulture: An analysis of the private sector and its institutional framework. LEI Wageningen UR, The Hague, 2008.

17. Schaechter, M., Desk Encyclopedia of Microbiology. 2010: Elsevier Science.

18. Paulitz, T.C. and R.R. Blanger, Biological control in greenhouse systems. Annual Review of Phytopathology, 2001. 39(1): p. 103-133.

19. van Lenteren, J.C., A greenhouse without pesticides: fact or fantasy? Crop Protection, 2000. 19(6): p. 375-384.

20. Neto, M., et al., A Greenhouse Tomato Crop Grey Mould Disease Early Warning System. 2011.

21. Elad, Y., N.E. Malathrakis, and A.J. Dik, Biological control of Botrytis-incited diseases and powdery mildews in greenhouse crops. Crop Protection, 1996. 15(3): p. 229-240.

22. Cook, R. and U. Braun, Conidial germination patterns in powdery mildews. Mycological Research, 2009. 113(5): p. 616-636.

23. Jansen, R. M. C., Hofstee, J. W., Wildt, J., Verstappen, F. W. A., Bouwmeester, H. J., Posthumus, M. A., Van Henten, E. J. (2009). Health monitoring of plants by their emitted volatiles: trichome damage and cell membrane damage are detectable at greenhouse scale. Annals of Applied Biology, 154(3), 441-452.

Chapter 2

Plant Disease Detection: Tools and Methods

2.1 Chapter Overview

The purpose of this chapter is two-fold: **first**, a review of plant diseases, their causes and symptoms will be given. Additionally, the plant's disease detection tools, molecular methods and procedures will be reviewed. Potential imaging and biomarkers approaches suitable to be deployed for a rapid and non-destructive disease detection will be briefly reported outlining the previous research conducted in the field. **Second**, this chapter presents the current state of knowledge about the non-destructive plants disease detection and identifies practical implications, challenges and experimental gaps that should be addressed.

2.2 Introduction

A 1950 publication by Chester et al. [1] presented the principles of plant disease appraisal and since then other studies measured production losses caused by plant diseases in agricultural and horticultural settings [2-5]. Cheatham et al. [6], presented a framework in which the direct and indirect plant disease impact on the entire ecosystem of food services were outlined. However, the most commonly considered impact of plant disease is on crop yield, and, at times, losses are so great that famine results [7].

James et al. [8], in 1974, characterised the relationship between plant disease and major loss in yield. More recently, it was reported that by controlling 20% of the *phakopsora pachyrhizi* (a fungus diseases commonly known as soybean rust), a $11 million profit may be achieved and if 80% of fungal infection is successfully removed, a $299 million profit would be potentially attained by US soybean producers over the scenarios considered [9]. Similar study [10] revealed that a 12% reduction in crop yields were caused by pathogens in US, representing around $33 billion in lost crop production annually which is based on the total potential value of all US crops of more than $267 billion/year. In United Kingdom, the economic loss due to plant pathogens amounts to 8.3% of potential production representing $2.7 billion a year [11]. Australia, with total crop production of $22 billion a year, suffers from 15.2% of crop losses being attributed to plant pathogens which represents $3.3 billion in economic terms [11]. Such patterns exists in other continents around the world. Plant pathogens in South Africa cause an estimated 15.6% or $2.1 billion a year loss of potential crop production. In India, pathogens reduce potential crop

production by 16% for a total of $48 billion a year [12].

2.3 Plant Diseases

There are about 50,000 parasitic and non-parasitic plant diseases [13]. A plant disease may be defined as any disturbance that prevents the normal development of a plant, interferes with the regular function of part of a plant or reduces its yield, quality or aesthetic value. Disease in plants are caused by living agents (micro-organisms) and non-living agents (environmental factors, faulty nutrition, and chemical substances). The former group, are also known as pathogens or biotic agents and the latter group are referred to as abiotic agents [14].

Fungi are among the most important plant pathogens. They are microscopic organisms which unlike plants, lack chlorophyll and conductive tissue. There are more than 100,000 species of fungi found so far, of which around 8000 species are known to cause disease in plants. Fungi reproduce mainly by means of spores which are specialised propagative or reproductive bodies, consisting of one or a few cells. Figure 2.1 illustrates the microscopic view of two common fungi (i.e. *Oidium neolycopersici* and *Leveillula taurica*) which cause the powdery mildew disease in tomato plants.

Bacteria, Mycoplasma-like organisms and viruses are also among the plant pathogens [16]. Universally, plant diseases target forests, farmlands and greenhouses.

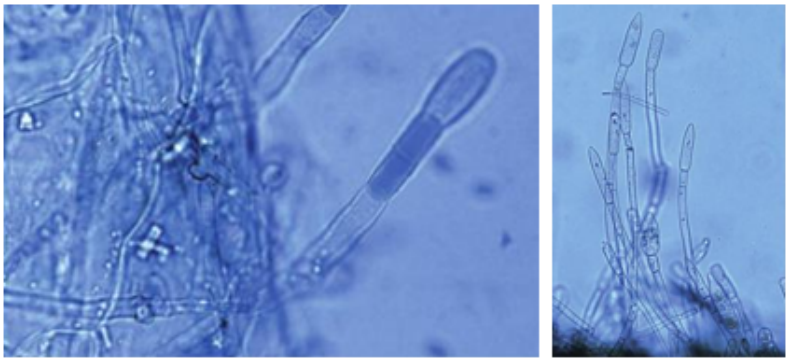

Figure 2.1: Left: Microscopic view of Oidium neolycopersici, right: Microscopic view of Leveillula taurica [15].

2.4 Greenhouse Diseases

It is falsely assumed that greenhouse environments are relatively free of disease and pests because the system is mostly enclosed. Pathogens, viruses and pests may be introduced when greenhouse vents are opened and through the movement of individuals or plantations through accidental introduction of infected plant material [17]. Another route for the spread of pathogens is through ornamental plants that act as hosts.

The fungal and viral infections, along with infestations by insects result in plant diseases and damage. Table 2.1 summarises the most common pests and diseases found in a greenhouse settings.

Pests		
Whiteflies	Spider Mites	Broad mites
Thrips	Broad mites	Caterpillars
Rutherglen bug	Flies (fungus gnats)	Aphids
Diseases		
Fungal moulds and mildews		
Botrytis (grey mould)	Downy mildew	Sclerotinia (white mould)
Leaf mould	Powdery mildew	
Bacterial leaf spots and soft rots		
Angular leaf spot	Bacterial speck	Bacterial spot
Bacterial soft rot		
Fungal leaf spots, blights and cankers		
Alternaria leaf spot	Anthracnose leaf spot	Grey leaf spot
Gummy stem blight		
Bacterial wilts		
Bacterial canker	Bacterial pith necrosis	Bacterial wilt
Fungal wilts and root rots		
Black root rot	Damping off	Fusarium
Verticillium		
Viruses		
Mosaic viruses	Cucumber yellows	Tomato spotted wilt virus

Table 2.1: Common greenhouse pest and diseases

2.5 Disease Symptoms

Plant's generic disease symptoms are briefly reviewed in this section since various non-destructive disease detection tools are activated when disease symptoms occur. Upon infection, a plant develops symptoms that appear on different parts of the plants causing a significant visual or agronomic impact. These include wilting, stunting, yellowing, whitening, death and abnormal growth of part or all of a plant. Diseases are sometimes classified as the basis of the kind of symptoms as follow: rusts, smuts, mildews, root-rots, blights, leaf spots, cankers and fruit-rots [18]. Image 2.2 illustrates visual symptoms of powdery mildew disease on tomato which is caused by fungi known as *oidium neolycop-*

ersici.

Figure 2.2: Left: powdery mildew colonies scattered around the plant, middle: powdery mildew colonies covers the entire leaf, right: colonies are visible on the stem [15].

The following images (2.3) illustrate the visual symptoms of diseases caused by bacteria and viruses in tomato plant.

Figure 2.3: Left to right: bronzed colour caused by Tomato Spotted Wilt Virus (TSWV), yellowing leaf is caused by Pepion Mosaic Virus (PEMV), angular small brown to black spots caused by Pseudomonas syrigae bacteria, Chlorotic, wilted and dried leafs caused by Clavibacter michigensis bacteria [15].

A plant disease develops over a period of time, whereas an injury that is caused by an insect feeding on a plant or damage from equipment or machinery occurs immediately or over a very short period of time. Usually a disease has been developing for several days before any symptoms on the plant are visible. For instance, it takes four to five days for leaf spots and potato late blight to become visible whereas symptoms of many other pathogens may take seven to 14 days to become visible [19].

2.6 Disease Diagnosis

After the onset of plant disease symptoms, the presence of disease in plants is verified using disease detection techniques.

Although experienced growers can diagnose diseases quickly by visual examination, others require the use of laboratory based methods since accurate diagnosis of a plant disease relies on the identification of the pathogen or causal agent. Conventional methods for detection of plant diseases such as light microscopy [20] have been practiced for many years. Additionally, molecular techniques have been employed to detect different pathogens in plants and hence identify the plants diseases. For the purpose of this study, disease detection techniques can be broadly classified into direct (a.k.a invasive, destructive) and indirect(a.k.a non-invasive, non-destructive) methods as outlined in table 2.2.

Disease Detection	
Direct Methods	Indirect Methods
Serological Methods	Biomarkers for disease detection
Flow Cytometry	Gaseous metabolite profiling
Enzyme-Linked	Plant metabolite profiling
Immunosorbent assay (ELISA)	
Molecular Methods	Plant Properties/stress
Fluorescence in situ hybridisation (FISH)	Imaging Techniques
Polymerase chain reaction (PCR)	Spectroscopic Techniques
DNA Arrays	

Table 2.2: Direct and indirect disease detection techniques

2.7 Molecular Techniques

Detection and diagnosis of plant viruses has included molecular and serological laboratory tests since the 1960s [21]. Molecular methods for plants disease detection includes characterising, isolating, and manipulating the molecular components of cells and organisms such as nucleic acids, that include deoxyribonucleic acid (DNA, the repository of genetic information) and ribonucleic acid (RNA, which serves the structural, functional, enzymatic, and information carrier role) [22].

The key performance measure of the molecular techniques are: a) sensitivity and b) speed of detection. The sensitivity of the molecular techniques refers to the minimum amount of microorganism that can be detected in the sample. The speed of detection refers to the length of time required to collect, prepare, analyse and interpret the results of the procedure. In this section two of the most widely used laboratory based techniques for plant disease detection will be briefly reviewed.

2.7.1 Enzyme-linked Immunosorbent Assay (ELISA)

Enzyme-linked Immunosorbent Assay (ELISA) is a rapid and sensitive serological method [23] which tests for the presence of the specific protein that the transgene produces in the plant and is employed for the identification of viral [24-26], bacterial [27] and fungal plant pathogens [28]. Applications of ELISA technique for the diagnosis of plant diseases have already been reviewed by Schaad et al. [29] and Henson et al. [30]. The following steps construct a typical ELISA procedure in a laboratory:

Step 1: Coat solid phase with either antibody or analyte.
Step 2: Block remaining binding sites on the solid phase.
Step 3: Add either analyte or anti-analyte antibody to be detected.
Step 4: Wash out excess reagent. This separates bound from free analyte.
Step 5: If reagent in step 4 is an analyte, add a second anti-analyte antibody with detection molecule attached. If reagent is an anti-analyte antibody, add an anti-Ig antibody with detection molecule attached.
Step 6: Wash out excess reagent
Step 7: Add substrate. The colour change or amount of light emitted is proportional to the level of target analyte.

Advantages of the ELISA tests are speed [31], relative ease of use, low cost [32] and tolerance to foreign material such as soil. Alternatives to ELISA are Immunofluorescence-Antibody Staining (IFAS) and Immunofluorescence-Colony Staining (IFCS) [33].

2.7.2 Polymerase Chain Reaction (PCR)

Polymerase Chain Reaction (PCR) is a technique used to make copied DNA sequences of interest through repetitive temperature cycling. PCR has been used in molecular biology, medical diagnosis, forensic analysis, plant biology, evolutionary and medical diagnosis [34]. The following tasks are required to be completed for a typical PCR procedure conducted in a laboratory.

Step 1 – Denaturation: DNA fragments are heated at high temperatures, which reduce the DNA double helix to single strands. These strands become accessible to primers.

Step 2 – Annealing: The reaction mixture is cooled down. Primers anneal to the complementary regions in the DNA template strands, and double strands are formed again between primers and complementary sequences.

Step 3 – Extension: The DNA polymerase synthesises a complementary strand. The enzyme reads the opposing strand sequence and extends the primers by adding nucleotides in the order in which they can pair. The whole process is repeated over and over as required.

As demonstrated in table 2.3, both ELISA and PCR have been extensively employed to detect different types of pathogens in plants. Other available molecular techniques includes Immunofluorescence (IF) [43], Flow Cytometry [44], Fluorescence In Situ Hydridization (FISH) [45], and DNA microarrays [46].

Reference	Plant	Source	Type	Method
[35, 36]	Citrus	Xylella fastidiosa	Bacteria	PCR, ELISA
[37]	Onion	Sclerotium cepivorum	Fungi	ELISA
[38]	Coffee Leaf	Xylella fastidiosa	Bacteria	PCR
[39]	Olive	Pseudomonas savastanoi	Bacteria	PCR
[40]	Potato	Candidatus Liberibacter	Bacteria	PCR
[41]	Tomato	Pepino mosaic virus	Virus	PCR, ELISA
[42]	Almond	Candidatus Phytoplasma	Bacteria	PCR, ELISA

Table 2.3: Examples of ELISA and PCR deployment for disease detection

2.7.3 Limitations and boundaries

Ready to use self-contained ELISA and PCR kits are produced in large quantities to allow detection of specific pathogens including Calibrachoa mottle virus [47], Xanthomonas fragariae [48], Ralstonia solanacearum [49], Tobacco mosaic virus [50] and Tomato spotted wilt virus [51]. Alvarez et al. [52] reported that there are around 100 commercially available immunodiagnostic tools for the detection pathogens in plants. In spite of the availability of these tools, the laboratory based techniques are time consuming, and require destructive sampling and thus they cannot be deployed as a preliminary screening tool for processing large number of plant samples due to the complexity involved in the process. Some of the specific and tangible limitations of the molecular techniques are as follow:

Time consuming: although some of the techniques may produce conclusive result in few minutes, the overall time to collect, prepare and analyse the sample may be significantly long. Time is the most crucial factor as the disease has to be detected and treated within the shortest time to avoid contaminating other crops within the greenhouse.

Labour-intensive: The molecular techniques requires skilled botanists or

horticulturalists to be able to prepare the samples and interpret the results. Hiring skilled technicians to collect and analyse samples on daily basis is impracticable and is considered economically unviable. Additionally, not all the tests conducted produces conclusive result. Obtaining reliable and accurate results requires skill. More importantly, the fact that human interaction is required for conducting the procedures eliminates the opportunity of such procedures to be integrated to the greenhouse management systems.

Destructive sampling: molecular techniques require a part of the plant to be detached for sampling. Destructive methods of disease detection are not suitable for rapid detection of diseases.

Elaborate procedure is required: especially during sample collection, extraction and preparation.

Cost: The overall cost of equipment, training and maintenance is high. Additionally, these techniques require consumable reagents that must be tailored to detect each specific pathogen (e.g. sequence-specific primers for PCR).

Considering the limitations outlined above, there is a demand for a fast, sensitive, and selective method for the non-destructive detection of plant diseases in early stages for economic, production and agricultural benefits.

2.8 Non-Destructive Methods

This section of the chapter reviews two approaches for a rapid, non-invasive and non-destructive plant disease diagnosis tool. The first approach involves the application of spectroscopic and imaging techniques for disease detection, whereas the second approach describes the application of Volatile Organic Compounds (VOCs) as possible biomarkers for disease detection. These two

approaches were selected as a) they offer non-destructive testing and b) they could possibly be integrated with an automated agricultural management system for a fast, reliable, and real-time plant disease monitoring for disease control and management.

Novel methods such as spectroscopic and imaging techniques for disease detection are among the non-destructive approaches since they do not required to detach any part(s) of the plant.

2.8.1 Spectroscopic and Imaging Techniques

Various spectroscopic and imaging techniques have been studied for the detection of symptomatic and asymptomatic plant diseases including fluorescence imaging [53], multispectral or hyperspectral imaging [54], infrared spectroscopy [55, 56], fluorescence spectroscopy [57], and Nuclear Magnetic Resonance (NMR) spectroscopy [58]. Such imaging and spectroscopic technologies have been applied for plant stress detection including water-stress and nutrient-stress detection. In addition, there have also been applications for monitoring the quality of postharvest fruits and vegetables [59].

2.8.2 Fluorescence Spectroscopy

Fluorescence Spectroscopy refers to a type of spectroscopic method, where the fluorescence from the object of interest is measured after excitation with a beam of light (usually ultraviolet spectra).

The laser-induced fluorescence has been used for vegetative studies to: a)

detect stress caused by water or other environmental factors or b) identify diseases based on plants visual symptoms. Two types of fluorescence: a) blue-green fluorescence (400-600 nm range), and b) chlorophyll fluorescence (650-800 nm), are produced by green leaves in plants [60]. In Fig. 2.4 a typical fluorescence spectrum of a healthy leaf for excitation at 532nm is shown which is due to the chlorophyll emission. The relative intensities of chlorophyll and blue-green fluorescent bands are highly sensitive to intrinsic leaf properties and environmental factors and therefore could be utilised to monitor nutrient deficiencies, nitrogen stress [61], environmental conditions based stress levels, and diseases in plants [62]. Lenk et al. [63] described the multispectral fluores-

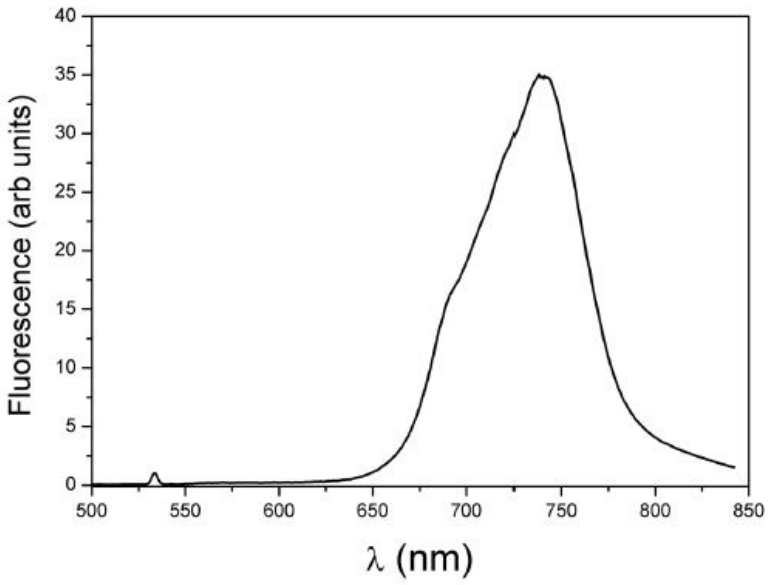

Figure 2.4: Typical fluorescence spectrum for a normal leaf experiencing no stress [62].

cence and its possible application in monitoring fruit quality, photosynthetic activities, tissue structures, and disease symptoms in plants; and the basic instrumentation required [64]. Belasque et al. [62] investigated the detection of mechanical and disease stresses in citrus plants (Citrus limonia L. Osbeck)

caused by the (Xanthomonas axonopodis pv. Citri) bacteria using 532nm, 10 mW excitation laser. Marcassa [65] used a system which composed of a spectrometer with the range of 350-850nm to detect water stress in orange trees (Citrus aurantium L.). Finally, Brling et al. [66] applied laser-induced fluorescence spectroscopy measured between 370 and 800 nm to detect leaf rust (Puccinia triticina) in wheat (Triticum aestivum L.) cultivars. In all investigations, the laser power has unanimously [62, 65] reported to be on the order of 10mW, assuring no thermal effect on the plant.

2.8.3 Visible and Infrared Spectroscopy

Studies have also been conducted on the detection of stress, injury, and diseases in plants using visible and infrared spectroscopy. The visible and infrared regions of the spectra is reported [60] to provide the valuable information on the physiological stress levels in the plants and thus, some of these wavebands specific to a disease can be used to detect plant diseases [67].

Xu et al. [68], characterised the leaf reflectance spectra of tomato leaves damaged by leaf miner and reported that spectral reflectance decreases significantly with the increasing damage severity level at the short wavelengths of near infrared 800-1100 nm but changes for individual bands of 1450 and 1900 nm where spectral reflectance increases with the increasing severity level. Wang et al. [69] using a diodearray NIR spectrometer measured reflectance spectra from 400 to 1,700 nm and classified healthy and damaged seeds with a 90% accuracy. Naidu et al. [70] investigated the potential of leaf spectral reflectance changes between virus infected and uninfected grapevines (Vitis vinifera) and

observed specific differences in vegetation indices and wavelength intervals between virus-infected and uninfected leaves in the 550, 900, 1600 and 2200nm regions.

Other imaging and spectrometry techniques such as hyperspectral imaging was investigated by Huang et. al [71], Chen et. al [72] and Delalieux et. al [73] to detect the symptoms of Sclerotinia Rot disease in celery crop (Apium graveolens), Verticillium wilt in cotton canopy and stress caused by Venturia inaequalis in apple trees respectively. In hyperspectral imaging, the spectral reflectance of each pixel is acquired for a range of wavelengths in the electromagnetic spectra. The wavelengths may include the visible and infrared regions of the electromagnetic spectra. The resulting information is a set of pixel values (intensity of the reflectance) at each wavelength of the spectra in the form of an image.

The following table summarises the studies previously conducted using spectroscopic methods.

Reference	Method	Plant	Application
[59]	NIR spectroscopy	Nectarines	Fruit Ripening
[74]	NIR spectroscopy	Apples	Sugar Content
[75]	NIR spectroscopy	Tomato	Rhizopus stolonifer spores
[62]	Fluorescence spect.	Citrus	Xanthomonas axonopodis pv
[76]	Fluorescence spect.	Tomato	Field monitoring
[71]	Hyperspectral sensing	Celery	Sclerotinia rot
[77]	Hyperspectral sensing	Citrus	Citrus canker
[78]	NMR Spectroscopy	Rose	Phytoplasma Infection

Table 2.4: Studies in which imaging and spectroscopic methods were employed for disease detection

2.8.4 Limitations and Boundaries

Most of the imaging techniques are relying on the visible symptoms and therefore the higher the visual symptoms, better is the accuracy of the technique. This is considered as a major drawback since the visual symptoms indicate that the disease has been developed already. Additionally, majority of wavelengths used in imaging techniques are limited to the ones that are produced by the photosynthesis process. Although such imaging techniques may be able to indicate the plant stress or photosynthesis deficiencies, there are not yet proficient in indicating underlying complex plant diseases [79]. Besides, the instrumentation and tools required for such detection are expensive, especially if techniques such as hyperspectral imaging are used. Predictably, fewer the wave bands used, cheaper will be the instrument. Standalone or networked computer systems are also needed for data collection and analysis which may add to the cost and may require an IT infrastructure. Such systems are not often rigorously ruggedized and therefore may not be suitable for intense weather conditions found in horticultural settings. Last but not the least, the devices need to be calibrated on regular basis which may affect the consistency of the result generated by the system.

2.9 Plant's Volatile Organic Compounds

Plants are a sedentary organism and to compensate for their immobility, they have evolved various mechanisms for their interactions with the environment including the synthesise and release of arrays of Volatile Organic Compounds (VOCs) from their leaves, flowers and fruits into the atmosphere and from

roots into the soil [80]. VOCs are lipophilic liquids with high vapour pressures which can cross membranes freely and be released into the atmosphere or soil in the absence of a diffusion barrier [81]. The VOC released by plants contribute to approx. 60% of the total VOC emissions present in the atmosphere. Various studies [82, 83] have been conducted to explore the VOCs emitted from different species of plants around the world because of their important role in: a) shaping global atmospheric and tropospheric chemistry, b) regional photochemical formation, c) balancing the global carbon cycle, and d) production of organic acids which contribute to acidic deposition in rural areas [84].

VOCs are produced by a range of physiological processes in many different plant tissues and are extremely diverse. In 1985, Isidorov et al. [85] attempted to sample and analyse the air containing VOC emissions from 22 species of living plants of northern hemisphere forests and determined the rate of isoprene and terpenes as well as another 70 different substances. Lelieveld et al. reported aircraft measurements of atmospheric trace gases performed over the pristine Amazon forest and effect of plant VOCs on atmosphere [86]. Knudsen et al. has listed 1719 VOCs including analyses of 991 species of flowering plants from 90 families [87]. They include oxygen, carbon dioxide, alkanes, alcohols, water vapour and aldehydes [88]. In addition to simple gases plants emit an enormous wealth of different terpenes, acid derivatives, benzenoids, phenylpropanoids, and amino acid derived metabolites [89, 90].

2.9.1 VOCs and Plant Defence

The principal functions of airborne VOCs are as follow: a) to defend plants against herbivores and pathogens [81], and b) to provide a potential reproductive advantage by attracting pollinators and seed dispersers [91]. VOCs emitted from vegetative tissues, as a part of the plant defence strategy, can repel or intoxicate [92] microbes and animals [93]. This is also known as a direct defence. VOCs can also attract natural predators of attacking herbivores, protecting the plant via tri-trophic interactions [94]. This is known as an indirect defence.

By releasing VOCs, a signalling plant not only reduces the number of attacking herbivores but can also warn the neighbouring plants about the herbivore or pathogen attack [95]. These warnings induce the expression of defence genes or emission of VOCs in neighbouring plants [96] or prime these plants to respond faster to future herbivore attack [97]. VOCs emitted from roots can contribute to a below-ground defence system by acting as anti-microbial or anti-herbivore substances, or by attracting enemies of root feeding herbivores [98].

2.10 VOCs and Disease Indication

Plants VOCs have multiple functions in plant physiology, biochemistry and health. The VOCs released by the plants depend on various physico-chemical factors [99] such as humidity [100], temperature [89], light [90], soil condition, and fertilisation [83], as well as biological factors such as growth and develop-

mental stage of the plant, insects, and presence of other herbs. These VOCs may vary qualitatively and quantitatively in response to abiotic and biotic stresses, including infection. The VOC profiles emitted from attacked plants show a degree of specificity and exclusivity which is associated with the category of attackers, and these profiles are different from those of undamaged or healthy plants [96]. Suitably, by examining the change of such profiles a non-destructive means of plant health evaluation may be developed.

Jansen et al. investigated whether plant-emitted volatiles can be used to detect a Botrytis Cinerea infection [101]. In a similar study, Sankaran reviewed the methods that can be employed in sensing diseases by analysing the plants VOCs [60]. Cevallos-Cevallos [102] reported that compounds such as hesperidin, naringenin, and quercetin present in the leaves could be used as a biomarker to identify huanglongbing disease in citrus trees. Finally, in a paper published by Tholl [103], the methods for VOC sampling and analysis for in-situ experiments as well as some for field experiments were described.

The two common methods for assessing the profile of VOCs released by plants are using Gas Chromatography-Mass spectrometry based and gas sensor array based techniques. Followings are the motives for selecting these two approaches: a) they could be easily integrated within an horticultural settings for a fast, reliable, and real-time plant disease monitoring for disease control and management, b) the approaches offer a non-destructive method of plant disease detection, c) these methods do not rely on visual symptoms of the disease and therefore may be able to detect the disease even before the appearance of the visual symptoms and d) gas sensors are becoming cheaper and

more portable which make them a suitable choice for deploying in large scale and multi-side operation.

2.11 VOCs and GC-MS Based Analysis

The most prominent technique in use for examining plant species VOCs is Gas Chromatography - Mass Spectrometry also known as GC-MS. GC-MS is an instrumental technique, comprising a gas chromatograph (GC) coupled to a mass spectrometer (MS), by which complex mixtures of chemicals may be separated in time, identified and quantified using electron or chemical ionisation techniques allowing the analysis of the hundreds of relatively low molecular weight compounds found in environmental materials. In order for a compound to be analysed by GC-MS it must be sufficiently volatile and thermally stable.

GC-MS systems with distinct topologies are used but for analysing VOCs the GC-MS need to be coupled with a thermal desorption unit which enables the analysis of concentration samples including air pollutants and living entities (i.e. plants). Figure 2.5 shows a typical installation of GC-MS which includes a GC unit, MS unit, thermal desorption unit and a PC for data analysis.

A number of studies were performed using GS-MS to investigate different plants species [104, 105]. For instance, in a study conducted by Hayase et al., 130 compounds where identified when VOCs obtained from two varieties of tomato fruits at various ripening stages were examined [106]. Table 2.5 summarises the studies in which the emission of exclusive VOCs were investigated to detect a particular plant disease.

Figure 2.5: A typical GC-MS setup with thermal desorption unit and data analysis unit ready for VOC sampling.

Reference	Plant	Cause of disease
[107]	Cucumber, Pepper	Oidium neolycopersici
[108]	Blueberry fruit	Botrytis cinerea
[109]	Tomato	Trichoplusia ni
[110]	Potato	Phytophthora infestans
[102]	Citrus	Huanglongbing
[111]	Carrots	Botrytis cinerea
[112]	Mango	Lasiodiplodia theobromae

Table 2.5: Analysis of VOC fingerprints for disease detection using GC-MS in previous studies

2.11.1 Limitations and Boundaries

Although GC-MS based systems are proven to be very effective in identifying the plants VOCs, the technology is costly, bulky, and requires skilled operators to process the resultant data. Therefore, these devices are unlikely to be suitable for use as user-friendly, practical and fully automated systems for early warning of pest and disease attacks in commercial greenhouses.

Furthermore, collecting, preparing and delivering the samples requires a lengthy and complicated procedure which makes the deployment of the system in any greenhouse settings to be literally impossible. GC-MS system requires a car-

rier gas (usually helium) to be fully operational. Selecting and supplying the appropriate carrier gas is a major drawback for a portable and rapid diagnosis tool.

Alternatively, gas sensor array systems (i.e. Electronic Noses) are known to offer a more attractive means of investigating VOCs as they are relatively cheaper, portable and can facilitate automated sampling procedures. Chapter 4 will investigate the use of Electronic Noses in detecting the plant's VOCs and hence discriminating between healthy and infected plants. Chapter 5 introduces a novel technique in which High-Field Asymmetric Waveform Ion Mobility Spectrometry (FAIMS) is utilised to sample the VOCs emitted from healthy and infected plants, thus, discriminating between them.

2.12 Summary

In this chapter different methods of disease detection including the established laboratory-based techniques were reviewed. The practicalities, challenges, experimental constrains and cost implications of the methods were clearly delineated. Although some of the techniques have already proved to be effective and are being used extensively, the need for a non-destructive, rapid and reliable technique for detection of diseases is certainly noticeable. In the next chapter the details of the practical plant VOC analysis including experimental procedure and data analysis techniques will be presented.

2.13 References

1. Chester, K.S., Plant disease losses: their appraisal and interpretation. Plant Disease Reporter (Suppl.), 1950(193): p. 190-362.

2. Alam, K. and J. Rolfe, Economics of plant disease outbreaks. Agenda, 2006. 13(2): p. 133-146.

3. Bowers, J.H., et al., The impact of plant diseases on world chocolate production. 2001: APSnet.

4. Chakraborty, S. and A.C. Newton, Climate change, plant diseases and food security: an overview. Plant Pathology, 2011. 60(1): p. 2-14.

5. Peterson, R.K.D. and L.G. Higley, Biotic Stress and Yield Loss. 2010: Taylor & Francis.

6. Cheatham, M.R., et al., Beyond Yield: Plant Disease in the Context of Ecosystem Services. Phytopathology, 2009. 99(11): p. 1228-1236.

7. Verdin, J., et al., Climate science and famine early warning. Philosophical Transactions of the Royal Society B: Biological Sciences, 2005. 360(1463): p. 2155-2168.

8. James, W.C., Assessment of plant diseases and losses. Annual Review of Phytopathology, 1974. 12(1): p. 27-48.

9. Roberts, M.J., et al., The value of plant disease early-warning systems: A case study of USDA's Soybean Rust Coordinated Framework, 2006, United States Department of Agriculture, Economic Research Service.

10. Pimentel, D., R. Zuniga, and D. Morrison, Update on the environmental and economic costs associated with alien-invasive species in the United States. Ecological Economics, 2005. 52(3): p. 273-288.

11. Oerke, E.-C., et al., Crop production and crop protection: estimated losses in major food and cash crops. 1994: Elsevier Science Publishers.

12. David Pimentel, P.D., Biological Invasions: Economic and Environmental Costs of Alien Plant, Animal, and Microbe Species. 2010: Taylor & Francis.

13. Pimentel, D., et al., Environmental and economic costs associated with non-indigenous species in the United States. Biological Invasions. CRC, Boca Raton, 2002: p. 285-303.

14. Lucas, G.B., C.L. Campbell, and L.T. Lucas, Introduction to Plant Diseases: Identification and Management. 1992: Springer.

15. Blancard, D., et al., Tomato Diseases: Identification, Biology and Control. 2012: Manson Publishing Limited.

16. Parry, D., Plant pathology in agriculture. 1990: Cambridge University Press.

17. Jensen, M.H. and A.J. Malter, Protected agriculture: a global review. 1995: World Bank Publications.

18. Sharma, P.D., Plant Pathology. 2004: Rastogi Publications.

19. Lamey, H.A. and M.P. McMullen, Plant Diseases: Development and Management. 1993: NDSU Extension Service.

20. Putnam, M.L., Evaluation of selected methods of plant disease diagnosis. Crop Protection, 1995. 14(6): p. 517-525.

21. Martin, R.R., D. James, and C.A. Lvesque, Impacts of Molecular Diagnostic Technologies On Plant Disease Management. Annual Review of Phytopathology, 2000. 38(1): p. 207-239.

22. Singh, A., et al., Chapter 13 - Molecular Techniques, in Chemical Analysis of Food: Techniques and Applications. 2012, Academic Press: Boston. p. 407-461.

23. Khan, J.A. and J. Dijkstra, Plant viruses as molecular pathogens. 2002: Food Products Press.

24. Narayanasamy, P., Microbial Plant Pathogens-Detection and Disease Diagnosis: Viral and Viroid Pathogens. 2011: Springer London, Limited.

25. Maramorosch, K., Plant Diseases and Vectors: Ecology and Epidemiology. 1981: Elsevier Science.

26. Hobbs, H., et al., Use of direct antigen coating and protein A coating ELISA procedures for detection of three peanut viruses. Plant disease, 1987. 71(8): p. 747-749.

27. Flood, J. and P.D. Bridge, Ganoderma diseases of perennial crops [electronic resource]. 2000: CABI Publ.

28. Vargas, V.M.L. and F.V. Flota, Plant Cell Culture Protocols-2006: Humana Press.

29. Schaad, N.W. and R.D. Frederick, Real-time PCR and its application for rapid plant disease diagnostics. Canadian Journal of Plant Pathology, 2002. 24(3): p. 250-258.

30. Henson, J.M. and R. French, The Polymerase Chain Reaction and Plant Disease Diagnosis. Annual Review of Phytopathology, 1993. 31(1): p. 81-109.

31. Miller, S.A. and R.R. Martin, Molecular Diagnosis of Plant Disease. Annual Review of Phytopathology, 1988. 26(1): p. 409-432.

32. Kole, C., Transgenic Crop Plants: Principles and development. Volume 1. 2010: Springer Berlin Heidelberg.

33. Gnanamanickam, S.S., Plant-Associated Bacteria. 2007: Springer.

34. Lim, C.T. and J.C.H. Goh, 13th International Conference on Biomedical Engineering. 2009: Springer Berlin Heidelberg.

35. Pooler, M. and J. Hartung, Specific PCR detection and identification of Xylella fastidiosa strains causing citrus variegated chlorosis. Current Microbiology, 1995. 31(6): p. 377-381.

36. Arajo, W.L., et al., Diversity of endophytic bacterial populations and their interaction with Xylella fastidiosa in citrus plants. Applied and Environmental Microbiology, 2002. 68(10): p. 4906-4914.

37. Haq, M.A., et al., Detection of Sclerotium cepivorum within onion plants using PCR primers. Physiological and molecular plant pathology, 2003. 62(3): p. 185-189.

38. De Lima, J., et al., Coffee leaf scorch bacterium: Axenic culture, pathogenicity, and comparison with Xylella fastidiosa of citrus. Plant Disease, 1998. 82(1): p. 94-97.

39. Penyalver, R., et al., Detection of Pseudomonas savastanoi pv. savastanoi in olive plants by enrichment and PCR. Applied and Environmental Microbiology, 2000. 66(6): p. 2673-2677.

40. Secor, G., et al., Association of 'Candidatus Liberibacter solanacearum' with zebra chip disease of potato established by graft and psyllid transmission, electron microscopy, and PCR. Plant Disease, 2009. 93(6): p. 574-583.

41. Martinez-Culebras, P., et al., A RTPCR assay combined with RFLP analysis for detection and differentiation of isolates of Pepino mosaic virus (PepMV) from tomato. European journal of plant pathology, 2002. 108(9): p. 887-892.

42. Chalak, L., et al., Attempts to eliminate Candidatus phytoplasma phoenicium from infected Lebanese almond varieties by tissue culture techniques combined or not with thermotherapy. European journal of plant pathology, 2005. 112(1): p. 85-89.

43. Odell, I.D. and D. Cook, Immunofluorescence Techniques. J Invest Dermatol, 2013. 133(1): p. e4.

44. Dpooleel, J., P. Binarov, and S. Lcretti, Analysis of nuclear DNA content in plant cells by flow cytometry. Biologia Plantarum, 1989. 31(2): p. 113-120.

45. Singh, R., J. Jiang, and B.S. Gill, Current status and the future of fluorescence in situ hybridization (FISH) in plant genome research. Genome, 2006. 49(9): p. 1057-1068.

46. Wan, J., M.F. Dunning, and A.F. Bent, Probing plant-pathogen interactions and downstream defense signaling using DNA microarrays. Functional & integrative genomics, 2002. 2(6): p. 259-273.

47. Liu, H.-Y., et al., First report of Calibrachoa mottle virus infecting petunia. Plant Disease, 2003. 87(12): p. 1538-1538.

48. Roberts, P., et al., Survival of Xanthomonas fragariae on strawberry in summer nurseries in Florida detected by specific primers and nested polymerase chain reaction. Plant Disease, 1996. 80(11): p. 1283-1288.

49. Elphinstone, J., et al., Sensitivity of different methods for the detection of Ralstonia solanacearum in potato tuber extracts. EPPO Bulletin, 1996. 26(34): p. 663-678.

50. Van Regenmortel, M. and J. Burckard, Detection of a wide spectrum of tobacco mosaic virus strains by indirect enzyme-linked immunosorbent assays (ELISA). Virology, 1980. 106(2): p. 327-334.

51. Zindovic, J., et al., First Report of Tomato spotted wilt virus on Pepper in Montenegro. Plant Disease, 2011. 95(7): p. 882-882.

52. Alvarez, A.M., Integrated Approaches For Detection of Plant Pathogenic Bacteria And Diagnosis Of Bacterial Diseases. Annual Review of Phytopathology, 2004. 42(1): p. 339-366.

53. Sauer, M., J. Hofkens, and J. Enderlein, Handbook of Fluorescence Spectroscopy and Imaging: From Ensemble to Single Molecules. 2010: Wiley.

54. Chang, C.I., Hyperspectral imaging: techniques for spectral detection and classification. 2003: Kluwer Academic/Plenum Publishers.

55. Stuart, B.H., Infrared Spectroscopy: Fundamentals and Applications. 2004: Wiley.

56. Nicola, B.M., et al., Nondestructive measurement of fruit and vegetable quality by means of NIR spectroscopy: A review. Postharvest Biology and Technology, 2007. 46(2): p. 99-118.

57. Lakowicz, J.R., Principles of fluorescence spectroscopy. 2009: Springer London, Limited.

58. Keeler, J., Understanding NMR Spectroscopy. 2011: Wiley.

59. Prez-Marn, D., et al., Non-destructive determination of quality parameters in nectarines during on-tree ripening and postharvest storage. Postharvest Biology and Technology, 2009. 52(2): p. 180-188.

60. Sankaran, S., et al., A review of advanced techniques for detecting plant diseases. Computers and Electronics in Agriculture, 2010. 72(1): p. 1-13.

61. Tremblay, N., Z. Wang, and Z. Cerovic, Sensing crop nitrogen status with fluorescence indicators. A review. Agronomy for Sustainable Development, 2012. 32(2): p. 451-464.

62. Belasque, J.J., M.C.G. Gasparoto, and L.G. Marcassa, Detection of mechanical and disease stresses in citrus plants by fluorescence spectroscopy. Appl. Opt., 2008. 47(11): p. 1922-1926.

63. Lenk, S., et al., Multispectral fluorescence and reflectance imaging at the leaf level and its possible applications. Journal of Experimental Botany, 2007. 58(4): p. 807-814.

64. Usha, K. and B. Singh, Potential applications of remote sensing in horticultureA review. Scientia Horticulturae, 2013. 153(0): p. 71-83.

65. Marcassa, L.G., et al., Fluorescence spectroscopy applied to orange trees. Laser Physics, 2006. 16(5): p. 884-888.

66. Brling, K., et al., UV-induced fluorescence spectra and lifetime determination for detection of leaf rust (Puccinia triticina) in susceptible and resistant wheat (Triticum aestivum) cultivars. Functional Plant Biology, 2011. 38(4): p. 337-345.

67. Muhammed, H.H. Using hyperspectral reflectance data for discrimination between healthy and diseased plants, and determination of damage-level in diseased plants. in Applied Imagery Pattern Recognition Workshop, 2002. Proceedings. 31st. 2002. IEEE.

68. Xu, H.R., et al., Near-infrared Spectroscopy in detecting Leaf Miner Damage on Tomato Leaf. Biosystems Engineering, 2007. 96(4): p. 447-454.

69. Wang, D., et al., Classification of Fungal-Damaged Soybean Seeds Using Near-Infrared Spectroscopy. International Journal of Food Properties, 2004. 7(1): p. 75-82.

70. Naidu, R.A., et al., The potential of spectral reflectance technique for the detection of Grapevine leafroll-associated virus-3 in two red-berried wine grape cultivars. Comput. Electron. Agric., 2009. 66(1): p. 38-45.

71. Huang, J.F. and A. Apan, Detection of sclerotinia rot disease on celery using hyperspectral data and partial least squares regression. Journal of Spatial Science, 2006. 51(2): p. 129-142.

72. Chen, B., et al., Spectrum Characteristics of Cotton Canopy Infected with Verticillium Wilt and Inversion of Severity Level, in Computer And Computing Technologies In Agriculture, Volume II, D. Li, Editor. 2008, Springer US. p. 1169-1180.

73. Delalieux, S., et al., Detection of biotic stress (Venturia inaequalis) in apple trees using hyperspectral data: Non-parametric statistical approaches and physiological implications. European Journal of Agronomy, 2007. 27(1): p. 130-143.

74. Nicola, B.M., K.I. Theron, and J. Lammertyn, Kernel PLS regression on wavelet transformed NIR spectra for prediction of sugar content of apple. Chemometrics and Intelligent Laboratory Systems, 2007. 85(2): p. 243-252.

75. Hahn, F., I. Lopez, and G. Hernandez, Spectral Detection and Neural Network Discrimination of Rhizopus Stolonifer Spores on Red Tomatoes. Biosystems Engineering, 2004. 89(1): p. 93-99.

76. Saito, Y. Laser-induced fluorescence spectroscopy/technique as a tool for field monitoring of physiological status of living plants. in 14th International School on Quantum Electronics: Laser Physics and Applications. 2007. International Society for Optics and Photonics.

77. Qin, J., et al., Citrus canker detection using hyperspectral reflectance imag-

ing and PCA-based image classification method. Sensing and Instrumentation for Food Quality and Safety, 2008. 2(3): p. 168-177.

78. Choi, Y.H., et al., Metabolic discrimination of Catharanthus roseus leaves infected by phytoplasma using 1H-NMR spectroscopy and multivariate data analysis. Plant Physiology, 2004. 135(4): p. 2398-2410.

79. Cerovic, Z., et al., The use of chlorophyll fluorescence excitation spectra for the nondestructive in situ assessment of UVabsorbing compounds in leaves. Plant, Cell & Environment, 2002. 25(12): p. 1663-1676.

80. Hewitt, C.N., et al., Quantification of VOC emission rates from the biosphere. TrAC Trends in Analytical Chemistry, 2011. 30(7): p. 937-944.

81. Pichersky, E., J.P. Noel, and N. Dudareva, Biosynthesis of plant volatiles: nature's diversity and ingenuity. Science Signaling, 2006. 311(5762): p. 808.

82. Komenda, M., et al., Measurements of biogenic VOC emissions: sampling, analysis and calibration. Atmospheric environment, 2001. 35(12): p. 2069-2080.

83. Karl, T., et al., Chemical sensing of plant stress at the ecosystem scale. Biogeosciences Discuss., 2008. 5(3): p. 2381-2399.

84. Fehsenfeld, F., et al., Emissions of volatile organic compounds from vegetation and the implications for atmospheric chemistry. Global Biogeochemical Cycles, 1992. 6(4): p. 389-430.

85. Isidorov, V.A., I.G. Zenkevich, and B.V. Ioffe, Volatile organic compounds in the atmosphere of forests. Atmospheric Environment (1967), 1985.

19(1): p. 1-8.

86. Lelieveld, J., et al., Atmospheric oxidation capacity sustained by a tropical forest. Nature, 2008. 452(7188): p. 737-740.

87. Knudsen, J., et al., Diversity and distribution of floral scent. The Botanical Review, 2006. 72(1): p. 1-120.

88. Peuelas, J. and J. Llusi, Plant VOC emissions: making use of the unavoidable. Trends in Ecology & Evolution, 2004. 19(8): p. 402-404.

89. Holopainen, J.K. and J. Gershenzon, Multiple stress factors and the emission of plant VOCs. Trends in Plant Science, 2010. 15(3): p. 176-184.

90. Kesselmeier, J. and M. Staudt, Biogenic Volatile Organic Compounds (VOC): An Overview on Emission, Physiology and Ecology. Journal of Atmospheric Chemistry, 1999. 33(1): p. 23-88.

91. Reinhard, J., M.V. Srinivasan, and S. Zhang, Olfaction: scent-triggered navigation in honeybees. Nature, 2004. 427(6973): p. 411-411.

92. Vancanneyt, G., et al., Hydroperoxide lyase depletion in transgenic potato plants leads to an increase in aphid performance. Proceedings of the National Academy of Sciences, 2001. 98(14): p. 8139-8144.

93. De Moraes, C.M., M.C. Mescher, and J.H. Tumlinson, Caterpillar-induced nocturnal plant volatiles repel conspecific females. Nature, 2001. 410(6828): p. 577-580.

94. Mercke, P., et al., Combined transcript and metabolite analysis reveals genes involved in spider mite induced volatile formation in cucumber plants. Plant Physiology, 2004. 135(4): p. 2012-2024.

95. Shulaev, V., P. Silverman, and I. Raskin, Airborne signalling by methyl salicylate in plant pathogen resistance. 1997.

96. Arimura, G.-i., et al., Herbivory-induced volatiles elicit defence genes in lima bean leaves. Nature, 2000. 406(6795): p. 512-515.

97. Engelberth, J., et al., Airborne signals prime plants against insect herbivore attack. Proceedings of the National Academy of Sciences of the United States of America, 2004. 101(6): p. 1781-1785.

98. Rasmann, S., et al., Recruitment of entomopathogenic nematodes by insect-damaged maize roots. Nature, 2005. 434(7034): p. 732-737.

99. Ebel, R.C., J.P. Mattheis, and D.A. Buchanan, Drought stress of apple trees alters leaf emissions of volatile compounds. Physiologia Plantarum, 1995. 93(4): p. 709-712.

100. Loreto, F. and J.-P. Schnitzler, Abiotic stresses and induced BVOCs. Trends in Plant Science, 2010. 15(3): p. 154-166.

101. Jansen, R., et al., Health monitoring of plants by their emitted volatiles: trichome damage and cell membrane damage are detectable at greenhouse scale. Annals of Applied Biology, 2009. 154(3): p. 441-452.

102. Cevallos, J.M., R. Rouseff, and J.I. Reyes De Corcuera, Untargeted metabolite analysis of healthy and Huanglongbinginfected orange leaves by CEDAD. Electrophoresis, 2009. 30(7): p. 1240-1247.

103. Tholl, D., et al., Practical approaches to plant volatile analysis. The Plant Journal, 2006. 45(4): p. 540-560.

104. Corrado, G., et al., Systemin regulates both systemic and volatile signaling in tomato plants. Journal of chemical ecology, 2007. 33(4): p. 669-681.

105. Deng, C., et al., Investigation of tomato plant defence response to tobacco mosaic virus by determination of methyl salicylate with SPME-capillary GC-MS. Chromatographia, 2004. 59(3): p. 263-268.

106. Hayase, F., T.Y. Chung, and H. Kato, Changes of volatile components of tomato fruits during ripening. Food Chemistry, 1984. 14(2): p. 113-124.

107. Laothawornkitkul, J., et al., Discrimination of plant volatile signatures by an electronic nose: a potential technology for plant pest and disease monitoring. Environmental science & technology, 2008. 42(22): p. 8433-8439.

108. Li, C., et al., Gas sensor array for blueberry fruit disease detection and classification. Postharvest Biology and Technology, 2010. 55(3): p. 144-149.

109. Miresmailli, S., et al., Herbivoreinduced plant volatiles allow detection of Trichoplusia ni (Lepidoptera: Noctuidae) infestation on greenhouse tomato plants. Pest management science, 2010. 66(8): p. 916-924.

110. De Lacy Costello, B.P.J., et al., Gas chromatographymass spectrometry analyses of volatile organic compounds from potato tubers inoculated with Phytophthora infestans or Fusarium coeruleum. Plant Pathology, 2001. 50(4): p. 489-496.

111. Vikram, A., et al., Metabolic fingerprinting to discriminate diseases of stored carrots. Annals of applied biology, 2006. 148(1): p. 17-26.

112. Moalemiyan, M., A. Vikram, and A.C. Kushalappa, Detection and discrimination of two fungal diseases of mango (cv. Keitt) fruits based on volatile metabolite profiles using GC/MS. Postharvest Biology and Technology, 2007. 45(1): p. 117-125.

Chapter 3

Pragmatic Approach To Plant VOC Analysis Via Gas Sensors

3.1 Chapter Overview

The focus of this chapter is on the sampling procedures for plant VOCs analysis. Different approaches will be presented outlining their practicality and viability for rapid and non-destructive sample collection. The chapter begins with an introduction of the instrumentations, apparatus, materials and the overall methodology used for VOC profile sampling and data acquisition in the experiments conducted at the University of Warwick. The chapter closes by introducing the state-of-the-art gas sensors including Electronic Nose (EN) and Field Asymmetric Ion Mobility Spectrometry (FAIMS).

3.2 Introduction

Plants VOC emission have been investigated most extensively in the airspace surrounding above-ground of plant parts including the stem, flowers, leaves and fruits. Major motivations for study of VOCs are as follow: **a)** analyses of VOCs in relation to pollination biology and reproduction [1], **b)** quantification of VOCs released from photosynthetic tissues in response to changes in environmental factors such as light, temperature and humidity [2], and **c)** identification of exclusive VOCs induced by biotic or abiotic infection or damage for direct or indirect defence strategy [3].

VOC sampling is a non-destructive method for collecting plant emitted profiles. Compared with solvent extractions [4] of volatiles from plant tissues, VOC profiles analysis provides in-depth view of the biomarkers emitted by plants making it suitable method for ecologically relevant applications including the non-destructive plant health monitoring tool.

Independent of sampling procedure, gas sensors are used to analyse the VOCs emitted from the plants. In this study, Electronic Nose and Field Asymmetric Ion Mobility Spectrometry are employed to examine the VOC profiles.

3.3 Electronic Nose

The Electronic Nose (EN) is referred to an instrument containing an array of gas sensors able to imitate some of the functions of human olfaction and may be used for detection and classification of VOCs. A multi-purpose EN system

was introduced in 1982 by Dodd and Persaud from the Warwick Olfaction Research Group, UK and since then several applications of EN have been investigated [5, 6]. More recently, EN technology has been used in a variety of fields, including food and fruit quality measurements [7-9], disease diagnosis [10, 11] and automotive industry [12, 13].

An EN device (Bloodhound ST214) manufactured by Scensive Technologies Ltd. (Normanton, UK) has been used as the gas sensor in this study (Fig 3.1).

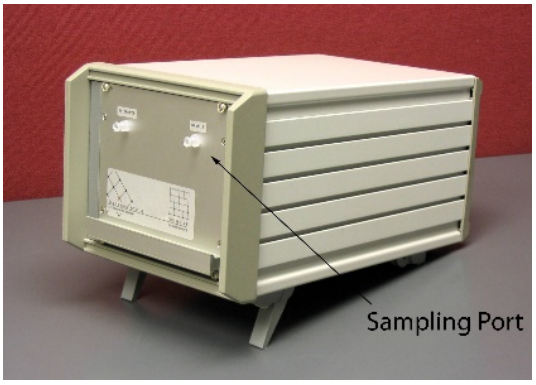

Figure 3.1: Bloodhound ST214 EN manufactured by Scensive Technologies Ltd.

The Bloodhound ST214 uses 13 conducting polymer sensors produced from a variety of materials and requires to be connected to a stand-alone PC/Laptop to capture and store the numerical data. The sensitivity of the EN device varies between ppm (part per million) and ppb (part per billion) levels depending on the built-in sensors. The headspace is conveyed from the sampling container via a sampling port (Fig. 3.1) to the sensor array using an internal

pump. A detailed description of EN's technology is given in chapter 4.

3.4 Field Asymmetric Ion Mobility Spectrometry (FAIMS)

The very first paper describing Field Asymmetric Ion Mobility Spectrometry (FAIMS) technology appeared in the literature in 1993 [14]. FAIMS has rapidly gained acceptance as a robust, versatile tool for post-ionisation separations prior to mass-spectrometric analysis and has been utilised in a variety of fields including bio-analytical, forensic, geological and defence applications [15, 16]. The more detailed description of FAIMS technology and its foundations will be given in chapter 5.

This study is the first to employ such FAIMS technology in horticultural settings to sample the VOCs emitted from a live plant in order to discriminate between healthy and infected species.

For this investigation a Lonestar FAIMS device produced by Owlstone (Cambridge, United Kingdom) was configured and used. Figure 3.2 demonstrates a Lonestar portable and self-contained unit. Lonestar compromises a full functioning PC, display screen, FAIMS sensor and a pump. The built-in sensor acts as a reprogrammable filter, which detects and separates chemicals according to their characteristic of ion mobility with high sensitivity (ppb detection level). This specific device has ambient and headspace input, high humidity tolerance (0% - 95%) and includes temperature, humidity, flow and pressure

Figure 3.2: Lonestar FAIMS unit manufactured by Owlstone Ltd.

sensors.

3.5 Sampling Procedures

A wide range of destructive sampling techniques have been employed for the collection of plant VOCs [17]. Although these approaches have significantly increased the understanding of plant VOCs, there are drawbacks to physically (artificially) wounding the plant [18, 19] during the sampling procedures. Wounding a plant not only causes the localised action of the phytohormones such as *jasmonic acid (JA)*, but it also generates chemical signals that act systemically through the plant. [20]. These signals stimulate the release of new volatiles including *ethylene* far from the site of damage and also cause quantitative and qualitative changes in the volatiles such as *terpene* relative to those from intact parts [21]. Therefore, contamination from the wound should be avoided or limited where possible.

In this section three of the most widely used sample collection techniques

for plants will be evaluated.

3.5.1 Static Collection

For full plant static VOC collection, the plant are enclosed in a container (Fig. 3.3a) and the emitted volatiles are trapped onto an adsorbent without any positive air pressure (no pulling). The air in the chamber is not circulated surrounding the plant and therefore remains static. VOCs are enriched on the adsorbing matrix without sampling impurities of a continuous air stream that may obscure the detection of target VOCs. Thus, this method is advantageous for sampling VOCs from low emitting or small plants. This method, however, is not suitable if the gas sensor is sensitive to humidity. Since there is no circulation within the chamber, perspiration occurs and humidity levels can reach up to 95%. Additionally, this technique is not suitable for monitoring the plant for a long period of time (in this case 30 days). Since there is no air circulation the plant will be stressed and can be destroyed after very few days. Another drawback is that watering the plant may be limited or not possible depending on the type of enclosure. Studies [22] were conducted in which static collection was only applied on a single leaf. This method is proven to be not practical for a rapid, non-destructive health monitoring tool application as: a) a single leaf may not reflect the overall status of the plant, b) attaching experimental appliances to a single leaf often result in injury, c) complex setup makes this procedure impractical for day-to-day usage, and d) no air circulation damage the plant in a short timeframe. Figure 3.3c demonstrates this technique.

3.5.2 Pull Only

In a pull only headspace collection the plant is enclosed in an open-top container (Fig. 3.3b). An air stream is pulled over the plant with and through a VOC collecting adsorbent trap. The air flow may be regulated by a flow meter. This method is not suitable for the proposed experiment as the open-top container will lead to the sampling impurities of a continuous air stream that may obscure the detection of target VOCs. Additionally, it will be practically impossible to control the disease in an open-top container as spread of pathogens may infect the control plant. In a simple pull collection from a single leaf, a device with an open-top chamber for collecting VOCs is attached to a single leaf (Fig. 3.6). This method is not recommended for the reasons discussed in sections 3.5.1.

3.5.3 Push & Pull

In a push–pull headspace collection system, pressurised air enters the top of the collection chamber regulated by a flow meter. Incoming air is purified by passing through a filtration system placed behind or in front of the flow meter. Alternatively, high-purity synthetic air may be used. After passing over the plant sample, the air is pulled through an adsorbent volatile trap at the lower side of the chamber at a defined rate controlled by a second flow meter. Excess air can escape through the vent on the lower side of the chamber (Fig. 3.3). Example of a modified push–pull headspace collection chamber for collecting VOCs from parts of a plant is demonstrated in Fig. 3.4. Teflon-coated blades close the base of the chamber around the stem of the plant allowing trapping of VOCs from the upper part of the plant. In order to minimise damage to a plant

during sampling of volatiles, a guillotine-style enclosure vessel may be used. This isolates part of or a whole plant, and clean air is blown into the enclosing vessel at a rate greater than that at which headspace is sampled through a trapping adsorbent. Typically, the main body of such vessels is made of glass and the guillotine of Teflon or aluminium. However, these heavy, bulky glass vessels require considerable support and are inconvenient for sampling plants growing naturally. Additionally, since the pot and soil is not included in the sampling chapter, the results will not reflect the actual real-life growing environment and for this reason this method may not be suitable for this study. The following image shows all the six plant sampling methods.

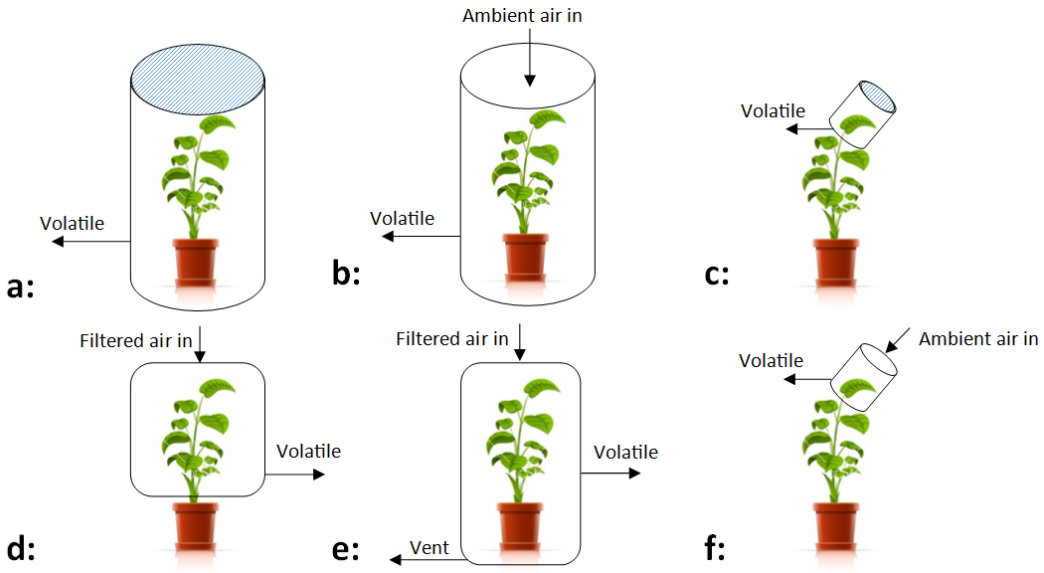

Figure 3.3: VOC sampling types: a) static collection (full plant), b) simple pull collection (full plant), c) static collection (part of plant), d) push and pull collection (part of plant), e) push and pull collection (full plant) and f) simple pull collection (part of plant)

Figure 3.4 illustrates the sampling procedures in a field or laboratory. Fig. 3.4-top-left shows a special cuvette used for simultaneous measurements of gas exchange and fluorescence properties of a single leaf. Fig. 3.4-bottom demonstrates static sample collection used to monitor gas exchanges from entire branches under field conditions. Fig. 3.4-top-right, shows a push-pull collection system for gas exchange analysis from the branch of Arabidopsis thaliana [23].

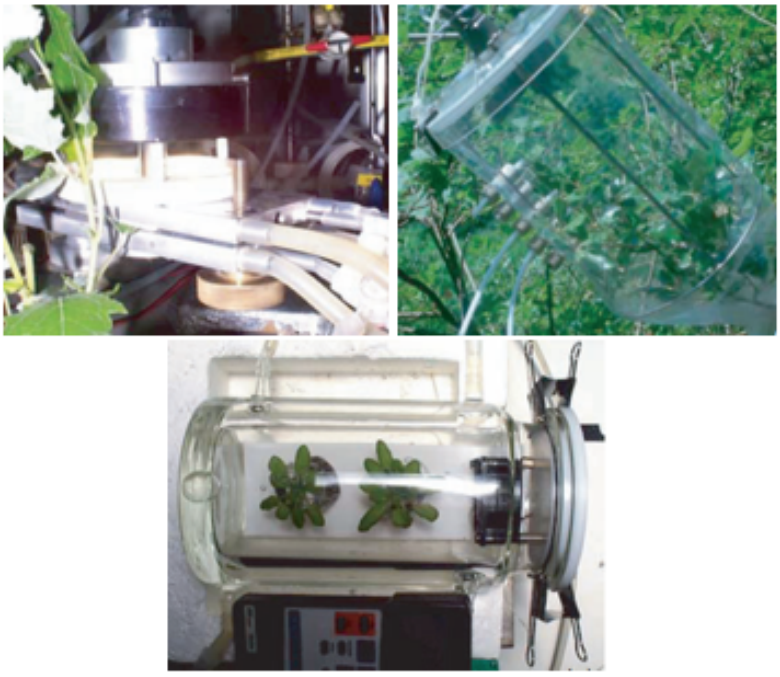

Figure 3.4: Field VOC sampling, top-left: Static collection (leaf), middle: static collection (branch) and top-right: push-pull collection (full plant) [23].

3.6 Experimental Design at University of Warwick

The experimental procedure reported in this thesis is designed in such a way in which a combination of static sample collection and push and pull sample collection is employed. In order to replicate the real-life growing environment in a small scale, plant-size glass chambers are designed and manufactured in School of Engineering, University of Warwick to house the infected and healthy plant. Since the experiment was going to be performed for a long period of time (approx. 30 days) the air needs to be circulated within the glass enclosure. The air is also required to be filtered and pumped into the chamber to regulate the humidity level as well as encouraging the plants normal growth. The air flow will be switched off approx. 3 hours prior to sampling so the VOC concentration within the glass enclosure could be built up ready for sample collection (static collection).

3.6.1 Plant Glass Chamber

Devices used for VOC collections need to be free of materials that retain volatiles or cause bleeding of compounds that may contaminate the system and interfere with volatile analysis. Commonly used materials that do not show bleeding include glass, metal and special plastics such as Teflon [22]. These sets of materials are considered to reduce adsorption of VOCs on parts of the apparatus. To replicate a real-life growing environment, clear glass and aluminium were used to construct a glass enclosure which will house one plant each. The glasses used were completely cleaned and disinfected using alco-

hol. The dimensions of the enclosure were: 150cm height, 50cm width and 50cm depth. Eight holes were drilled for sampling and watering purposes. As demonstrated in figure 3.5, three holes were drilled on the front panel of the enclosure for the sample volatile outlet. Three holes were drilled on the bottom side of the glass enclosure for watering tube, air tubing and ventilation. Two holes were drilled on the top of the enclosure for data loggers and other cables.

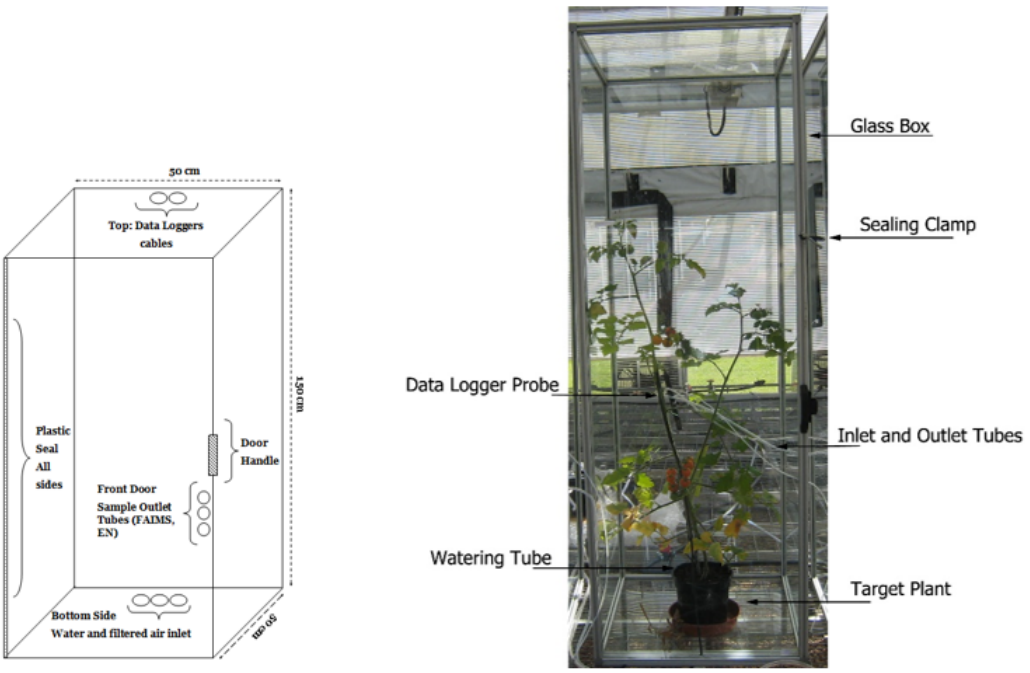

Figure 3.5: Left: The sampling glass enclosure and the positions of the holes, right: Components of a sampling glass enclosure (front view) at University of Warwick

Each glass enclosure was designed to house a single plant in a pot. The enclosures were kept reasonably distanced (50 cm) from each other. None of the sampling tubes, probes or watering pipes were shared between the enclosures so the possibility of cross contamination is minimised. Figure 3.6 illustrates experimental setup. A sealing clamp was used on all three glass enclosures

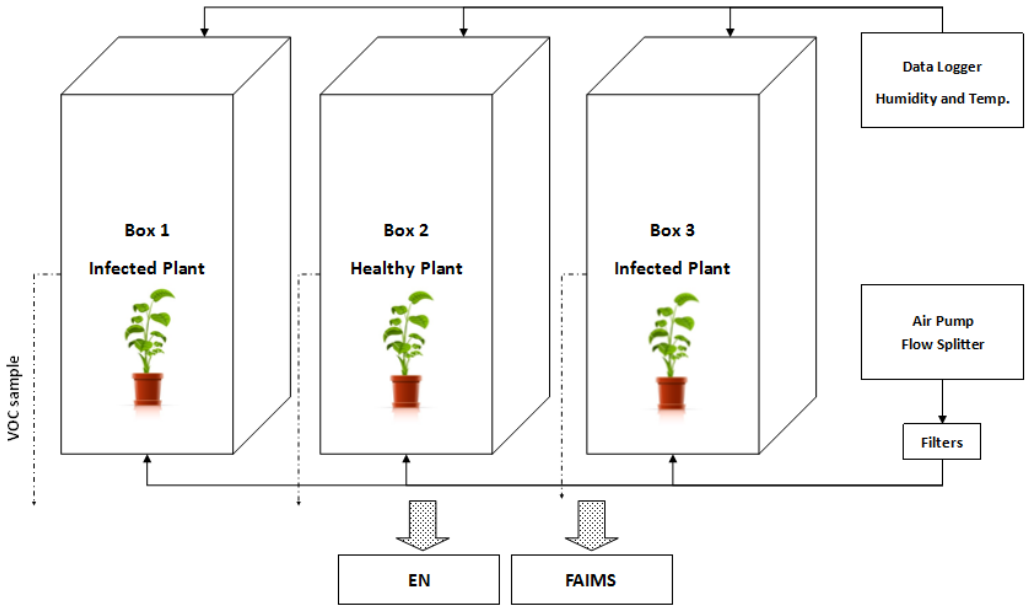

Figure 3.6: Schematic view of the experimental setup showing three glass enclosures for each plant

to seal the front door preventing cross contamination. The following image demonstrates the enclosures with all the three plants housed in them.

3.6.2 Watering System

Water stress has been proven to alter the emission of plant VOCs both qualitatively and quantitatively [24-27]. In tomato for instance, the emission of *abscisic acid (ABA)* is believed to increase due to water stress [26]. To minimise water stress, a regulated watering system was built in to the system. A watering tube was connected to a watering pump which was configured centrally so it automatically water the plants on daily basis. This also avoids the opening and closing of the front door for watering purposes which eliminated the possibility of cross contamination.

Figure 3.7: Experimental setup showing the position of each glass enclosure

3.6.3 Air Circulation

Pathogens such as *Oidiopsis sicula*, *Botrytis cinerea* and *Mycovellosiella fulva* may be introduced when enclosure doors are opened and through the movement of people or other random sources [28]. It is important that the air circulating in the glass enclosure is free of any infectious or undesirable particles. Since it is required that the plants should grow under normal conditions, a positive pressure is created inside the enclosures via injecting a clean and fresh air. To accomplish this, a set of air pumps, PTFE tubing and filters were used.

3.6.4 Pumps and Tubing

In order to create a positive pressure and air flush in a clean glass enclosure, an electronic air pump was employed. The cleanness of the pump and tubing was taken into consideration before flushing the enclosure. The pump flow rate was measured at 800 litter per hour and was initially regulated by a flow meter. Figure 3.8 illustrates the back of the enclosures where the air pump and the tubing are visible.

3.6.5 Filters

A series of filters were used to filter the ambient air outside the glass enclosures before it is pumped into the sampling setup. Helapet ISOVent, 0.2 micron filtration devices used for purifying air for gas detection applications and are capable of eliminating biological particles such as *Oidiopsis sicula* and other spores. Figure 3.9 illustrated one of the PTFE filters and the way the tubes are connected to it.

3.6.6 Environmental Factor Data Loggers and Probes

High temperatures increase the rapid stimulation and emission rate of VOC profiles such as *isoprene* in many plant species [25]. High humidity may also lead to a swelling and to the consequent explosion of the structures of emitted VOCs [29]. In order to monitor and control the environmental factors throughout the experiment three data loggers and probes were used. The HygroLog HL-NT2 devices (Rotronic Ltd.) were capable of logging long term data under severe conditions. Its working temperature and humidity range is -50 to

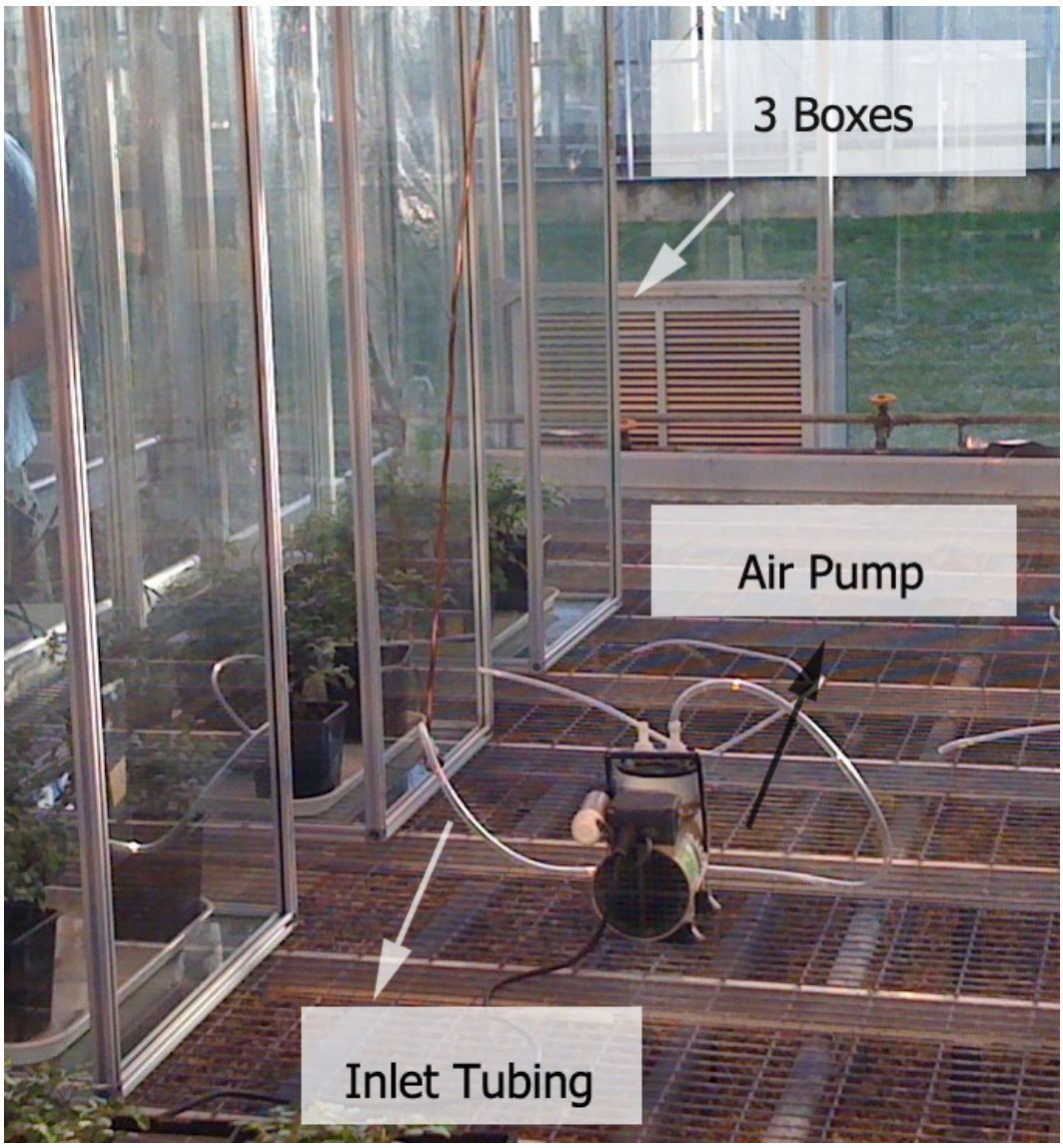

Figure 3.8: Components of a sampling glass enclosure (behind view) at the University of Warwick

+100 centigrade and 0 – 100 % relative humidity respectively. The sensing probes are attached to the data loggers via a 2m cable. Each probe is carefully placed in the middle of each glass enclosure away from the side glasses so the most accurate reading is achieved (Fig 3.10- right). The probes and the attached cables were not shared between the enclosures to avoid potential

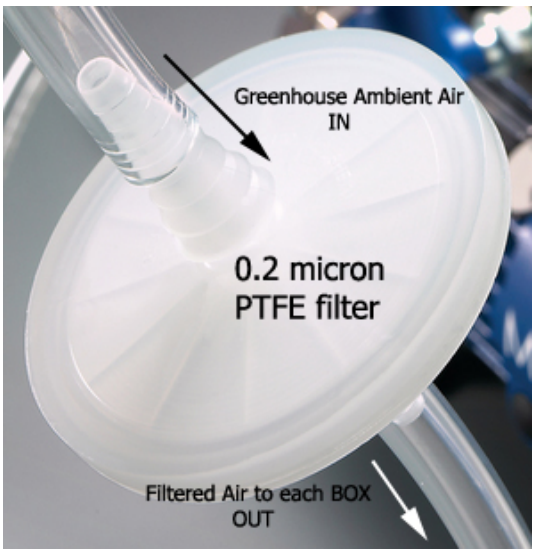

Figure 3.9: PTFE filter, the tubing and the direction of the air flow

cross contamination.

Figure 3.10: Left: Retronic Data Logger main unit, middle: field probe, right: position of the probe in the sampling glass enclosure at Warwick University

3.6.7 Lighting System

An appropriate lighting system for the plant is of important for two reasons: a) lighting is vital for the photosynthesis phenomena which is a process used by plants to convert light energy into chemical energy that can be used to fuel the organisms' activities and b) low or high light intensity stimulates VOC emission in a variety of different ways [25, 29]. Poor lightening has been proven to modify the VOC profiles such as *acetaldehyde* and *(E)-2-hexenal* emitted from plants both qualitatively and quantitatively [30]. In order to minimise the plant stress caused by high or low lighting, a timer was used to automatically switch on the greenhouse lights. The blinding curtains installed in the greenhouse was also centrally controlled. In addition to sunlight the supplementary light of 140 $molm^{-2s-1}$ was employed to provide 16 hours of day light. The light intensity was measured with a LX-105 light meter (REED Instruments, North Carolina, USA).

3.7 Samples

3.7.1 Tomato (Solanum lycopersicum)

Tomato plants (fig. 3.11) where obtained from University of Warwick's glasshouses at the School of life sciences. The plants were 4 weeks old, individually planted and grown in 17 cm pots in the controlled environment within the greenhouse with an ambient day and night temperatures of 20°c and 18°c respectively. All three plants were initially in healthy state with no stress or diseases. The plants were approximately 25cm tall at the start of the experiments and no

pesticides had been applied to them.

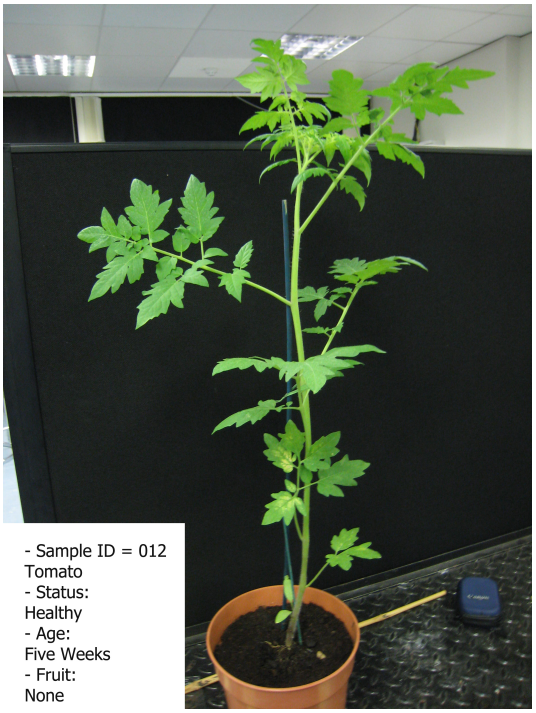

Figure 3.11: A sample of healthy (control) tomato plant at the University of Warwick

3.7.2 Powdery Mildew and Spider Mites

Powdery mildew fungal (Fig. 3.12) spores and spider mites were also provided by School of life sciences and were introduced to the target plants in a controlled fashion.

3.8 Inoculation Procedures

The inoculation procedures included culturing the spores and rubbing them to the surface of leaves at different parts of the plant. The spider mites were placed on the stem and leaves of the plant manually.

Figure 3.12: A tomato leaf covered with powdery mildew spores obtained from the University of Warwick

3.9 Visual Observation of Infection Symptoms

In regards to powdery mildew, in both experiments, approximately 24 hours after inoculation the first symptoms appeared which were in the form of small necrotic spots on some of the leaves. These spots remained small and restricted for the first five days after inoculation indicating a mild infection. In the later days, the lesions expanded rapidly, resulting in large unrestricted infected regions on leaves and stems indicating a severe infection. Spider mites were initially placed at different parts of the plant (i.e. leaves and stems). Approximately 48 hours after inoculation the spider mites were still at the initial place. In the later days, the spiders visibly moved around the plant

and were mostly located underneath the leaves. Small spider webs and white speckling were visible around the plant when it was severely infested by the spider mites.

3.10 Sampling Procedure

Prior to sampling, the air inflow was switched off for 3 hours to allow volatile concentration around the plants to build up. The EN device was switched on for one hour prior to taking readings to warm up/initialise the sensor arrays.

A solution of butan-2-ol (2% in distilled water) was used as a reference sample and also acted as a sensor wash to regenerate sensor surfaces. Figure 3.13 illustrates the procedure needed to wash the sensors.

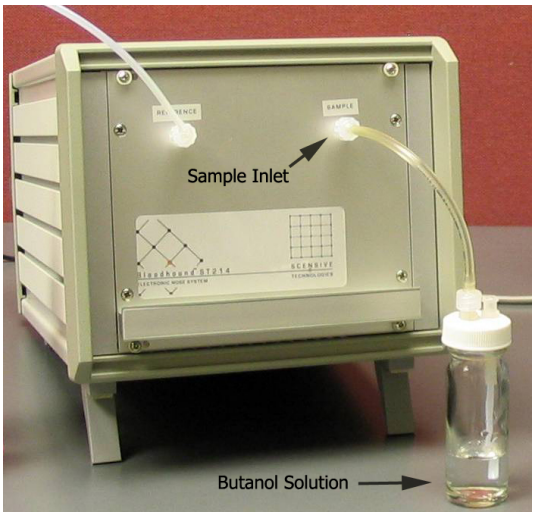

Figure 3.13: The procedure for EN's sensor regeneration with Butan-2-ol

Throughout the experiment, all the physical factors such as humidity and temperature remained constant. The doors of the glass enclosures were closed mostly to avoid cross contamination. The light system was precisely controlled by a timer to make sure that the plants had 16 hours of artificial daylight. Each plant was watered daily. The following table shows the tasks conducted sequentially for a single data acquisition.

Log ID	Time	Task
033	10:50	Air Pumps Switched OFF
034	14:05	Electronic Nose Switched on - Warm UP
035	14:05	FAIMS Switched on - Initiation
036	15:10	Electronic Nose - Start Sampling - Glass enclosure 1
037	15:15	FAIMS - Start Sampling - Glass enclosure 1
038	15:50	Electronic Nose - Start Sampling - Glass enclosure 2
039	15:45	FAIMS - Start Sampling - Glass enclosure 2
040	16:30	Electronic Nose - Start Sampling - Glass enclosure 3
041	16:15	FAIMS - Start Sampling - Glass enclosure 3
042	16:00	Air Pumps Switched ON

Table 3.1: Sequential tasks conducted on a single day

3.11 Data Acquisition

3.11.1 EN

During the experiment, the EN continuously recorded the responses from its array of 13 conducting polymer sensors and the data were saved as a data matrix for later processing. The following acquisition profile of the data was used for VOC analysis by the EN: 7 second absorption, 10 seconds pause, 20 second desorption and 5 second flush. The EN device was capable of sampling 10 replicas at each run. Each plant was sampled twice and therefore 20 replicas were taken from each plant (i.e. healthy and infected) on a daily basis. The

in-depth details of EN generated data files, structure, pre-processing and the analysis will be given in chapter four.

3.11.2 FAIMS

Since the FAIMS device used in this study is self-contained and do include a built-in PC, a pump, flow meter, humidity and temperature sensors, the data gathered was directly saved on the device and was later transfered for analysis. Following images (3.14) shows the FAIMS device on a trolley ready for sampling the VOC profiles.

Figure 3.14: Left: FAIMS device on a sampling bench with an external pump, right: FAIMS on sampling bench with built-in FAIMS

The full explanation of FAIMS data structure and data analysis will be presented in chapter five. The experiment were conducted at three different stages and each of which took 30, 33 and 15 consequent days respectively.

3.12 Summary

In this chapter the fundamentals of VOC sampling experimental design and setup conducted by the author was presented. The methodology, instrumentation, procedures and tasks were clearly outlined. In the next chapter the analysis of plants VOC using Electronic nose is presented.

3.13 References

1. Jrgens, A., A comparative investigation of floral scent in angiosperms in relation to phylogeny and pollination biology. South African Journal of Botany, 2013. 86(0): p. 170.

2. Laffineur, Q., et al., Impact of diffuse light on isoprene and monoterpene emissions from a mixed temperate forest. Atmospheric Environment, 2013. 74(0): p. 385-392.

3. Bchel, K., et al., How plants give early herbivore alert: Volatile terpenoids attract parasitoids to egg-infested elms. Basic and Applied Ecology, 2011. 12(5): p. 403-412.

4. Demeestere, K., et al., Sample preparation for the analysis of volatile organic compounds in air and water matrices. Journal of Chromatography A, 2007. 1153(12): p. 130-144.

5. Gardner, J.W., Detection of vapours and odours from a multisensor array using pattern recognition Part 1. Principal component and cluster analysis. Sensors and Actuators B: Chemical, 1991. 4(1): p. 109-115.

6. Hines, E., J. Gardner, and C. Potter, Olfactory feature maps from an electronic nose. Measurement and Control, 1997. 30(9): p. 262-8.

7. Borah, S., et al., Neural network based electronic nose for classification of tea aroma. Sensing and instrumentation for food quality and safety, 2008. 2(1): p. 7-14.

8. Ampuero, S. and J. Bosset, The electronic nose applied to dairy products: a review. Sensors and Actuators B: Chemical, 2003. 94(1): p. 1-12.

9. Peris, M. and L. Escuder-Gilabert, A 21st century technique for food control: Electronic noses. Analytica Chimica Acta, 2009. 638(1): p. 1-15.

10. Dutta, R., et al., Identification of Staphylococcus aureus infections in hospital environment: electronic nose based approach. Sensors and Actuators B: Chemical, 2005. 109(2): p. 355-362.

11. Sohn, J.H., et al., Implementation of an electronic nose for continuous odour monitoring in a poultry shed. Sensors and Actuators B: Chemical, 2008. 133(1): p. 60-69.

12. Kalman, E.-L., et al., Classification of complex gas mixtures from automotive leather using an electronic nose. Analytica Chimica Acta, 2000. 403(1): p. 31-38.

13. Sobaski, T., et al., Electronic nose applied to automotive fuel qualification. Sensors and Actuators B: Chemical, 2006. 116(1): p. 207-212.

14. Buryakov, I., et al., A new method of separation of multi-atomic ions by mobility at atmospheric pressure using a high-frequency amplitude-asymmetric strong electric field. International journal of mass spectrometry and ion processes, 1993. 128(3): p. 143-148.

15. Kolakowski, B.M. and Z. Mester, Review of applications of high-field asymmetric waveform ion mobility spectrometry (FAIMS) and differential mobility spectrometry (DMS). Analyst, 2007. 132(9): p. 842-864.

16. Wu, L. and F.G. Vogt, A review of recent advances in mass spectrometric methods for gas-phase chiral analysis of pharmaceutical and biological compounds. Journal of pharmaceutical and biomedical analysis, 2012.

17. De Boer, J.G., M.A. Posthumus, and M. Dicke, Identification of volatiles that are used in discrimination between plants infested with prey or nonprey herbivores by a predatory mite. Journal of Chemical Ecology, 2004. 30(11): p. 2215-2230.

18. Mumm, R., et al., Chemical analysis of volatiles emitted by Pinus svlvestris after induction by insect oviposition. J Chem Ecol, 2003. 29(5): p. 1235-52.

19. Choh, Y., et al., Exposure of lima bean leaves to volatiles from herbivore-induced conspecific plants results in emission of carnivore attractants: active or passive process? J Chem Ecol, 2004. 30(7): p. 1305-17.

20. Schmelz, E.A., H.T. Alborn, and J.H. Tumlinson, The influence of intact-plant and excised-leaf bioassay designs on volicitin-and jasmonic acid-induced sesquiterpene volatile release in Zea mays. Planta, 2001. 214(2): p. 171-179.

21. De Bruxelles, G.L. and M.R. Roberts, Signals regulating multiple responses to wounding and herbivores. Critical Reviews in Plant Sciences, 2001. 20(5): p. 487-521.

22. Tholl, D., et al., Practical approaches to plant volatile analysis. The Plant Journal, 2006. 45(4): p. 540-560.

23. Rohloff, J. and A.M. Bones, Volatile profiling of Arabidopsis thaliana Putative olfactory compounds in plant communication. Phytochemistry, 2005.

66(16): p. 1941-1955.

24. Ebel, R.C., J.P. Mattheis, and D.A. Buchanan, Drought stress of apple trees alters leaf emissions of volatile compounds. Physiologia Plantarum, 1995. 93(4): p. 709-712.

25. Holopainen, J.K. and J. Gershenzon, Multiple stress factors and the emission of plant VOCs. Trends in Plant Science, 2010. 15(3): p. 176-184.

26. Kesselmeier, J. and M. Staudt, Biogenic Volatile Organic Compounds (VOC): An Overview on Emission, Physiology and Ecology. Journal of Atmospheric Chemistry, 1999. 33(1): p. 23-88.

27. Karl, T., et al., Chemical sensing of plant stress at the ecosystem scale. Biogeosciences Discuss., 2008. 5(3): p. 2381-2399.

28. Jensen, M.H. and A.J. Malter, Protected agriculture: a global review. 1995: World Bank Publications.

29. Loreto, F. and J.-P. Schnitzler, Abiotic stresses and induced BVOCs. Trends in Plant Science, 2010. 15(3): p. 154-166.

30. Schuh, G., et al., Emissions of Volatile Organic Compounds from Sunflower and Beech: Dependence on Temperature and Light Intensity. Journal of Atmospheric Chemistry, 1997. 27(3): p. 291-318.

31. Michie, D., D.J. Spiegelhalter, and C.C. Taylor, Machine Learning, Neural and Statistical Classification. 1994: Ellis Horwood.

32. Nemati, H.R. and C.D. Barko, Organizational Data Mining: Leveraging Enterprise Data Resources for Optimal Performance. 2004: Idea Group Pub.

33. Milligan, G.W. and M.C. Cooper, Methodology review: Clustering methods. Applied Psychological Measurement, 1987. 11(4): p. 329-354.

34. Handl, J. and B. Meyer, Improved ant-based clustering and sorting in a document retrieval interface. Parallel Problem Solving from NaturePPSN VII, 2002: p. 913-923.

35. Haralick, R.M. and L.G. Shapiro, Image segmentation techniques. Computer vision, graphics, and image processing, 1985. 29(1): p. 100-132.

36. Wen, J.R., J.Y. Nie, and H.J. Zhang. Clustering user queries of a search engine. 2001. ACM.

37. Jolliffe, I.T., Principal component analysis. Vol. 487. 1986: Springer-Verlag New York.

38. Buljak, V., Inverse Analyses with Model Reduction: Proper Orthogonal Decomposition in Structural Mechanics. 2012: Springer Berlin Heidelberg.

39. Gil-Snchez, L., et al., A novel humid electronic nose combined with an electronic tongue for assessing deterioration of wine. Sensors and Actuators A: Physical, 2011. 171(2): p. 152-158.

40. Dbska, B. and B. Guzowska-wider, Application of artificial neural network in food classification. Analytica chimica acta, 2011. 705(1): p. 283-291.

41. Kostesha, N.V., et al. Development of the colorimetric sensor array for detection of explosives and volatile organic compounds in air. in Proc. SPIE. 2010.

42. Mai, Q., A review of discriminant analysis in high dimensions. Wiley Interdisciplinary Reviews: Computational Statistics, 2013. 5(3): p. 190-197.

43. Feng, T., et al., Analysis of volatile compounds of Mesona Blumes gum/rice extrudates via GCMS and electronic nose. Sensors and Actuators B: Chemical, 2011. 160(1): p. 964-973.

44. Cozzolino, D., et al., Usefulness of chemometrics and mass spectrometry-based electronic nose to classify Australian white wines by their varietal origin. Talanta, 2005. 68(2): p. 382-387.

45. Gmez, A.H., et al., Evaluation of tomato maturity by electronic nose. Computers and electronics in agriculture, 2006. 54(1): p. 44-52.

46. Mehrotra, K., C.K. Mohan, and S. Ranka, Elements of artificial neural networks. 1997: MIT Press.

47. Graupe, D., Principles of artificial neural networks. 2007: World Scientific.

48. Taylor, W.A., What every engineer should know about artificial intelligence. 1988: MIT Press.

49. Shepherd, G.M., The synaptic organization of the brain. 2004: Oxford University Press.

50. Rojas, R., Neural networks: a systematic introduction. 1996: Springer-Verlag.

51. Nelson, M.M.C. and W.T. Illingworth, A practical guide to neural nets. 1994: Addison-Wesley.

52. Raol, J. and S. Mankame, Artificial neural networks. Resonance, 1996. 1(2): p. 47-54.

53. Medsker, L.R. and L.C. Jain, Recurrent neural networks: design and applications. 2000: CRC Press.

54. Soucek, B., Neural and concurrent real-time systems: the sixth generation. 1989: Wiley.

55. Anthony, M. and P.L. Bartlett, Neural Network Learning: Theoretical Foundations. 2009: Cambridge University Press.

56. Hrl, W.H., Replacement of Renal Function by Dialysis. 2004: Kluwer Academic Publishers.

57. Haykin, S.S., Neural networks: a comprehensive foundation. 1999: Prentice Hall.

58. Smith, A.J., Applications of the self-organising map to reinforcement learning. Neural Netw., 2002. 15(8-9): p. 1107-1124.

59. Bishop, C.M., Neural Networks for Pattern Recognition. 1995: Oxford University Press, Incorporated.

60. Lisboa, P.J.G. and M.J. Taylor, Techniques and applications of neural networks. 1993: E. Horwood.

61. Hastie, T., R. Tibshirani, and J.J.H. Friedman, The elements of statistical learning. Vol. 1. 2001: Springer New York.

62. Kotsiantis, S.B., I.D. Zaharakis, and P.E. Pintelas, Machine learning: a review of classification and combining techniques. Artificial Intelligence Review, 2006. 26(3): p. 159-190.

63. Webb, A.R., Statistical pattern recognition. 2003: Wiley.

64. Platt, J.C., 12 Fast Training of Support Vector Machines using Sequential Minimal Optimization. 1999.

65. Keerthi, S.S. and E.G. Gilbert, Convergence of a generalized SMO algorithm for SVM classifier design. Machine Learning, 2002. 46(1-3): p. 351-360.

66. Weston, J. and C. Watkins, Multi-class support vector machines, 1998, Citeseer.

67. Kordon, A., Applying Computational Intelligence: How to Create Value. 2010: Springer Berlin Heidelberg.

68. Byvatov, E. and G. Schneider, Support vector machine applications in bioinformatics. Appl Bioinformatics, 2003. 2(2): p. 67-77.

69. Baccarini, L.M.R., et al., SVM practical industrial application for mechanical faults diagnostic. Expert Systems with Applications, 2011. 38(6): p. 6980-6984.

70. Kim, S.-K., et al., SVM-based feature extraction for face recognition. Pattern Recognition, 2010. 43(8): p. 2871-2881.

71. Brudzewski, K., S. Osowski, and T. Markiewicz, Classification of milk by means of an electronic nose and SVM neural network. Sensors and Actuators B: Chemical, 2004. 98(2): p. 291-298.

72. El Barbri, N., et al., Electronic nose based on metal oxide semiconductor sensors as an alternative technique for the spoilage classification of red meat. Sensors, 2008. 8(1): p. 142-156.

73. Thaler, E.R. and C.W. Hanson, Use of an electronic nose to diagnose bacterial sinusitis. American journal of rhinology, 2006. 20(2): p. 170-172.

Chapter 4

Non-destructive Plant VOC analysis using Electronic Nose

4.1 Chapter Overview

This chapter is concerned with the analysis of data acquired from sensor arrays, particularly Electronic Noses (EN). The unique experimental methodology described in the previous chapter was constructed in which the VOCs released by tomato plants were sampled by EN.

Data collected by EN from two distinct experiments are analysed using clustering and classification methods in order to detect infected samples. The chapter closes by evaluating and discussing the results in detail.

4.2 Introduction

Disease-induced VOCs in plants presents a number of characteristics. For instance, the time course of disease-induced VOC emission has been of interest [1] as the emission of various VOCs may rise rapidly after the onset of disease followed by a rapid decrease, whereas the increased emission of other substances may be delayed for a while after the start of the disease. Although the time period between the VOC inductions may be indicative of the disease it is unlikely that plant disease can be identified solely based on the time course of disease-induced VOC emission [2].

Emissions of chemical substances including *ethylene*, *hexenol*, *methyl salicylate*, *ocimene*, *linalool*, *farnesene* and *trimethyl-tridecatetraene* are frequently reported [3, 4] to be changed when a plant is stressed, independent of plant species and disease type. For example, release of ethylene significantly regulates environmentally and developmentally induced processes including stress resistance, germination, ripening, senescence and abscission [5]. Ethylene production is also induced by mechanical wounding, environmental stresses and interaction with various micro-organisms [6]. However, such generic substances are not sufficiently exclusive to characterise a specific disease.

In tomato *(Solanum lycopersicum)* plants, different parts release a set of VOCs including *Benzaldehyde*, *Limonene*, *2-Isobutylthiazole*, *2-Phenylethanol* and *Phenylacetaldehyde* [7]. Fresh tomato fruit itself has been shown to produce compounds including *hexanal*, *methylbutanols*, *heptenal* and *methyl* [8]. For the purpose of this study, it is necessary to identify the compounds that rep-

resent a degree of exclusivity when a tomato plant is infected with powdery mildew *(Oidium neolycopersici)* and infested with spider mite *(Tetranychus urticae Koch)*.

The compounds that are specific to the infection caused by powdery mildew in tomato plants have been quantified by GC-MS analysis and reported in several studies [9]. They include *(Z)-3-heptenol, butanolmethylacetate*, *1-6-anhydro-β-D-glucopyranose*, *1-fluorododecane*, *α-humulene*, *β-phellandrene*, *y-terpiene*, *β-pinene* and *α-caryophyllene*.

When VOCs emitted by spider mite infested plants of 11 species were compared, it was evident that almost all of the investigated plant species produced compounds that dominated the volatile blend [10]. Moreover, infestation-induced release of *3,7,11-tridecatetraene*, *(E, E)-4,8,12-trimethyl-1* and *(E)-β-ocimene* attract the carnivorous mite *(Phytoseiulus persimilis)*, a specialist predator of the spider mites that exterminates entire prey populations contributing indirectly to plant defence [11]. The wound-induced release of methanol increases dramatically [12, 13] when larvae attack plants. VOC emission rates of *β-myrcene*, *α-pinene*, *carene* and *phellandrene* are increased several-fold relative to un-attacked plants [9, 12-14]. Emission of *cis-3-hexen-1-ol*, *linalool*, and *cis-α-bergamotene* is proven to reduce the number of herbivores by more than 90% [4]. These VOCs are among the ones that are targeted to be traced and identified by EN which will enable differentiation between healthy and infested plants. Some of the exclusive compounds released by tomato plants when attached by spider mites are *7-bromo-heptanoicacid*, *1-bromobicyclo-decan-8-one*, *bicyclo-octane*, *δ-3-carene*, *β-ocimene*, *decane*, *12-*

trimethyl, *11-tridecatetraene* and *α-farnesene* [9].

The above compounds are chemically verified to be detectable by the array of conducting polymer gas sensors (EN) in other applications previously [9, 15-22].

4.3 EN Sensors

EN sensitivity and detection performance is directly correlated to the type and number of sensors built into them. Different types of EN sensors are as follow.

Optical sensors are based on changes in fluorescence, wavelength absorption or reflection. The light source of these sensors excites volatile molecules, generating a signal that can be measured via absorbance, reflectance, fluorescence or refractive index [23]. Such output signals are detected using various detectors, including CMOS cameras [24].

Thermal sensors in ENs act as pellistor sensors which measure temperature changes specific for combustible gases like methane. Thermal detection is based on a key assumption that the gas needs to be oxidised or thermally decomposed by which heat will be produced and measured. They are manufactured using platinum and palladium coupled with a heater to maintain the sensors operating temperature [25].

Chemiresistive sensors are consisted of metal oxide semiconducting sensors (MOS) and conducting polymer sensors (CP) and are most suited for large

volume low cost applications because of their small size combined with their high sensitivity and selectivity, and easy manufacturability [26].

MOS sensors consist of a heating coil within a ceramic cylinder. The outer side is coated with metal oxides such as Tindioxide (SnO_2), Titanium dioxide (TiO_2), Indium dioxide (In_2O_3), Tungsten trioxide (WO_3) or Nickel oxide (NiO). The semiconducting material is covered with traces of different metals like Platinum (Pt), Gold (Au) or Palladium (Pd).

In common with metal oxide semiconductors, the response of CP sensors is expressed as a change of conductivity because of the adsorption of volatile compounds to a sensitive layer. These polymers are typically made of Pyrrole (C_4H_5N), Aniline ($C_6H_5NH_2$) or other semi-conducting materials. CP sensor arrays consist of unique polymers with different reversible physicochemical properties and sensitivity to groups of volatile compounds. These compounds interact with and attach to the polymer surface, changing the resistance under ambient temperature conditions. This, in turn, changes the signal, which is monitored for each sensor type, enabling an array to be constructed that has overlapping detection ranges for different groups of volatile compounds [23]. Other advantages of conductive polymers include wide selectivity, high sensitivity and operation at ambient temperatures. Additional types of EN sensors includes Metal Oxide Field Effect Transistors sensors [27], Amperometric sensors [28] and Gravimetric sensor [29] systems.

4.4 EN Sampling

The sensors in the ST214 EN device used for this experiment are housed within a PTFE sample chamber, into which sample headspace is drawn with a rate of 200 $mlmin^{-1}$. The following tasks were conducted during sampling: **a)** Baseline: A sample reading is initiated and then the instrument records the baseline resistance of the sensors for 5 second, before the sample headspace is pumped into the chamber, **b)** Absorption: During exposure to a gaseous sample the composite resistances of the sensor materials change. These changes are brought about by the interaction of VOCs with the active surface of each sensor, **c)** Pause: during which the flow of sample over the sensors ceases and **d)** Desorption: cleaned external air is again passed over the sensors and the composite resistance returns to the baseline values as the volatiles leave the sensor surface.

The sample acquisition settings are required to be properly set based on type and quality of headspace. During the experiments conducted in this study, it was heuristically identified that better results are obtained using longer absorption settings.

The following acquisition profile of the data was used in this experiment: 30 second absorption, 5 seconds pause, 20 second desorption and 5 second flush. The EN device was capable of sampling 10 replicas at each run. Each plant was sampled twice and therefore 20 replicas were taken from each plant (healthy and infected) on a daily basis.

4.5 EN's Data Structure

Figure 4.1 is the response of the EN sensors when sampling the tomato plant. The data are the representation of the raw reading from the 13 CP sensors built into the EN device. The shape of a sensor response curve is determined by the lengths of the absorption, pause, and desorption phases of the sample routine. As shown, each single sensor may react differently from the others and some may not react at all.

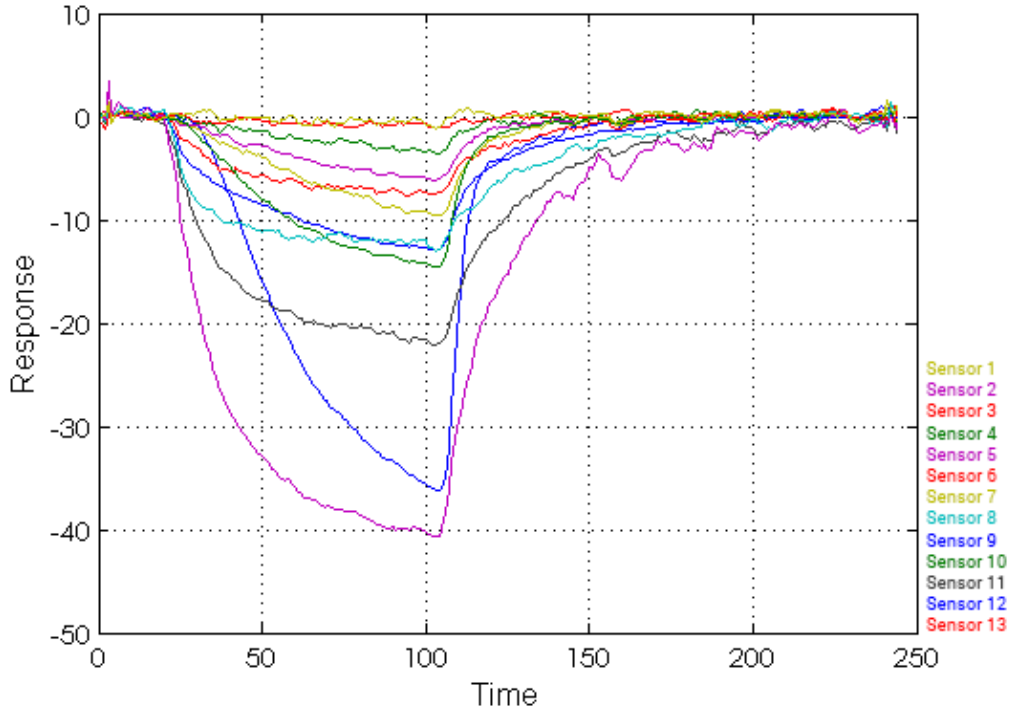

Figure 4.1: Typical EN response (raw data) acquired from a tomato plant. Each line representing a single sensor.

Since ENs sensors are highly sensitive to humidity and are required to be replaced frequently, it is common that one or multiple sensors produce in-

correct observations. As discussed in the previous chapter, the humidity and temperature levels were constantly controlled and logged to ensure consistency. The temperature levels were observed to be $20°c - 24°c$ and the humidity was maintained between $40\% - 50\%$.

The dataset generated from the experiment, contained four specific and crucial days within the infection process which were 4 Day Post Infection (DPI), 6 DPI, 8 DPI and 9 DPI. Four parameters were calculated and extracted from the raw dataset: **A)** Divergence: maximum step response **B)** Absorption: maximum rate of change of resistance, **C)** Desorption: maximum negative rate of change of resistance and **D)** Area: area under the curve (Fig. 4.2). These values later formed the preliminary dataset.

The very first stage of data analysis was to investigate the differences in the sensor responses produced by EN. Figure 4.3 compares the mean (normalised) divergence response of healthy and infected samples of 4 DPI. It is evident that there is difference in response between healthy and infected samples.

4.6 Data Analysis

In this section the statistical and Intelligent Systems (IS) techniques used for analysing the data generated by the gas sensors will be presented. Clustering and classification techniques are both employed in this study for analysing the experimental datasets. Classification in the context of data mining may refer to two tasks: **a)** to establish the existence of classes or group within a set of observations and **b)** to establish a rule whereby a new and unseen ob-

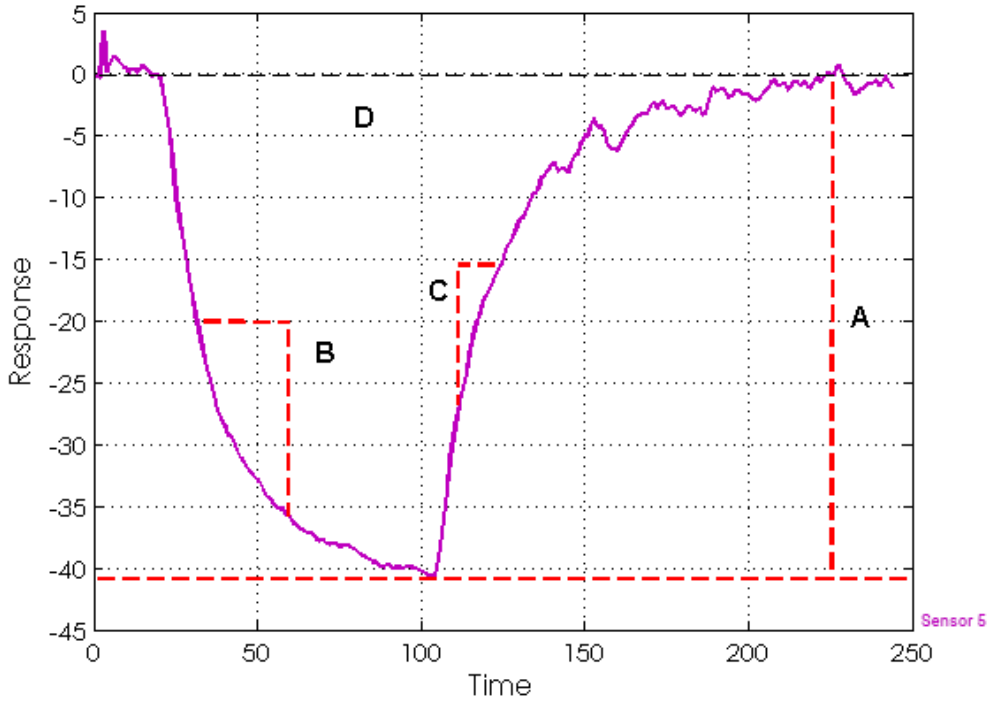

Figure 4.2: Parameters extracted from the raw data, a: Divergence (maximum step response - positive or negative) - b: Absorption (maximum positive rate of change) - c: Desorption (maximum negative rate of change) d: Area under the curve.

servation could be classified into one of the existing classes [30]. The process involves the mapping of values into classes using a function which provides a class representation of past trends enabling predication based on classification dependencies [31].

Clustering is concerned with the grouping of a given collection of unlabelled patterns into meaningful clusters. Milligan [32] established a seven-step structure to organise the clustering process. **a)** entity selection which is commonly done by choosing a sample population, **b)** variable selection which consists of selecting the variables containing sufficient information to permit the clus-

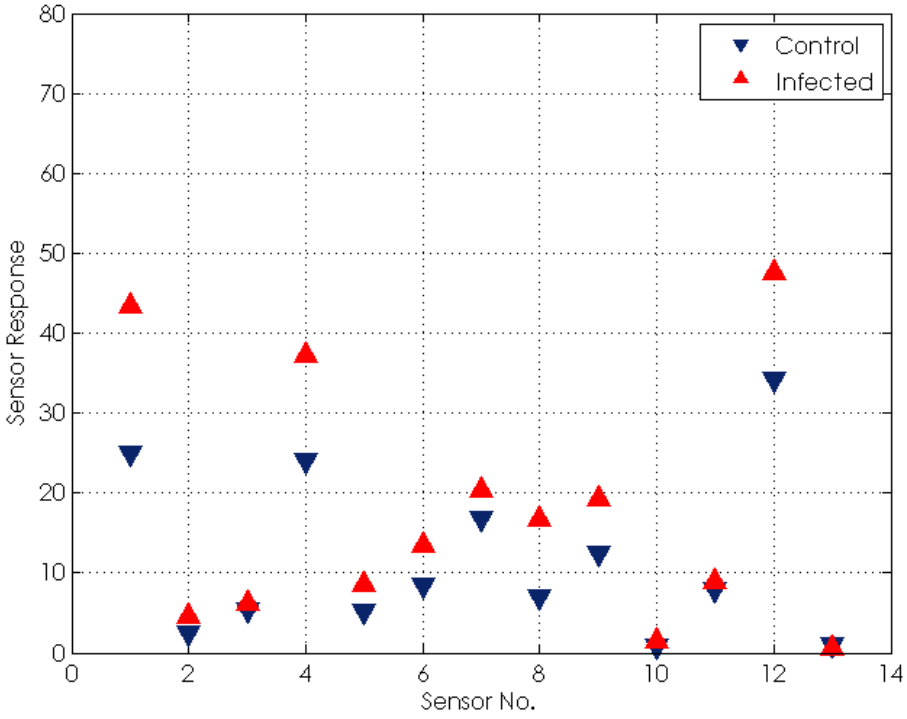

Figure 4.3: Mean divergence of control and infected samples on 4 DPI

tering of the objects, **c)** standardisation if required, this step also includes normalisation, **d)** selection of similarity or dissimilarity measure which indicates the degree of closeness or separation between objects,**e)** selection of clustering method, **f)** selection of number of clusters and **g)** interpretation, assessment and replication of the results. The above steps are highly dependent on the application at hand and may need to be modified by the domain expert. Clustering is beneficial in several exploratory data mining situations, including data document retrieval [33], image segmentation [34], and search engine optimisation [35].

4.6.1 Principal Component Analysis (PCA)

The central idea of Principal Component Analysis (PCA) is to reduce the dimensionality of a data set consisting of a large number of variables, while attempting to retain as much as possible of the variation present in the dataset [36]. PCA is obtained from the eigenvectors of the covariance matrix and gives directions in which the data have maximal variance [37]. PCA has a further use in data visualisation, namely to give a two dimensional representation of the observations by selecting the 2 eigenvectors with the largest eigenvalues. Such a two-dimensional representation can give a visual means of either detecting or verifying the existence of clusters provided that most of the variation falls in the two-dimensional subspace defined by the first two PCs.

PCA has been shown to be effective for processing the response of an EN and is extensively used in almost all studies employing EN [38, 39]. Borah et al.[40] used PCA to visualise the different categories of tea aroma profiles. Ampuero et al. [41] grouped UHT milk aged 18 days, and 13 days of pasteurised milk using PCA performed on EN generated data. Kalman et al. [42] investigated complex gas mixtures from automotive leather using an EN and PCA. In a similar study, PCA and EN were coupled to assess the automotive fuel qualification [43]. Finally, Peris et al. [44] reviewed several studies in which PCA was employed to analyse the EN generated datasets.

Here, PCA was applied to 4 datasets each representing 4, 6, 8 and 9 DPIs during the first experimental period. Each dataset contained 60 samples and 26 variables (Area under curve and Divergence of 13 sensor responses) and was

normalised. Figure 4.4 – 4.7 shows the plot of PC_1 and PC_2 of the 4 different DPIs. On 6 and 8 DPI, the cluster group representing powdery mildew infected and healthy plants are separated significantly. The first two PCs accounted for 86%, 95%, 98% and 97% of the variance, in 4, 6, 8 and 9 DPIs respectively. The image of the plant infected with powdery mildew is also provided indicating the health status of the plant on each DPI. Three main clusters (healthy, powdery mildew-infected and spider mites-infested) are visible.

It is evident that the health of the infected plant is degraded as the 9 DPI was approached on which most parts of the plant is severely covered by the powdery mildew white spores potentially increasing the emission of *(Z)-3-heptenol, butanolmethylacetate*, *1-6-anhydro-β-D-glucopyranose*, *1-fluorododecane* and *α-humulene*. At this point it is highly unlikely for growers to be able to save the plant without the use of chemicals. Since powdery mildews only colonise the upper layer of cells, chemical eradication is possible.

PCA analysis is important from both biological and data analysis perspective as it **a)** is a perfect foundation for investigating how the pattern of plants health status changes in respect to DPIs and **b)** signifies whether the limited number of projected variables in the dataset carries a significant amount of variations. The PCA analysis revealed that PC_1 and PC_2 are able to sufficiently represent the valuable information (overall variance) in order to discriminate between healthy and infected plants.

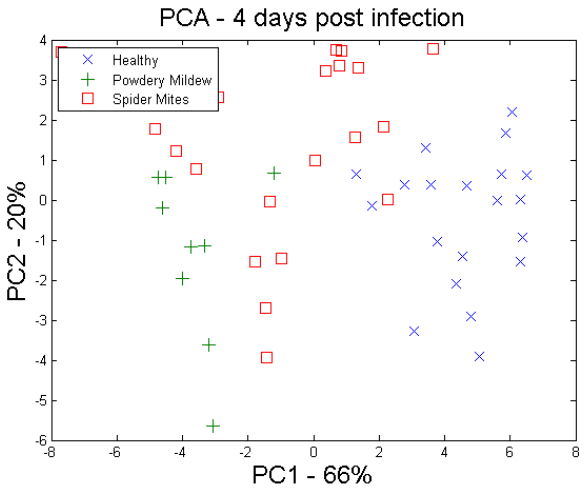

(a) (b)

Figure 4.4: 4 DPI - a) Plant's visual status - b) PCA projection

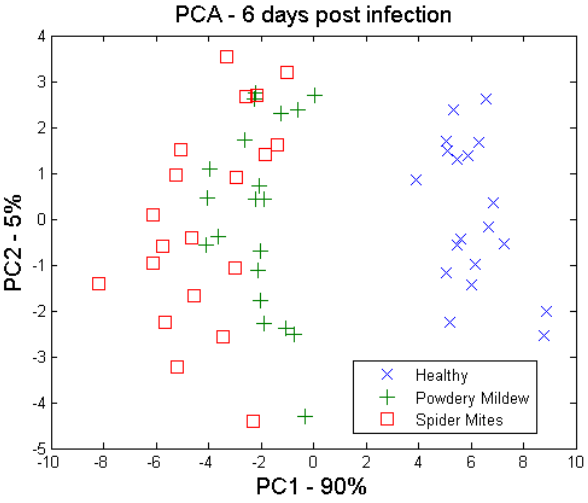

(a) (b)

Figure 4.5: 6 DPI - a) Plant's visual status - b) PCA projection

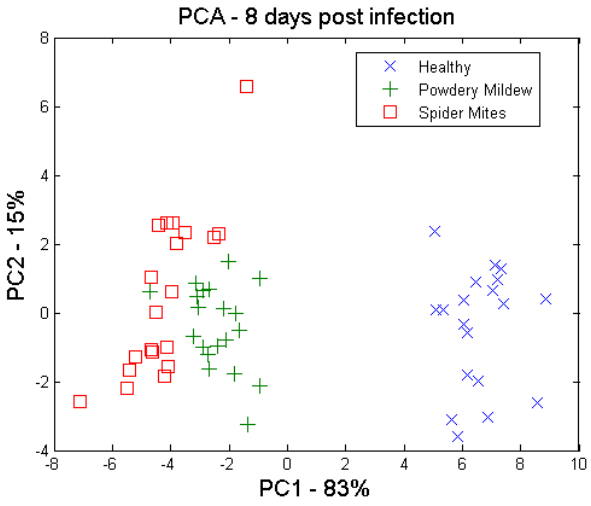

(a) (b)

Figure 4.6: 8 DPI - a) Plant's visual status - b) PCA projection

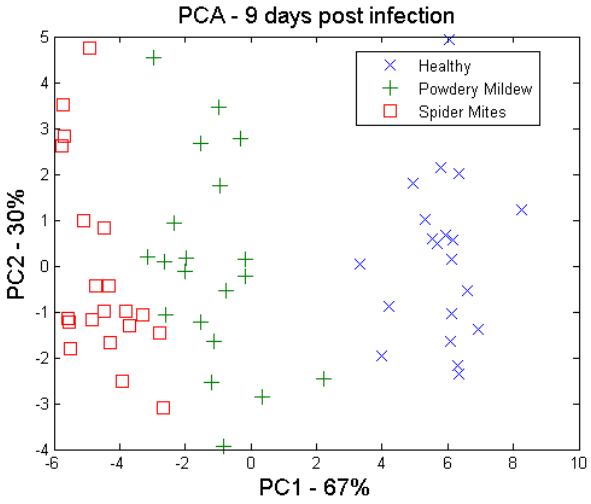

(a) (b)

Figure 4.7: 9 DPI - a) Plant's visual status - b) PCA projection

4.6.2 K-Means

K-means clustering is a method for finding clusters and cluster centres in a set of unlabelled data. One chooses the desired number of cluster centres, the k-means procedure iteratively moves the centres to minimise the total

within cluster variance. Given an initial set of centres, the k-means algorithm alternates the two steps:

- For each centre, k-means identify the subset of training points (its clusters) that is closer to it than any other centre.
- The means of each feature for the data points in each cluster are computed, and this mean vector becomes the new centre for that cluster.

These two steps are iterated until convergence. Typically the initial centres are randomly chosen observations from the training data. K-means clustering has been widely used for clustering the EN generated datasets and subsequent categorisation of different VOC profiles [45, 46] including explosives [47].

The four datasets from the first experiment were subjected to the k-means technique so the differences between clusters could be investigated based on each DPI. The set of observations which is the entire population of our samples (60 samples) is plotted on a 3D plane. K-means managed to find three categories especially in the 6 DPI dataset allocated to the healthy, powdery mildew and spider mite infected plants. The centroids 1, 2 and 3 of K clusters are also visible in the graph and are separated favourably (Figure 4.8).

K-means algorithm require the number of clusters, k, to be specified in advance, which is considered to be a drawback of such algorithms. Here, the k value is constant an equal to 3 since it was known that this was the expected number of clusters. Figure 4.9, investigates the changes in cluster patterns and their member data points when k value is increased. The silhouette plot shows that when k is 3, most points in all three clusters have a large silhouette

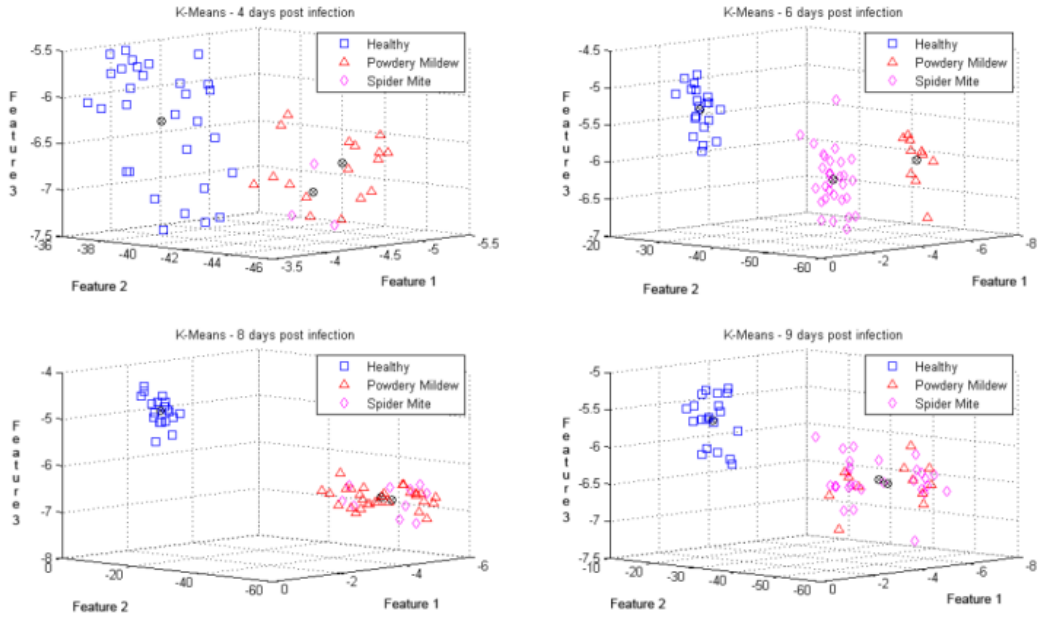

Figure 4.8: K-means clustering showing projections on 4, 6, 8 and 9 DPIs

value, greater than 0.6, indicating that the clusters are rather separated from neighbouring clusters. However, when k is increased, clusters contain many points with low silhouette values, indicating that those clusters are not well separated. When $k = 5$, there are few points with negative silhouette values

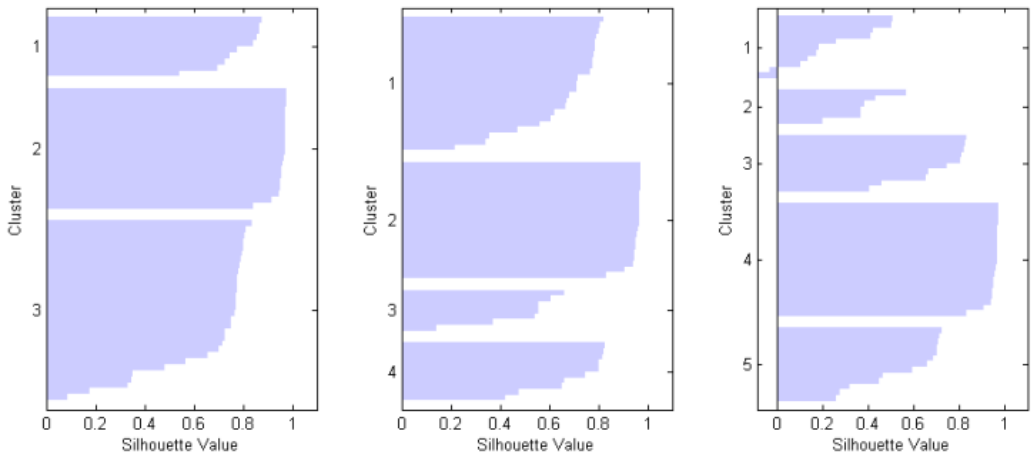

Figure 4.9: Silhouette plot with k = 3, k = 4 and k = 5

indicating that they are most probably classified incorrectly. The average silhouette values for the three cases are 0.7784, 0.7417, and 0.6322 respectively. Evidently, as k increases the silhouette value decreases indicating that the optimal value for k is three which is the expected value.

4.6.3 Linear Discriminant Analysis

Linear discriminant analysis (LDA) is commonly [41, 44] used to separate classes of objects or assign new objects to appropriate classes (both bi-class and multi-class problems). The discriminants are the combinations of the measured variable in this case, ENs sensor responses [72]. Discriminant functions are calculated with the objective of maximising the distance between classes relative to the variation within classes. LDA arises in the special case when it is assumed that the classes have a common covariance matrix.

Using LDA with cross validation, classification accuracy of 80%, 91%, 90% and 85% on 4 DPI, 6 DPI, 8 DPI and 9 DPI datasets was achieved respectively. The procedure was conducted in Matlab using the PRtools data analysis package. Figure 4.10 demonstrates the performance of LDA on 6 DPI dataset. It is evident that LDA applied to dataset with 60 samples (20 healthy, 20 PM and 20 SM) gave an average discrimination percentage of 86% ($p < 0.05$), while only few samples were not correctly classified in the validation procedure.

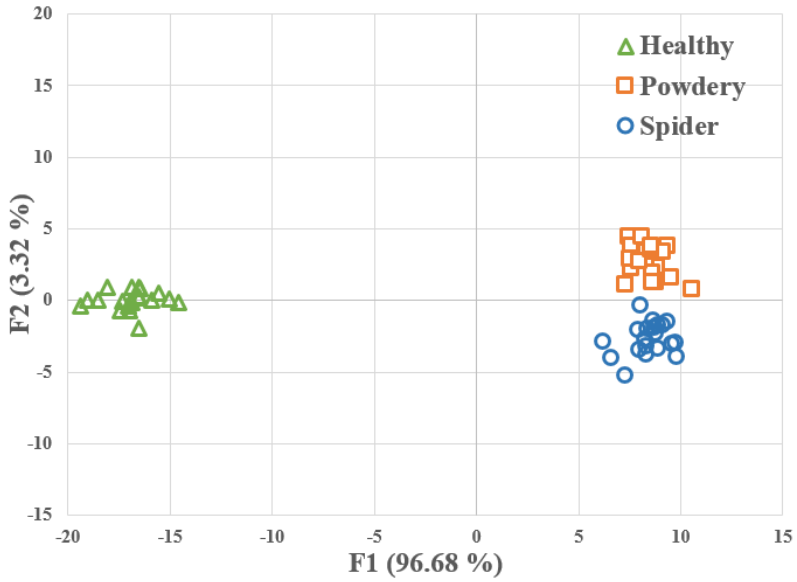

Figure 4.10: LDA result of 6 DPI with discriminant function 1 and discriminant function 2

4.7 Second Set of Experiments

The first set of experiment was conducted and the preliminary results from PCA, k-Means and LDA indicated that EN was capable of discriminating between healthy and infected plants between 4-9 DPI. In order to replicate the results and verify the initial findings, a second set of experiments was conducted 8 months after the first experiments. Extra care was taken to make sure that environmental factors, devices and instruments as well as experimental procedures were remained identical. The exact EN device, data loggers, tubing and glass enclosures (described in chapter 3) were employed in the second set of experiments. The glass champers, entire PTFE tubing system and apparatus were thoroughly cleaned and disinfected using a 5% alcohol solution. Six fresh, healthy, hand-planted, 4 weeks old tomato plants were acquired from glasshouses in the University of Warwick and used for the second

set of experiments. The repeated experiment took 33 consecutive days and were conducted by the author at HRI, School of life sciences, University of Warwick. The data generated by the EN device was identical to the one described in section 4.6. In this section, Artificial Neural Networks and Support Vector Machines were used to analyse the sensory dataset generated by EN.

4.7.1 Feed-Forward Neural Networks

Artificial Neural Networks (ANNs) refer to both computer software and hardware systems whose methodology is derived from the analogy of biological Neural Networks found in human brain and the simulation of the nerve cell (neurons) network [48]. The feed-forward neural network (FFNN) is considered as the most widely used ANN technique for the analysis of data from sensor arrays (i.e. ENs) [40, 43, 44]. These networks are a member of a larger group of ANNs known as MLPs (multilayer perceptrons) which is often accompanied by the back-propagation algorithm (method of optimising the network weights). Generally, the FFNN network includes the following components: an input layer, a hidden layer, and an output layer. For sensor arrays, the number of neurons in the input layer is frequently reported [72] to be equal to the number of sensors in the array, or the optimal number of sensors in the array. Each input is injected to the hidden layer along with a weight (the weights could initially set to have a constant value or be randomised). The number of neurons in the output layer is often dictated by the application at hand. Finally, cross-validation is used to avoid over-training of the FFNN. This occurs when the network memorises the features of the training data and loses its ability to generalise [50]. The network training may be stopped in

one of the following conditions: a) the maximum number of epochs is reached, b) The maximum amount of time is exceeded, c) performance is minimised to the goal, d) the performance gradient falls below minimum gradient value and e) validation performance has increased more than maximum times since the last time it decreased.

The first stage in EN data classification was to design and train an FFNN using the datasets acquired from the second experiment. The EN data from sensor responses (13 divergence features) were used to train the ANN for the purpose of comparing and identifying the correct class to which each sample belongs. A FFNN with back-propagation was employed to classify the datasets. The ratio of training, testing and validation data was set as 70%, 15% and 15% respectively. The dataset contained 60 samples (20 healthy samples, 20 powdery mildew-infected samples and 20 spider mite-infested samples). The maximum number of epochs was set to 1500. The learning rate was initialised at 0.2. Through trial and error, the FFNN design and parameters were chosen in a format which guaranteed the high classification performance through cross validation. Figure 4.11 demonstrates the training and validation MSE for the 6 DPI dataset.

The classification was conducted using the neural network toolbox in Matlab. The overall time of training was 42 seconds. This times was based on the calculation conducted on an 8 Core Xenon PC with 24 GB of RAM. A value of $p < 0.052$ was calculated which is considered statistically significant and therefore rejects the suggestion that the classification accuracy reported have arisen by chance. The MSE falls within the range of 9.23 and 14.77 with 95%

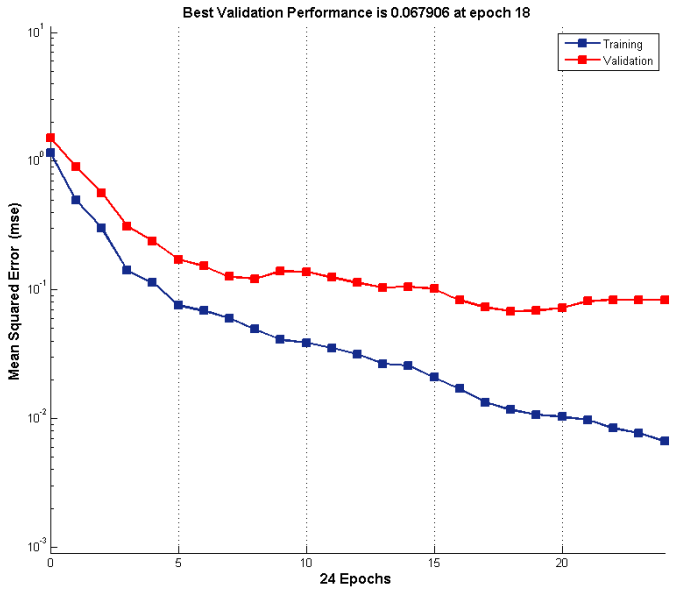

Figure 4.11: ANN's training and validation error

CI (Confidence Interval). The average classification accuracy of 87%, 90%, 92% and 91% was achieved when FFNN with BP was applied on 4 DPI, 6 DPI, 8 DPI and 9 DPI respectively (Fig. 4.12).

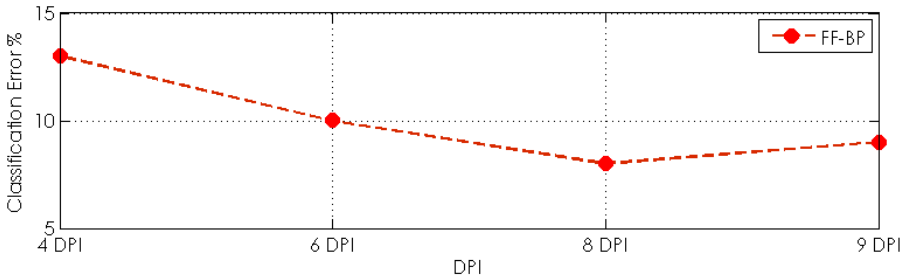

Figure 4.12: FFNN with BP, classification performance on 4, 6, 8 and 9 DPI

4.7.2 Generalisation

The goal of network training is not to learn an exact representation of the training data itself, but rather build a statistical model of the process which

generates the data. This is important if the network is to exhibit good generalisation, that is, to make good predictions for new inputs [51]. This highlights the need to optimise the complexity of the model in order to achieve the best possible generalisation. Considerable insight into this phenomenon can be obtained by introducing the concept of the bias-variance trade-off, in which the generalisation error is decomposed into the sum of the bias squared plus the variance [51]. A model which is too simple, or too inflexible, will have a large bias, while one which has too much flexibility in relation to the particular data set will have a large variance. Bias and variance are complementary quantities, and the best generalisation is obtained when one have the best compromise between the conflicting requirements of small bias and small variance. In order to find the optimum balance between bias and variance one need to have a way of controlling the effective complexity of the model. In the case of ANNs, the complexity can be varied by changing the number of adaptive/free parameters in the network. One way to implement this in practice is to compare a range of models having different numbers of hidden units. Alternatively, one can start with a relatively large network and prune out the least significant connections. Similarly, it is possible to start with a small network, and add units with the goal of arriving at an optimal network structure. Concepts such as cross-validation, early training stopping, regularisation and prior probability adjusting are used to improve the generalisation ability of a network [51].

4.7.3 Support Vector Machines

Support Vector Machines (SVM) first introduced by Vapnik are fundamentally known to be capable of constructing an optimal separating hyperplane

between two separated classes. This maybe generalised to the non-separable case, where the classes may not be separable by a linear boundary [52].

Since the joint probability distribution is unknown, Vapnik suggested to use the Empirical Risk Minimization (ERM) principle which is an induction principle that can be used to train the classifier with the limited number of data samples at hand. ERM generates an approximation using the training set known as empirical risk. Empirical risk estimation employs a specific loss function and depends on the given training set. Then the empirical risk minimisation estimate the minimum value of the risk through the minimum value of the empirical risk. SVM also adopts Structural Risk Minimization (SRM) principle, and finds the best compromise between the learning ability and the complexity of the model to get the best generalisation ability according to the limited sample information [53].

Mathematically, the SVM algorithm can be expressed as follow. Considering the training sample $z_n, n = 1, \ldots, N_s$ and for each sample a label $c_n \in \{1, -1\}$, indicating to which of the two classes the sample belongs. Then a linear classifier $g(z) = w^T z + b$ is therefore declared in the following format [73]:

$$\begin{aligned} w^T z_n + b \geq 1 \quad if \quad c_n = +1 \\ w^T z_n + b \leq 1 \quad if \quad c_n = -1 \end{aligned} \tag{4.1}$$

These two constraints can be rewritten into one inequality:

$$c_n(w^T z_n + b) \geq 1 \tag{4.2}$$

To maximise the margine, $\|w\|^2$ needs to be minimised. Using *Lagrange multipliers*, the constraints (4.2) could be incorporate into the minimisation:

$$L = \frac{1}{2}\|w\|^2 + \sum_{n=1}^{N} \alpha_n [c_n(w^T z_n + b) - 1], \tag{4.3}$$

L should be minimised with respect to w and b, and maximised with respect to the Lagrange multipliers α_n. Setting the partial derivates of L w.r.t. w and b to zero results in the constraints [73]:

$$w = \sum_{n=1}^{N} \alpha_n c_n z_n \tag{4.4}$$

$$\sum_{n=1}^{N} \alpha_n c_n = 0 \tag{4.5}$$

Resubstituting this into (4.3) gives the so-called dual form [73]:

$$L = \sum_{n=1}^{N} \alpha_n - \frac{1}{2} \sum_{n=1}^{N} \sum_{m=1}^{N} \alpha_n \alpha_m c_n c_m z_n^T z_m \qquad \text{subject to } \alpha_n \geq 0. \tag{4.6}$$

L is a quadratic optimisation problem and should be maximised with respect to the α_n. In order to cope with overlapping classes, the SVM can be extended to have some samples erroneously classified. For that, the hard constraints (4.1) are replaced by soft constraints:

$$\begin{aligned} w^T z_n + b &\geq 1 - \xi_n \quad if c_n = 1 \\ w^T z_n + b &\leq 1 + \xi_n \quad if c_n = -1 \end{aligned} \tag{4.7}$$

Here, so-called *slack* variables $\xi_n \geq 0$ are introduced. These should be minimised in combination with the w^2. The final optimisation problem is in the following form [73]:

$$L = \frac{1}{2}w^2 + C\sum_{n=1}^{N}\xi_n + \sum_{n=1}^{N}\alpha_n(c_n[w^T z_n + b] - 1 + \xi_n) + \sum_{n=1}^{N}\gamma_n\xi_n, \qquad \alpha_n, \gamma_n \geq 0 \tag{4.8}$$

The second term expresses the desire to have the slack variables as small as possible. C is a trade-off parameter that determines the balance between having a large overall margin at the cost of more erroneously classified samples, or having a small margin with less erroneously classified samples.

Kernels are considered as the key component of the SVM algorithm [54] and is often used to improve the classification of non-separable and overlapping datasets. The selection of an appropriate kernel function is important, since the kernel function defines the feature space in which the training set instances will be classified. The following are some of the most commonly used kernels [55]: **a)** Polynomial, **b)** Gaussian and **c)** Sigmoid. It is common practice to estimate a range of potential settings and use cross-validation over the training set to find the best kernel. One of the limitation of SVMs is the low speed of the training. Platt [56] developed an optimised algorithm for training of SVMs called Sequential Minimal Optimization (SMO) which is an algorithm that can quickly solve the SVM QP problem by decomposing the overall QP problem into a series of smallest possible QP problems. Note that other studies [57] have also presented modied versions of SMO.

SVM classifiers have been shown to produce lower prediction error in many

applications and fields including bioinformatics [60], fault diagnosis [61] and face recognition [62] when large number of features are considered for sample description. SVM has been found to perform well in discriminating between the olfactory sensor responses and has been extensively used to classify the data generated by an EN in [32, 33]. SVM capabilities has been previously harvested to classify VOC profiles and odour of milk [63], meat [64] and bacterial sinusitis [65] and therefore is a suitable candidate for data analysis in this study.

A number of SVM configurations with different kernels is applied on the EN generated dataset in the second experiment. Firstly, the objective was to separate the two classes of each of the DPI datasets which represent the healthy and infected plants using a linear kernel. Then the more complex kernels namely Gaussian and Polynomial kernels which are often used for non-separable datasets were investigated. Finally, the multi-class SVM to categorise between three classes were evaluated.

4.7.3.1 Linear Kernel

An SVM with a linear kernel (LSVM) was constructed to classify the sensor responses. Once the SVM is trained, assuming a single dataset belongs to either of two classes, it simply determines on which side of the hyperplane a given test vectors lies and assigns to it the corresponding class label [66]. After applying the LSVM, the network was able to distinguish between the VOCs of the control tomato plants and the infected plants (Fig. 4.13). The LSVM results in Figure 4.13-left also show that classification of healthy and infected plant on 4 DPI is possible with a performance rate of 85% (4 standard

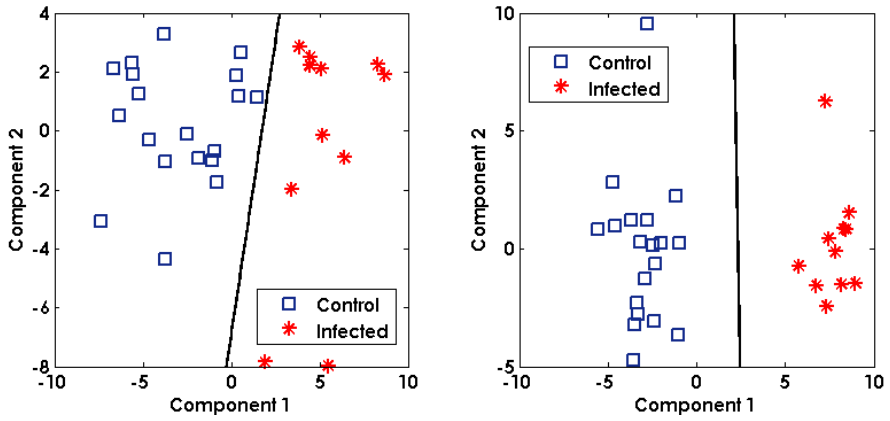

Figure 4.13: SVM with Linear - left: 4 DPI - right: 6 DPI

deviations from the mean, $p < 0.05$). The 6 DPI dataset were discriminated at a performance level of 90% ($p < 0.05$) (Figure 4.13-right). Ten-fold cross-validation was used to avoid the evaluation to become optimistically biased.

4.7.3.2 Polynomial Kernel

So far the discussion has been limited to training data that are linearly separable. It may not be feasible to attempt to separate the data precisely, when only a limited amount of training data is available. For the first non-separable kernel investigation, a *polynomial* kernel is used. The polynomial kernel is capable of producing more hyperplanes than the linear kernel.

As shown in Figure 4.14, using SVM with a polynomial kernel ($d = 2$) improved the healthy/infected classification of 4 DPI from 86% to 91% ($p < 0.05$). The highest classification accuracies were achieved with polynomial degree of 2 polynomial kernel, with an average error of 10%. As the third kernel, a Gaussian Radial Basis Function (RBF) kernel which has previously received significant attention [67] is investigated. Using multiple training and

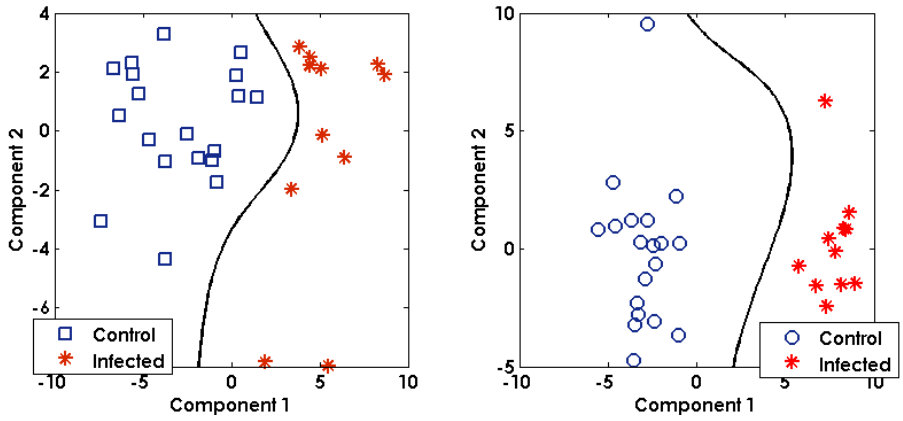

Figure 4.14: SVM with Polynomial kernel - left: 4 DPI right: 6 DPI

cross validation, the optimum $\sigma = 1$ was calculated. The RBF kernel enabled the SVM to match the performance rate of polynomial kernel when classifying datasets with 91% correct classification. The statistical t-test revealed that SVM with RBF kernel did not significantly improve the classification performance compared to polynomial kernel when presented with the EN dataset.

4.7.3.3 Multiclass SVM

SVM methods are binary and were originally designed for two-class classification problems. Various approaches including one-against-all and one-against-one multiclass SVMs [59] have been developed in order to extend standard SVM to be able to classify multiclass datasets [59]. The simplest solution for obtaining a classifier with more than two classes is to train K classifiers to distinguish one class from the rest. The classifier with the highest output then determines the class label [68]. In this case, both RBF and the polynomial kernels were applied to the multi-class datasets. The multi-class dataset consisted of VOCs from control (20 samples), PM (20 samples) and SM (20 samples) plants. Each sample contained 13 divergence features extracted from

the raw dataset. Initially, PCA was used to reduce the number of variables and the PCs where injected to the SVM classifier implemented in PRtools. The multi-class SVM technique was able to categorise the whole dataset with 89% and 91% performance rates with the Polynomial and RBF kernels respectively. Figure 4.15 demonstrate the decision boundaries produced by polynomial kernel on 6 DPI.

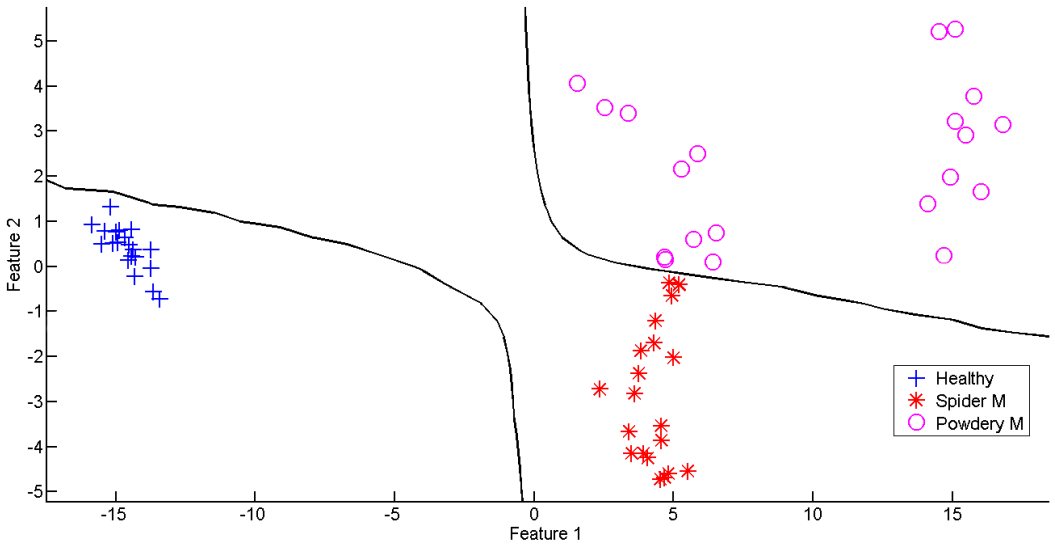

Figure 4.15: Multi-Class classification with polynomial kernel 91%

Cross-validation was employed to produce a realistic result as well as avoiding false positives/negatives. Both the polynomial and RBF kernels, as well as the linear kernel, showed discrimination classifying the datasets with a high performance rate. Here, it is possible to argue that the linear kernel can discriminate the separable datasets 6DPI with better accuracy. Linear classifiers have potential advantages such as: **a)** simpler training algorithms; **b)** requiring smaller training set and **c)** demanding fewer computational resources. For

other nonlinear non separable datasets, complex kernels may be used.

4.7.3.4 SVM Advantages and Disadvantages

Unlike conventional classifiers, SVMs offer a mechanism to maximise the margins of class boundaries. They also perform well when the number of the training data instances is small and the number of input variables is large. Other SVM benefits are the ability to control complexity independently of dimensionality of the problem. More importantly, SVMs operation is based on global optimisation methods and therefore will not trapped in local minima. Another major difference between SVMs and ANNs is that since initial parameter randomisation is not conducted in SVMs, the result is guaranteed to be repeatable. The SVM has a few weaknesses in that the kernels it uses are problem dependent so model development is extremely sensitive to the selection of an appropriate kernel function and initial parameters [69].

4.7.4 Discussion

From the findings of the experimental procedure presented in chapters 3 and 4, it appears that the VOC profiles of plants with powdery mildew infection *(Oidium neolycopersici)* and spider mite infestation *(Tetranychus urticae Koch)* are different from that of plants without it. Both unsupervised and supervised statistical analyses showed satisfactory classification performance of infected tomato samples, then proving the ability of ST214 EN to reveal possible infection.

One of the major drawbacks of EN is that, in case of sensor deterioration

or breakage, it would be extremely difficult to replace the sensor by another one having exactly the same behaviour and performance. This dramatically jeopardises the use of previously trained models, which are compulsory for data comparison purposes and for the classification of new unknown samples. This problem may be addressed by improving the sensors reproducibility. SMO gas sensor variability, for instance, was found to be of the order of 40% for different metal oxides and is mainly related to the deposition procedure of the sensitive layers [25]. At an industrial level this problem is fixed by producing a large number of sensors and then by selecting the most similar on the basis of an application specific test protocol [25]. Proper adjustment of priors and cost values in classifiers proved to be helpful in this study.

In regards to the rapidity of the EN, although the instrument may require flushing time and this might contradict the fact of having a rapid instrument, the technique remains much faster than any traditional laboratory based procedure (as discussed in chapter 2) that requires several hours/days for plate cultures, while the samples throughput is comparable to what can be achieved by complex analytical methods (i.e. GC-MS) with the advantage of having much simpler and cheaper analysis method [70, 71].

To conclude, this study with the aid of two separate experiments showed that an EN can differentiate between healthy and powdery mildew infected tomatoes, as well as between healthy and spider mite infested tomato plants. EN could thus be of large value for disease management not only for rapid detection of infected plants, but also potentially for the monitoring of the plant overall status.

4.7.5 Summary

In this chapter, an effort has been made to explore the ability of a sensor array (EN) in examining the VOCs emitted from greenhouse crops in both healthy and infested conditions and hence explore the possibility of replacing existing biological and laboratory based diagnosis. The Bloodhound ST214, EN system was employed to collect data from control and artificially inoculated tomato plants. Clustering and classification methods were used independently and in conjunction with each other to analyse the data gathered by EN.

PCA, k-means, LDA, SVM and ANN with different configurations were employed to scrutinise the data. In the next chapter the data acquired from High-Field Asymmetric Waveform Ion Mobility Spectrometry (FAIMS) in the same experimental settings will be analysed.

4.8 References

1. Huang, J., et al., Differential volatile emissions and salicylic acid levels from tobacco plants in response to different strains of Pseudomonas syringae. Planta, 2003. 217(5): p. 767-775.

2. Jansen, R., et al., Detection of diseased plants by analysis of volatile organic compound emission. Annual Review of Phytopathology, 2011. 49: p. 157-174.

3. Jansen, R., et al., Health monitoring of plants by their emitted volatiles: trichome damage and cell membrane damage are detectable at greenhouse scale. Annals of Applied Biology, 2009. 154(3): p. 441-452.

4. Kessler, A. and I.T. Baldwin, Defensive Function of Herbivore-Induced Plant Volatile Emissions in Nature. Science, 2001. 291(5511): p. 2141-2144.

5. Yang, S.F. and N.E. Hoffman, Ethylene Biosynthesis and its regulatioon in higher-plants. Annual Review of Plant Physiology and Plant Molecular Biology, 1984. 35: p. 155-189.

6. Harren, F.J.M. and S.M. Cristescu, Online, real-time detection of volatile emissions from plant tissue. AoB Plants, 2013. 5.

7. Berna, A.Z., et al., Mapping consumer liking of tomatoes with fast aroma profiling techniques. Postharvest Biology and Technology, 2005. 38(2): p. 115-127.

8. Buttery, R.G., R. Teranishi, and L.C. Ling, Fresh tomato aroma volatiles: A quantitative study. Journal of Agricultural and Food Chemistry, 1987. 35(4): p. 540-544.

9. Laothawornkitkul, J., et al., Discrimination of plant volatile signatures by an electronic nose: a potential technology for plant pest and disease monitoring. Environmental science & technology, 2008. 42(22): p. 8433-8439.

10. Van Den Boom, C.E., et al., Qualitative and quantitative variation among volatile profiles induced by Tetranychus urticae feeding on plants from various families. Journal of chemical ecology, 2004. 30(1): p. 69-89.

11. Song, G. and C.-M. Ryu, Two Volatile Organic Compounds Trigger Plant Self-Defense against a Bacterial Pathogen and a Sucking Insect in Cucumber under Open Field Conditions. International Journal of Molecular Sciences, 2013. 14(5): p. 9803-9819.

12. von Dahl, C.C., et al., Caterpillar-elicited methanol emission: a new signal in plant-herbivore interactions? Plant J, 2006. 46(6): p. 948-60.

13. Penuelas, J., et al., Caterpillars of Euphydryas aurinia feeding on Succisa pratensis leaves induce large foliar emissions of methanol. New Phytologist, 2005. 167(3): p. 851-857.

14. Raghava, T., et al., Spatial and temporal volatile organic compound response of select tomato cultivars to herbivory and mechanical injury. Plant Science, 2010. 179(5): p. 520-526.

15. Maul, F., et al., Aroma volatile profiles from ripe tomatoes are influenced by physiological maturity at harvest: an application for electronic nose

technology. Journal of the American Society for Horticultural Science, 1998. 123(6): p. 1094-1101.

16. Wilson, A.D. and M. Baietto, Advances in electronic-nose technologies developed for biomedical applications. Sensors, 2011. 11(1): p. 1105-1176.

17. van der Hooft, J.J., et al., Polyphenol identification based on systematic and robust high-resolution accurate mass spectrometry fragmentation. Analytical chemistry, 2010. 83(1): p. 409-416.

18. Emmerich, S.J. and A.K. Persily, State-of-the-art review of CO2 demand controlled ventilation technology and application. 2001: DIANE Publishing.

19. Lebrun, M., et al., Discrimination of mango fruit maturity by volatiles using the electronic nose and gas chromatography. Postharvest Biology and Technology, 2008. 48(1): p. 122-131.

20. Taurino, A., et al., Analysis of dry salami by means of an electronic nose and correlation with microbiological methods. Sensors and Actuators B: Chemical, 2003. 95(1): p. 123-131.

21. Hansen, T., M.A. Petersen, and D.V. Byrne, Sensory based quality control utilising an electronic nose and GC-MS analyses to predict end-product quality from raw materials. Meat science, 2005. 69(4): p. 621-634.

22. Dragonieri, S., et al., An electronic nose in the discrimination of patients with non-small cell lung cancer and COPD. Lung Cancer, 2009. 64(2): p. 166-170.

23. Turner, A.P.F. and N. Magan, Electronic noses and disease diagnostics. Nat Rev Micro, 2004. 2(2): p. 161-166.

24. Mills, A., A. Lepre, and L. Wild, Breath-by-breath measurement of carbon dioxide using a plastic film optical sensor. Sensors and Actuators B: Chemical, 1997. 39(13): p. 419-425.

25. James, D., et al., Chemical Sensors for Electronic Nose Systems. Microchimica Acta, 2005. 149(1-2): p. 1-17.

26. Jha, S.K. and R. Yaava, Power scaling of chemiresistive sensor array data for odor classification. J. Patt. Recog. Res, 2011. 1: p. 65-74.

27. Han, J.-W., et al., Liquid gate dielectric field effect transistor for a radiation nose. Sensors and Actuators A: Physical, 2012. 182(0): p. 1-5.

28. Stetter, J.R., et al., New sensor arrays and sampling systems for a modular electronic nose. Sensors and Actuators B: Chemical, 2000. 69(3): p. 410-419.

29. Fanget, S., et al., Gas sensors based on gravimetric detectionA review. Sensors and Actuators B: Chemical, 2011. 160(1): p. 804-821.

30. Michie, D., D.J. Spiegelhalter, and C.C. Taylor, Machine Learning, Neural and Statistical Classification. 1994: Ellis Horwood.

31. Nemati, H.R. and C.D. Barko, Organizational Data Mining: Leveraging Enterprise Data Resources for Optimal Performance. 2004: Idea Group Pub.

32. Milligan, G.W. and M.C. Cooper, Methodology review: Clustering methods. Applied Psychological Measurement, 1987. 11(4): p. 329-354.

33. Handl, J. and B. Meyer, Improved ant-based clustering and sorting in a document retrieval interface. Parallel Problem Solving from NaturePPSN VII, 2002: p. 913-923.

34. Haralick, R.M. and L.G. Shapiro, Image segmentation techniques. Computer vision, graphics, and image processing, 1985. 29(1): p. 100-132.

35. Wen, J.R., J.Y. Nie, and H.J. Zhang. Clustering user queries of a search engine. 2001. ACM.

36. Jolliffe, I.T., Principal component analysis. Vol. 487. 1986: Springer-Verlag New York.

37. Buljak, V., Inverse Analyses with Model Reduction: Proper Orthogonal Decomposition in Structural Mechanics. 2012: Springer Berlin Heidelberg.

38. Magan, N., A. Pavlou, and I. Chrysanthakis, Milk-sense: a volatile sensing system recognises spoilage bacteria and yeasts in milk. Sensors and Actuators B: Chemical, 2001. 72(1): p. 28-34.

39. Fend, R., et al., Monitoring haemodialysis using electronic nose and chemometrics. Biosensors and Bioelectronics, 2004. 19(12): p. 1581-1590.

40. Borah, S., et al., Neural network based electronic nose for classification of tea aroma. Sensing and instrumentation for food quality and safety, 2008. 2(1): p. 7-14.

41. Ampuero, S. and J. Bosset, The electronic nose applied to dairy products: a review. Sensors and Actuators B: Chemical, 2003. 94(1): p. 1-12.

42. Kalman, E.-L., et al., Classification of complex gas mixtures from automotive leather using an electronic nose. Analytica Chimica Acta, 2000. 403(1): p. 31-38.

43. Sobaski, T., et al., Electronic nose applied to automotive fuel qualification. Sensors and Actuators B: Chemical, 2006. 116(1): p. 207-212.

44. Peris, M. and L. Escuder-Gilabert, A 21st century technique for food control: Electronic noses. Analytica Chimica Acta, 2009. 638(1): p. 1-15.

45. Gil-Snchez, L., et al., A novel humid electronic nose combined with an electronic tongue for assessing deterioration of wine. Sensors and Actuators A: Physical, 2011. 171(2): p. 152-158.

46. Dbska, B. and B. Guzowska-wider, Application of artificial neural network in food classification. Analytica chimica acta, 2011. 705(1): p. 283-291.

47. Kostesha, N.V., et al. Development of the colorimetric sensor array for detection of explosives and volatile organic compounds in air. in Proc. SPIE. 2010.

48. Taylor, W.A., What every engineer should know about artificial intelligence. 1988: MIT Press.

49. Rojas, R., Neural networks: a systematic introduction. 1996: Springer-Verlag.

50. Haykin, S.S., Neural networks: a comprehensive foundation. 1999: Prentice Hall.

51. Bishop, C.M., Neural Networks for Pattern Recognition. 1995: Oxford University Press, Incorporated.

52. Hastie, T., R. Tibshirani, and J.J.H. Friedman, The elements of statistical learning. Vol. 1. 2001: Springer New York.

53. Li, D. and C. Zhao, Computer and Computing Technologies in Agriculture III: Third IFIP TC 12 International Conference, CCTA 2009, Beijing, China, October 14-17, 2009, Revised Selected Papers. 2010: Springer.

54. Kotsiantis, S.B., I.D. Zaharakis, and P.E. Pintelas, Machine learning: a review of classification and combining techniques. Artificial Intelligence Review, 2006. 26(3): p. 159-190.

55. Webb, A.R., Statistical pattern recognition. 2003: Wiley.

56. Platt, J.C., 12 Fast Training of Support Vector Machines using Sequential Minimal Optimization. 1999.

57. Keerthi, S.S. and E.G. Gilbert, Convergence of a generalized SMO algorithm for SVM classifier design. Machine Learning, 2002. 46(1-3): p. 351-360.

58. Weston, J. and C. Watkins, Multi-class support vector machines. 1998, Citeseer.

59. Byvatov, E. and G. Schneider, Support vector machine applications in bioinformatics. Appl Bioinformatics, 2003. 2(2): p. 67-77.

60. Baccarini, L.M.R., et al., SVM practical industrial application for mechanical faults diagnostic. Expert Systems with Applications, 2011. 38(6): p. 6980-6984.

61. Kim, S.-K., et al., SVM-based feature extraction for face recognition. Pattern Recognition, 2010. 43(8): p. 2871-2881.

62. Brudzewski, K., S. Osowski, and T. Markiewicz, Classification of milk by means of an electronic nose and SVM neural network. Sensors and Actuators B: Chemical, 2004. 98(2): p. 291-298.

63. El Barbri, N., et al., Electronic nose based on metal oxide semiconductor sensors as an alternative technique for the spoilage classification of red meat. Sensors, 2008. 8(1): p. 142-156.

64. Thaler, E.R. and C.W. Hanson, Use of an electronic nose to diagnose bacterial sinusitis. American journal of rhinology, 2006. 20(2): p. 170-172.

65. Distante, C., N. Ancona, and P. Siciliano, Support vector machines for olfactory signals recognition. Sensors and Actuators B: Chemical, 2003. 88(1): p. 30-39.

66. Luan, F., et al., Classification of estrogen receptor-[beta] ligands on the basis of their binding affinities using support vector machine and linear discriminant analysis. European journal of medicinal chemistry, 2008. 43(1): p. 43-52.

67. Brudzewski, K., et al., Classification of gasoline with supplement of bioproducts by means of an electronic nose and SVM neural network. Sensors and Actuators B: Chemical, 2006. 113(1): p. 135-141.

68. Distante, C., N. Ancona, and P. Siciliano, Support vector machines for olfactory signals recognition. Sensors and Actuators B: Chemical, 2003. 88(1): p. 30-39.

69. Kordon, A., Applying Computational Intelligence: How to Create Value. 2010: Springer Berlin Heidelberg.

70. Concina, I., et al., Early detection of microbial contamination in processed tomatoes by electronic nose. Food Control, 2009. 20(10): p. 873-880.

71. Covington, J. A., Wedlake, L., Andreyev, J., Ouaret, N., Thomas, M. G., Nwokolo, C. U., Arasaradnam, R. P. (2012). The detection of patients at risk of gastrointestinal toxicity during pelvic radiotherapy by electronic nose and FAIMS: a pilot study. Sensors, 12(10), 13002-13018.

72. Jurs, P. C., Bakken, G. A., McClelland, H. E. (2000). Computational methods for the analysis of chemical sensor array data from volatile analytes. Chemical Reviews, 100(7), 2649-2678.

73. Van Der Heijden, F., Duin, R., De Ridder, D., Tax, D. M. (2005). Classification, parameter estimation and state estimation: an engineering approach using MATLAB. Wiley. com.

Chapter 5

Non-destructive Plant Disease Detection using Field Asymmetric Ion Mobility Spectrometry

5.1 Chapter Overview

In this chapter the plant's VOC profiles acquired using a Field Asymmetric Ion Mobility Spectrometry (FAIMS) device will be analysed and discussed. This study is the first to employ a FAIMS device in horticultural settings to sample the VOCs emitted from plants by conducting two distinct experiments. The aim is to determine the utility of a FAIMS instrument to detect plant diseases. Finally, the chapter closes by assessing the performance of FAIMS when coupled with classifiers in order to discriminate between healthy and infected plants.

5.2 Introduction

Recently, Ion mobility spectrometry (IMS) has become a significant technique for the detection of compounds in pharmaceutical [1], military [2, 3], food [4, 5], clinical [6, 7], environmental [8] and space exploration [9, 10] industries due to its fast and highly sensitive capabilities for separating and identifying gaseous molecules. IMSs are currently installed at commercial airports across the world to screen individuals and their luggage for explosives, explosive residues [11] or illegal substances [12]. Similarly, tens of thousands of hand-held/portable IMSs have been distributed for determining chemical warfare agents on battlefields in different regions of the world [13].

5.2.1 Ion Mobility Spectrometry (IMS)

IMS is an analytical technique for the determination of volatile and semi-volatile compounds (i.e. gas or vapour molecules) based on the gas-phase separation of the resulting ions under a weak electric field at ambient (atmospheric) pressure [14].

Four major components form the foundations of a typical IMS: **1)** an ion source region which typically is a 10 mCi of ^{63}Ni, **2)** An ion gate which electronically inject ions from the ion source into the drift region, **3)** a drift region in which an electric field is established using a voltage divider and **4)** a detector which creates a signal when hit by ions under the influence of electric field generated at drift region [2]. Fig. 5.1 illustrates the four major components of a typical IMS. These four components may be used on their own or

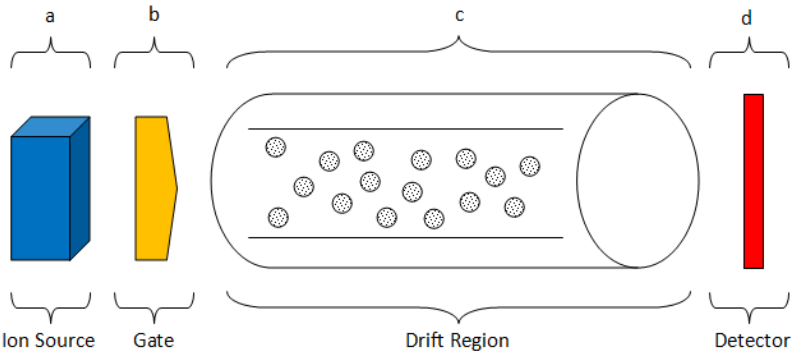

Figure 5.1: Schematic representation of the IMS device a: ion source, b: ion gate, c: drift region and d: detector

in conjunction with other separation or identification techniques (i.e. electrospray ionisation/ion mobility spectrometry) [15, 16] in order to enhance the detection of compounds according to the sensitivity or resolution required by various applications [17].

5.2.2 High-Field Asymmetric Ion Mobility Spectrometry

The very first paper describing Field Asymmetric Ion Mobility Spectrometry (FAIMS) technology appeared in the literature was written by Buryakov [18] in 1993. Since then, FAIMS has rapidly gained acceptance as a robust, versatile tool for ionisation separations prior to mass-spectrometric analysis and has been utilised in a variety of fields including bio-analytical, forensic, geological and defence applications [19, 20]. This study employs FAIMS technology in a horticultural settings to sample the VOCs emitted from a live plant in order to discriminate between healthy and infected samples.

5.2.3 Fundamentals of FAIMS

FAIMS technology discriminates compounds using a property known as mobility which is a measure of how quickly an ion moves through an electric field [21]. The mobility relates to size and mass, and is used to specifically distinguish the chemical of interest. A basic FAIMS device includes two parallel plates to which voltages can be applied and between which are introduced the ions of interest.

When a mixture of ionised compounds of different sizes and types is introduced between the two plates, a condition is created by the application of high voltage in an appropriate waveform to the plates where some types of ions drift and hit the plates while other types of ions remain between the plates. The *asymmetric waveform* is a square wave in which a high positive voltage is applied for a short time and a lower negative voltage is applied for a longer time (Fig. 5.2). The peak voltage of the waveform is called the dispersion voltage (DV). If the electric fields which are created by the application

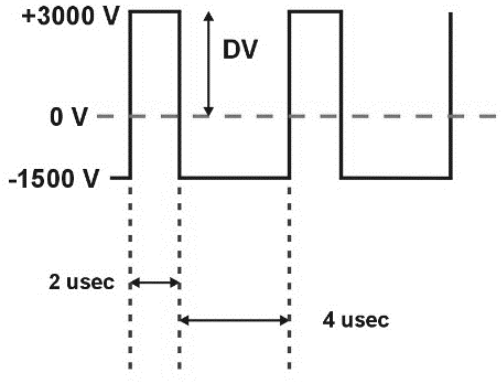

Figure 5.2: Example of an asymmetric waveform [22]

of the asymmetric waveform are weak, the ion will move back and forth, or

oscillate, during the waveform, but the ion will not be pushed towards either plate. If the electric field during the high-voltage part of the waveform is high, then the application of the waveform may cause the ion to drift in one or the other direction towards one of the plates. Figure 5.3 illustrates examples of ions drifting towards the lower and upper plates or when it is in a balanced condition.

Figure 5.3: Ions oscillating between the FAIMS plates. *left:* ion hits lower plate, *middle:* ion in balanced condition, *right:* ion hits upper plate

An ion must be in the balanced condition to exit from FAIMS plates. The reason the ion will drift towards a plate is that the ion mobility during the application of the high electric field is different than the ion mobility during the low electric field.

There are three types of ion behaviour observed in an electric field: **Type A:** these ions show an increase in ion mobility with increasing field strength, **Type B**: these ions display an initial increase in ion mobility with increasing fields, followed by decreasing mobility as the field strength increases further and **Type C**: ions that show a decrease in ion mobility with increasing field strength. Certain ions, such as the *Chloride ion* in *nitrogen (N)* or *oxygen (O)*, experience a very large change in mobility with field. During the application of the asymmetric waveform, the chloride ion will drift very rapidly towards

a plate. On the other hand, ions such as the *tetrapropylammonium* ion, experience a very small change in mobility with field and drift slowly towards one of the plates [22].

The drift of an ion towards one of the metal plates can be stopped by the application of a small *dc* voltage to either of the plates. If the voltage is applied with the appropriate magnitude and polarity, the ion will sense the force of this field and the drift of the ion will be stopped. The voltage which is applied to reverse or compensate for the ion drift is known as *Compensation Voltage* (CV). The CV necessary to stop the drift of the chloride ion will be high, since the mobility of this ion increases substantially at high electric field. Conversely, the CV necessary to stop the drift of the tetrapropylammonium ion will be small. In the nutshell, the CV is the force used to control the separation of ions [23].

Different types of ions, under a high voltage asymmetric waveform, will begin to migrate towards the plates at rates that are characteristic of those ions. When a CV is applied, most ions will hit the plates except the ions for which the CV is exactly the right voltage to balance the drift caused by the application of the asymmetric waveform. The types of ions which are in a balanced condition between the plates are selected by adjusting the voltage used for CV [23]. A mixture of ions carried by a gas flow can be resolved into several peaks by scanning CV and simultaneously detecting the ions successfully transported through the gap between the plates. Each type of ion travels through the plates at a specific characteristic value of CV [24]. The spectrum of peaks observed in this manner is called a *CV spectrum* and are the data

that are going to be analysed subsequently.

5.2.4 IMS vs. FAIMS

Both FAIMS and IMS operate at atmospheric pressure. However, they differ in several ways including but not limited to the following: **a)** FAIMS is an ion filter, where a mixture of ions is presented to the inlet, but only selected ions are transmitted through the analyser in a continuous fashion and **b)** the FAIMS instrument operates at room temperature, whereas the conventional IMS requires a sophisticated heated inlet system to increase the rate of desolvation of the hydrated analyte ions produced during the electrospray process. An elevated temperature is not required in FAIMS, because the heating of the ions by the high electric fields appears to promote desolvation [25].

5.3 Lonestar FAIMS device

For this investigation a Lonestar FAIMS device produced by Owlstone (Cambridge, United Kingdom) was configured and used. The Lonestar comprises a full functioning PC, display screen, FAIMS sensor and a pump. The built-in sensor acts as a filter, which detects and separates chemicals according to their characteristic ion mobility. The sensor filters out the background chemicals that do not have the correct mobility fingerprint.

5.4 Experimental Setup

The FAIMS technology described in section 5.2 was employed to sample the VOCs emitted from a healthy and infected tomato plants. The experimental

methodology, setup, samples and procedures including the environmental factors are comprehensively described in detail in chapter 3. The experiment was conducted in two rounds each taking 33 and 20 consequent days respectively.

It is important to note that this study is not attempting to identify the chemical compounds detected by FAIMS. This study, similar to other FAIMS studies for different applications [26, 27], is mainly focused on perceiving the changes/differences that occur between the samples. Hence, by just detecting these changes and examining the intensity of discrepancy, healthy plants can be distinguished from the infected ones.

The following parameters are required to analyse FAIMS data and so are explained here.

5.4.1 DF – Dispersion Field

The dispersion field, DF, is the field created by the dispersion voltage, DV. Dispersion voltage is the peak voltage of the asymmetric waveform applied to the electrodes in the FAIMS process. The DF can be scanned from 0% to 100% of its set range on the Lonestar unit. These parameters can be changed based on the resolution and accuracy required by the application at hand. For the purpose of this study, DF was scanned for the whole range (0% to 100%).

5.4.2 CV – Compensation Voltage

As mentioned earlier, the compensation voltage, CV, is the critical parameter in the FAIMS device. For these experiments the compensation voltage is

scanned from -6.0 V to 6.0 V when collecting Lonestar data. The detector will pick up different analyte molecules at different combinations of CV and DF.

5.4.3 Ion Current

The ion current is the current generated by the ions that pass through the separator electrodes and are picked up by the ion detector plate at the end of the drift tube.

5.4.4 DF Matrix

Finally, a DF matrix is the chart produced by scanning DF and CV and plotting the ion current produced. The DF matrix is the output of the FAIMS. An illustration is shown in Figure 5.4. DF matrices come in pairs: one for positive ions (positive mode) and one for negative ions (negative mode).

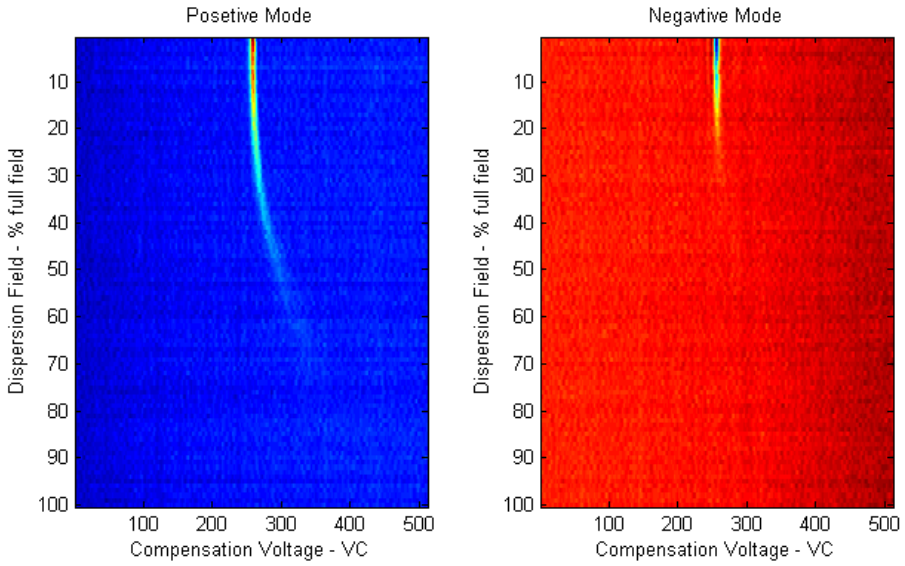

Figure 5.4: Typical FAIMS response - *left:* positive mode - *right:* negative mode

5.5 Data Pre-processing and Analysis

On each individual day of experiment, both control (healthy) and *Oidium neolycopersici*-infected tomato plants were sampled for the minimum of 10 runs. The data matrices were organised and saved as a MAT file in Matlab environment. For the first set of experiments, each MAT file contained an average of 12 runs of healthy and infected samples.

By extracting and visualising the FAIMS generated data (DF matrix), the location of the essential signal data points can conveniently be observed and examined to determine the area of significance. In order to extract and visualise the actual signal/response from the data generated by FAIMS the following algorithm was proposed, implemented in MATLAB (MathWorks ©) and applied to the original, raw dataset.

The threshold value, τ was obtained statistically as given in equation (5.1) below, where, μ, and σ are the mean and standard deviation of all of the intensities in a visualised data matrix (Fig. 5.4) . $I(i,j)$ corresponds to each intensity in the 2D matrix.

$$\tau = \mu + k\sigma \tag{5.1}$$

where

$$\mu = \frac{1}{(HW)} \sum_{i,j} I(i,j) \tag{5.2}$$

and

$$\sigma = \sqrt{\frac{1}{(HW)} \sum_{i,j} (I(i,j) - \mu)^2} \tag{5.3}$$

where H and W denote the height and width of the visualised data I (Fig. 5.5), respectively, k is determined heuristically for segmenting the corresponding area on the matrix. A threshold value is applied to remove the background on the data and then segment the corresponding area on the matrix with the following formula:

$$I_\tau(i,j) = \begin{cases} 0 \quad , & if I(i,j) > \tau \\ 255, & if I(i,j) \leq \tau \end{cases} \tag{5.4}$$

Figure 5.5 depicts the visualised data images with original sample followed by the obtained threshold image (Fig. 5.5 - right). The algorithm has the effect of accurately removing the area that evidently does not contribute to the forthcoming analysis.

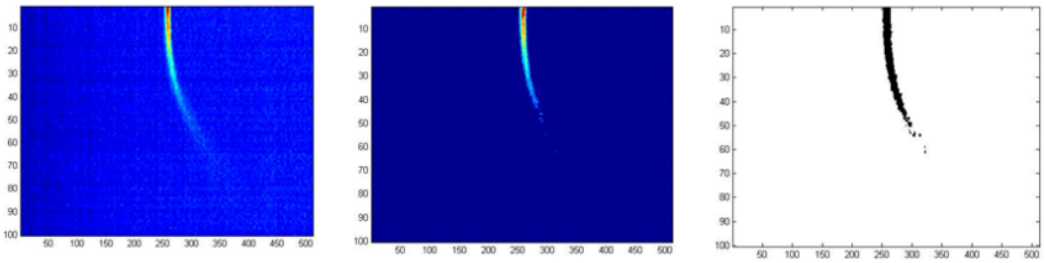

Figure 5.5: *Left:* normal FAIMS response - *middle:* processed FAIMS response - *Right*: gray-scaled signal

Figure 5.6 illustrates a single CV sweep corresponding to the position of a sin-

gle horizontal line on the DF matrix in both positive and negative modes. The single CV sweeps containing the signal intensity peaks are the foundations of the analysis and may be processed individually or in an array.

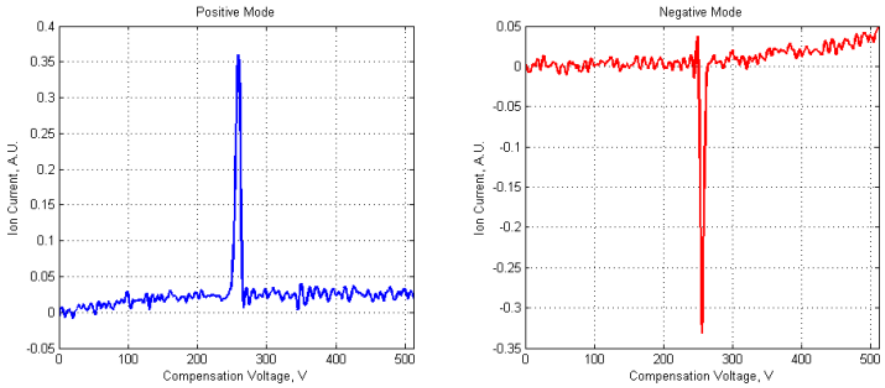

Figure 5.6: Positive and negative modes of the first sampling run

As demonstrated in section (5.4.4) each single FAIMS generated DF matrix contains a considerable bulk of redundant regions that only hinders the analysis and discrimination process. Such regions are commonly [28] eliminated by deleting all the data outside of a central spread of the signal/response. The procedure literally has the effect of reducing the data size by about 30-40% depending on the signal shape, while protecting the entire crucial discriminatory information. Thus, in order to mine the signal region from the insignificant background, a block cutting method was used. Using a customised batch process, all the single FAIMS observations (DF matrices) were further processed. A block of signal (150 by 80) was extracted from raw data as exemplified in figure 5.7. Note that the dimension of the extracted signal depends on the range of the scanned DF (i.e. 0% – 100% or 0% to 50%).

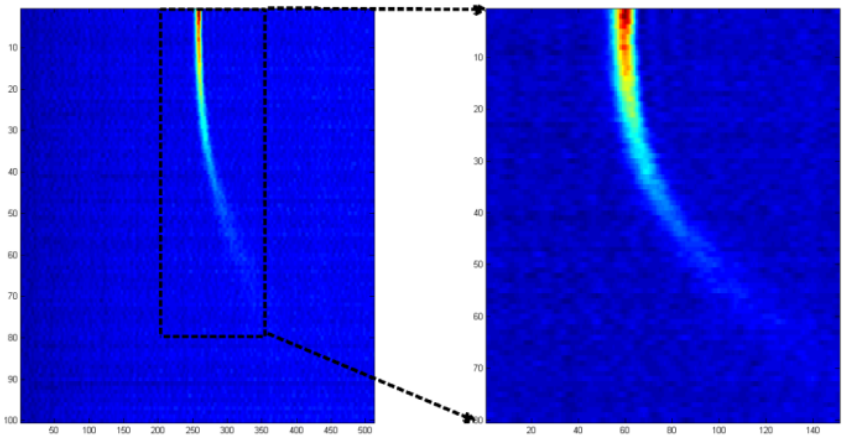

Figure 5.7: Extracting (cutting) signal block from the full spectra

In order to monitor the variations occurring at different DV levels, three sweeps were extracted and formed a dataset in the following fashion: for example, if the original DF matrix A is a $(p \times q)$ matrix, where $p = 3$ and $q = 150$, A was then reshaped into a new $(m \times n)$ matrix B, where $m = 1$ and $n = 450$ such that $(p \times q) = (m \times n)$. The elements of matrix B are taken column wise from the matrix A as shown in the following projection:

$$\begin{bmatrix} 1 & \dots & 150 \\ \vdots & & \\ 3 & & \end{bmatrix} \rightarrow \begin{bmatrix} 1 & \dots & 450 \end{bmatrix} \tag{5.5}$$

Figure 5.8 illustrates the three sweeps (lines 10, 15 and 20) extracted from the entire spectrum (DF matrix) which constructed matrix B. The red dashed line indicates the end of each single sweep. As expected, the peaks are clearly visible in each sweep and are shown to be decreased as DV increases.

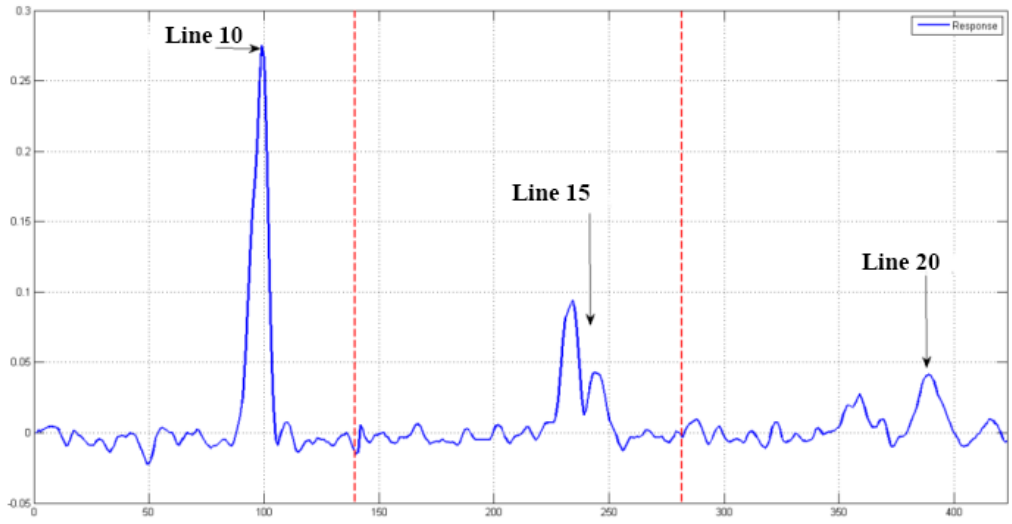

Figure 5.8: Extracted sweeps showing lines 10, 15 and 20 of a single DF matrix

As discussed earlier, as the compensation voltage, CV, is varied, a spectrum is produced. Figure 5.9 demonstrates two spectra from healthy (control) and powdery mildew samples from the 8^{th} DPI on which one of the plants was heavily infected with powdery mildew.

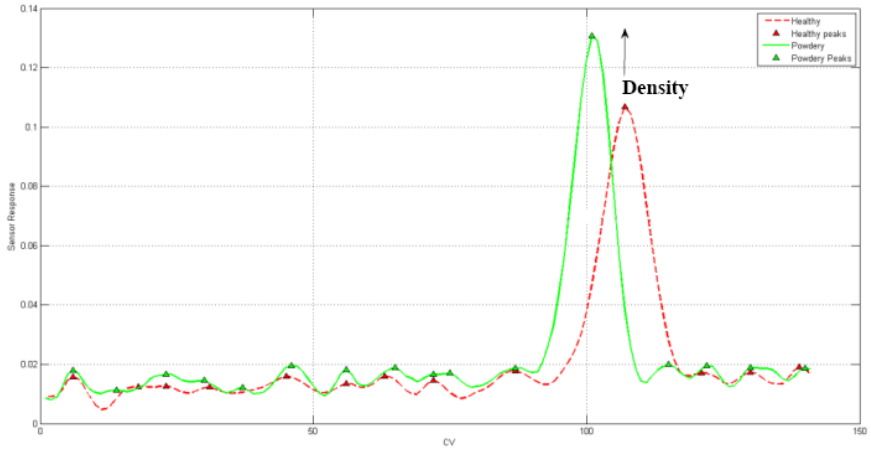

Figure 5.9: A single sweep extracted from the healthy and infected plants.

The difference in the height of the peak signifies the density change of the analyte detected. The peak shown in figure 5.9 is solely constructed from a single sweep extracted from the complete DF matrix. All the 80 DVs extracted from the entire DF matrix via the blocking method have been used to create the spectrum in Fig. 5.10. Individual peaks from each DV sweep are clearly visible. Matlab code was written to modify the built in Bioinformatics Toolbox to process the FAIMS data and create the spectrum. Each spectrum was baseline-corrected with the *msbackadj* routine and smoothed. Next, the peaks were identified by leveraging the *mspeaks* function. Figure 5.10 is the plot of the spectra with the peak position indicated with red crosses. Detecting the peaks as the discriminatory factor in IMS analysis is a natural procedure and have been frequently conducted in previous studies. Heuristically, the first 25 peak intensities have been used to form the attributes of each sample as they carry the significant discriminatory information. The negative part of the spectrum did not show significant contribution to the discrimination and therefore was discarded.

5.5.1 Disease Development

One of the core objectives of conducting the initial FAIMS experiment was to detect and identify a systematic pattern in the development of infection caused by *Oidium neolycopersici* in tomato plants. The FAIMS device has been employed to sample the plants on every single day of the experiment (33 Days). Hence, by observation and analysis of the consequent days one may be able to demonstrate the evolution of infection in the plant.

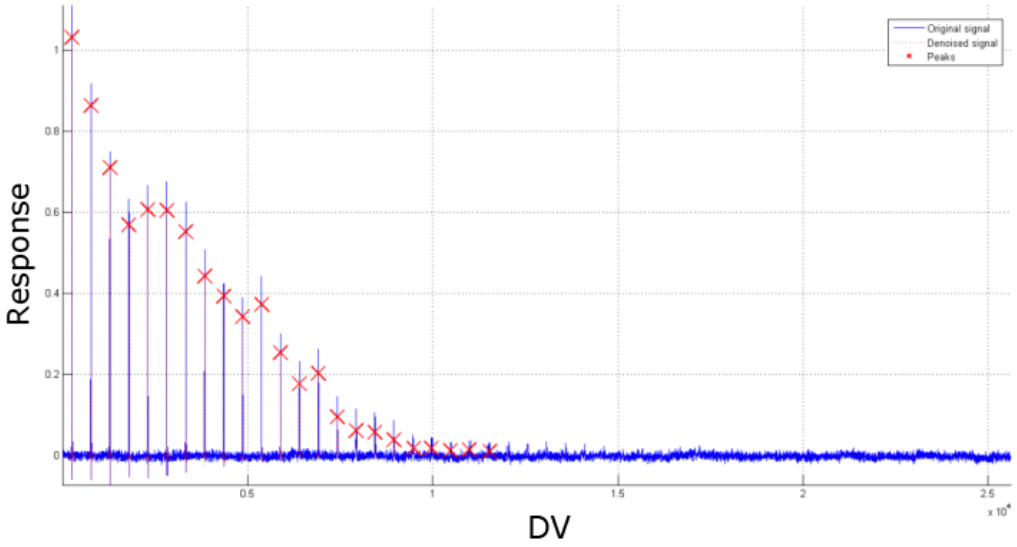

Figure 5.10: Intensity peaks detected on the pre-processed signal

Figure 5.11, illustrates the graph of peaks extracted from healthy and infected samples on 6 DPI. For demonstration purposes, the first 20 peaks were extracted and drawn. As shown, there is a visible difference between the intensity of peaks detected from the control and *Oidium neolycopersici*-infected tomato plants. This is potentially due to FAIMS detection of increased emission of ionised VOCs including *ethylene*, *hexenol*, *methyl salicylate*, *ocimene*, *linalool*, *farnesene* and *trimethyl-tridecatetraene*.

The next stage is to use PCA to evaluate the development of infection for each day of experiment. PCA has previously been used to process sensory data collected with respect to time [30]. The objective is to determine three stages of infection as follow: **a:** healthy stage in which the plant is healthy and not artificially inoculated, **b:** mild infection stage in which the plant is inoculated and therefore is mildly infected and **c:** severe infection stage in

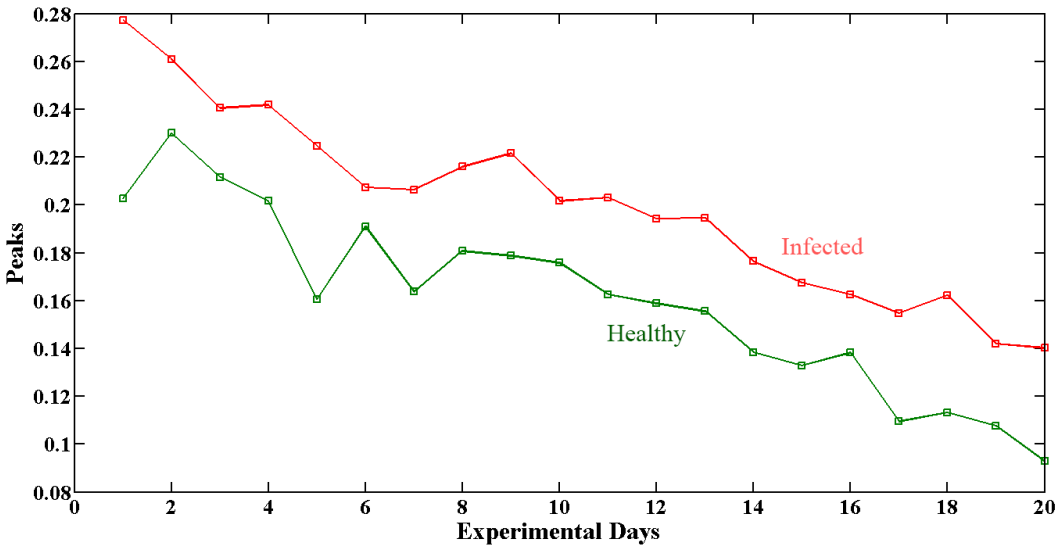

Figure 5.11: Peak intensity differences between the healthy and infected samples

which the plant is severely infected and the white powdery mildew is clearly visible on the leaves and stem of the plant. After data scaling, the principal components for each dataset were calculated. The first components (PC_1) of each dataset are plotted on a single graph since it carries the highest variance in the dataset (Fig. 5.12). On average PC_1 carried around 88% and PC_2 carried around 9% of the overall variance. The day of infection is indicated using a dashed red line.

In case of the infected plant, three stages of infection can be observed. The first four days including the day of inoculation formed a cluster. A significant jump can be seen from the healthy stage to mildly infected stage between 1 DPI to 10 DPI after which the gradual move to severe infection is noticed.

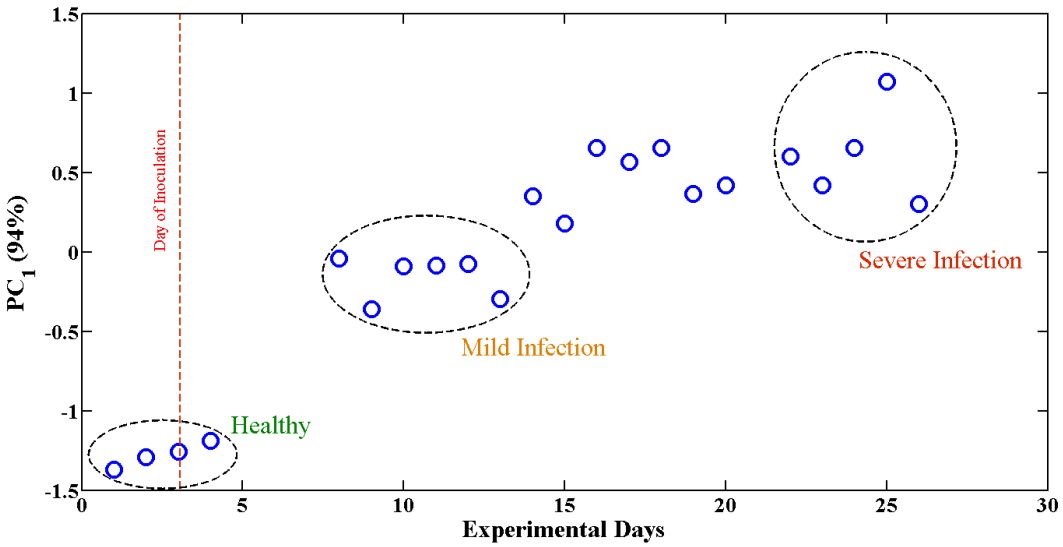

Figure 5.12: Development of powdery mildew disease from Day 1 to 26 DPI

The same analysis was conducted on the data acquired from the control (healthy) plant. As illustrated in Figure 5.13, although a minimal gradual increase could be seen in the responses, it does not follow the reactions found in the powdery mildew infected plant and may be considered negligible.

The preliminary analyses demonstrated that FAIMS technology was capable of materialising a pattern for disease development. This is particularly useful, as it can be a basis for a potential early detection tool. Such technology may be able to alert growers if the system has detected a disease development pattern.

5.6 Second Set of Experiment

In order to verify the preliminary results of the initial experiment, the author conducted a second set of experiments at HRI, University of Warwick. Three

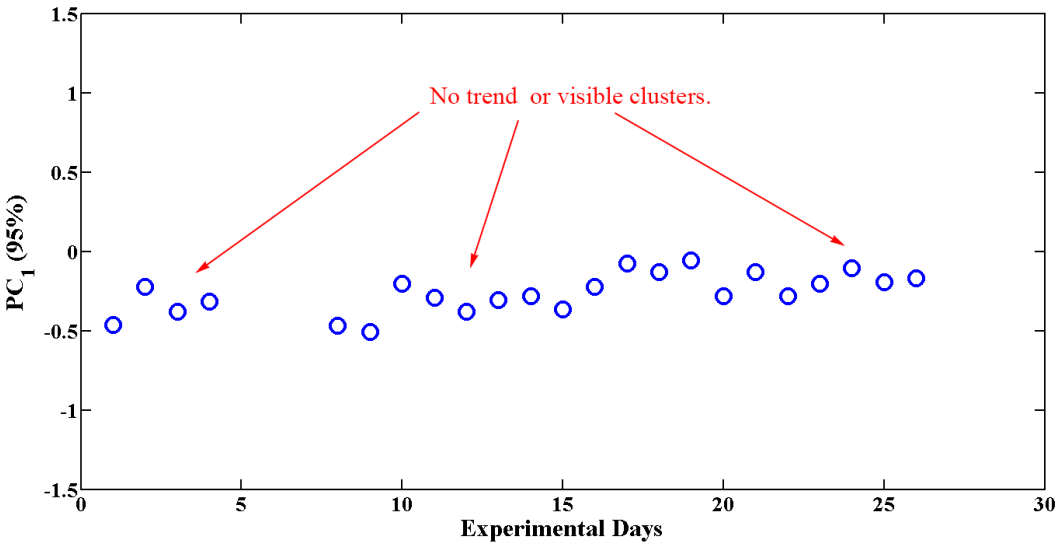

Figure 5.13: Status of healthy plant - from Day 1 to DPI 26 - No visible trend could be identified

fresh, healthy, 4 week old tomato plants were acquired and placed in glass chambers. One of the tomato plants remained healthy through out the experiment as a control. The others were inoculated as described in chapter 3. Temperature and humidity were logged constantly. Extra care was taken to ensure that the experiential setup, instrumentations and environmental factors were replicated so a reliable result can be obtained for comparison. The experiment took around 20 days. Four crucial days after inoculation was identified as follow: 2 DPI, 4 DPI, 6 DPI and 10 DPI. One glass chamber was kept as the control while the other contained the artificially infected plant.

PCA projection of the 2 DPI and 6 DPI are demonstrated in figure 5.14 with the first two PCs accounting for 91% and 93.12% of total variance respectively. It is plainly visible that the healthy and *Oidium neolycopersici*-infected samples are not separable on the 2 DPI. Conversely, two clusters are visible

on the 6 DPI figure each representing the healthy (red crosses) and infected (blue squares) samples respectively. The clusters are perfectly separated at each side of the graph.

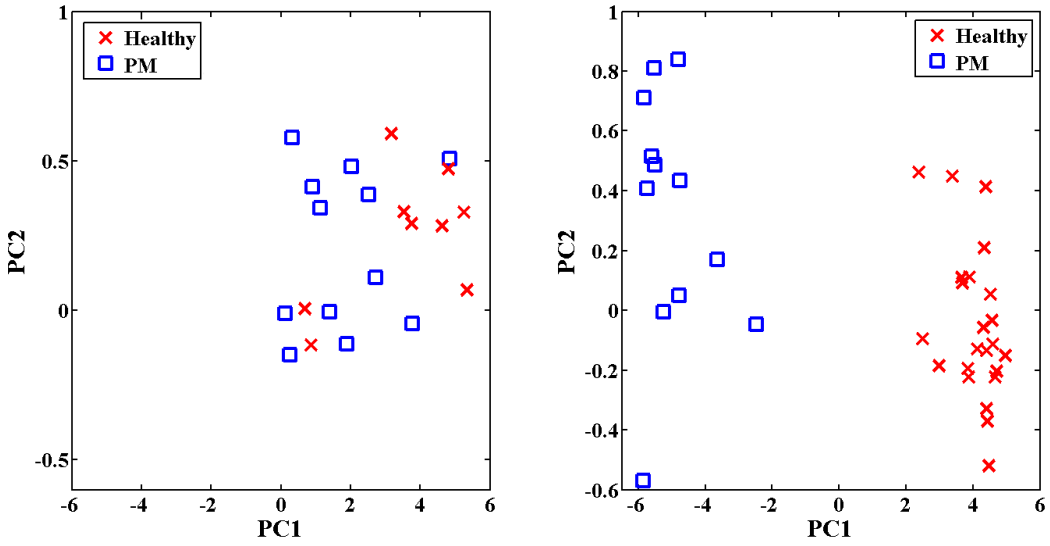

Figure 5.14: PCA projection of the second experiment: left: 2 DPI with pc_1 = 81% and pc_2 = 10%, right: 6 DPI with pc_1 = 82% and pc_2 = 11%

In the previous section a disease development pattern was identified. In this part using the data acquired from the second experiment, a dataset containing both healthy and powdery mildew infected samples was constructed to be classified.

Furthermore, Linear Discriminant Analysis (LDA) was employed on the FAIMS dataset (6 DPI) to discriminate between healthy and infected plants. The preprocessing technique described in section 5.5 was applied on the dataset. The data points representing healthy and infected samples formed two categories

each containing the peaks extracted from the DF matrix as the discriminatory features. The healthy samples which formed a dense cluster are represented by blue crosses. The infected plants were clearly separated from the healthy samples and have formed their own cluster but the inter-cluster distances are not as minimised as the healthy one. No outliers are visible from the graph. The distance between the clusters indicates that they may be linearly separable. As illustrated in Fig. 5.15 the LDA managed to produce a linear decision boundary which separates the healthy and powdery mildew infected samples.

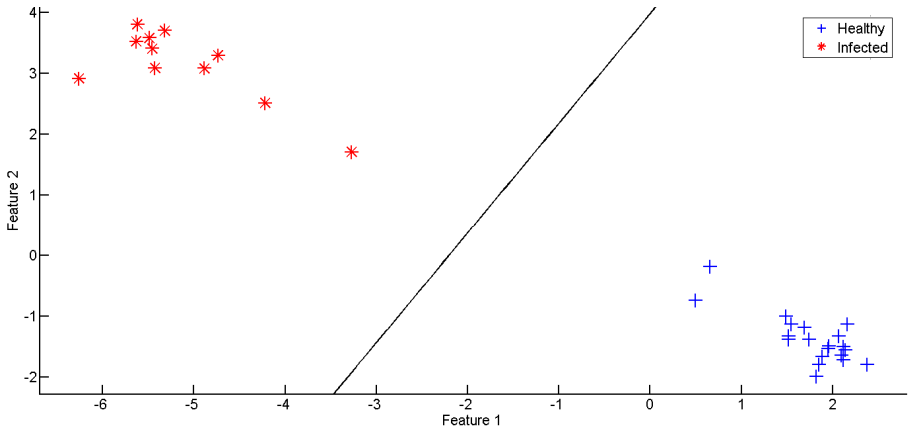

Figure 5.15: Decision boundary produced by LDA on 6 DPI

Using LDA with cross validation, classification accuracy of 83%, 89%, 90% and 90% on 2 DPI, 4 DPI, 6 DPI and 10 DPI datasets was achieved respectively. Classifying the dataset generated by the above method has took on average 79 seconds (including pre-processing). These times were based on the calculation conducted on an 8 Core Xenon PC with 24 GB of RAM.

5.7 Discussion

In this study, the utility of a novel, non-destructive and rapid technology to distinguish between VOC profiles released by healthy and infected tomato plants were demonstrated. VOC profiles of tomato plants were sampled using a FAIMS device based on the experimental procedure outlined in chapter 3. The uniqueness of this study is the use of such specific non-invasive tests which to the best of the author's knowledge is the first demonstration of the detection of diseases in plants via FAIMS technology. The results not only confirmed the previous studies which reported the substantial differences in VOC composition of the two groups but also proved that FAIMS technology is capable of detecting such differences. This was further verified by repeating the analysis in two separate experiments using the same instrument and in a similar conditions. Specifically, the findings from both experiments showed that LDA is able to classify the 4 DPI dataset with the accuracy of 90%. This is before the occurrence of severe visual symptoms on plant's leaves. Additionally, a pattern of disease development was observed by analysing samples for the period of the experiment.

As expressed in chapter 2, other analytical instruments such as GC-MS can successfully identify individual plant's VOCs but are often complicated, time consuming and expensive. Here, it was demonstrated that investigating the overall pattern (composition) of the plant VOC using FAIMS and EN is more decisive and yet accessible. Unlike gas sensor arrays (i.e. ENs) which have been extensively studies and commercialised, FAIMS is an interesting technology for future development. It offers the advantage of high sensitivity, can

operate at room temperature flawlessly and does not require special carrier gases (as with GC or GC-MS). The specific FAIMS devices employed in this study had built-in air pump, flow regulator and environmental sensors which offered a rapid solutions for sampling the VOCs. The analysis technique may be incorporated into the device for an all-in one solution. The device can be deployed in a short amount of time with a minimum time required for sampling and analysis of the result making it an attractive option for a non-destructive alternative. Unlike EN, the sensitivity of the sensors built into FAIMS does not change rapidly with time which means minimum maintenance, sensor replacement and calibration is required. Undoubtedly, FAIMS is still in its infancy but the technique is proved to be powerful, it therefore seems likely that as research continues the instrument will improve further making it applicable in different industries [28].

5.8 Summary

In this chapter the fundamentals of FAIMS technology were reviewed. A FAIMS device was employed to sample the VOCs emitted from healthy and diseased plants in order to discriminate between them. The classifiers managed to discriminate between healthy and infected plants with a high degree of accuracy. A time series was also produced outlining the development of powdery mildew disease in the plants. The overall result indicates that FAIMS when coupled with an appropriate processing techniques was able to detect powdery mildew infected tomato plant by sampling the emitted VOC profiles. The next chapter will introduce two potential applications using synchronisations of chaotic dynamical systems and external bias.

5.9 Reference

1. ODonnell, R.M., X. Sun, and P.d.B. Harrington, Pharmaceutical applications of ion mobility spectrometry. TrAC Trends in Analytical Chemistry, 2008. 27(1): p. 44-53.

2. Ewing, R.G., et al., A critical review of ion mobility spectrometry for the detection of explosives and explosive related compounds. Talanta, 2001. 54(3): p. 515-529.

3. Eiceman, G.A. and H. Schmidt, Chapter 9 - Advances in Ion Mobility Spectrometry of Explosives, in Aspects of Explosives Detection, M. Maurice and C.O. Jimmie, Editors. 2009, Elsevier: Amsterdam. p. 171-202.

4. Gursoy, O., P. Somervuo, and T. Alatossava, Preliminary study of ion mobility based electronic nose MGD-1 for discrimination of hard cheeses. Journal of Food Engineering, 2009. 92(2): p. 202-207.

5. Karpas, Z., et al., Determination of volatile biogenic amines in muscle food products by ion mobility spectrometry. Analytica Chimica Acta, 2002. 463(2): p. 155-163.

6. Lu, Y., R.M. ODonnell, and P.B. Harrington, Detection of cocaine and its metabolites in urine using solid phase extraction-ion mobility spectrometry with alternating least squares. Forensic Science International, 2009. 189(13): p. 54-59.

7. Shahdousti, P. and N. Alizadeh, Headspace-solid phase microextraction of selenium(IV) from human blood and water samples using polypyrrole film

and analysis with ion mobility spectrometry. Analytica Chimica Acta, 2011. 684(12): p. 67-71.

8. Mrquez-Sillero, I., et al., Ion-mobility spectrometry for environmental analysis. TrAC Trends in Analytical Chemistry, 2011. 30(5): p. 677-690.

9. Johnson, P.V., et al., Ion mobility spectrometry in space exploration. International Journal of Mass Spectrometry, 2007. 262(12): p. 1-15.

10. Palmer, P.T. and T.F. Limero, Mass spectrometry in the U.S. space program: past, present, and future. Journal of the American Society for Mass Spectrometry, 2001. 12(6): p. 656-675.

11. Buxton, T.L. and P.d.B. Harrington, Rapid multivariate curve resolution applied to identification of explosives by ion mobility spectrometry. Analytica Chimica Acta, 2001. 434(2): p. 269-282.

12. Lawrence, A.H., Detection of drug residues on the hands of subjects by surface sampling and ion mobility spectrometry. Forensic Science International, 1987. 34(12): p. 73-83.

13. Eiceman, G.A., Ion-mobility spectrometry as a fast monitor of chemical composition. TrAC Trends in Analytical Chemistry, 2002. 21(4): p. 259-275.

14. Armenta, S., M. Alcala, and M. Blanco, A review of recent, unconventional applications of ion mobility spectrometry (IMS). Analytica Chimica Acta, 2011. 703(2): p. 114-123.

15. Cudjoe, K.S., et al., Detection of Clostridium perfringens type A enterotoxin in faecal and food samples using immunomagnetic separation (IMS)-

ELISA. International Journal of Food Microbiology, 1991. 12(4): p. 313-321.

16. Reid Asbury, G., J. Klasmeier, and H.H. Hill Jr, Analysis of explosives using electrospray ionization/ion mobility spectrometry (ESI/IMS). Talanta, 2000. 50(6): p. 1291-1298.

17. Dworzanski, J.P., et al., Fieldportable, automated pyrolysisGC/IMS system for rapid biomarker detection in aerosols: A feasibility study. Field Analytical Chemistry & Technology, 1997. 1(5): p. 295-305.

18. Buryakov, I.A., et al., A new method of separation of multi-atomic ions by mobility at atmospheric pressure using a high-frequency amplitude-asymmetric strong electric field. International Journal of Mass Spectrometry and Ion Processes, 1993. 128(3): p. 143-148.

19. Kolakowski, B.M. and Z. Mester, Review of applications of high-field asymmetric waveform ion mobility spectrometry (FAIMS) and differential mobility spectrometry (DMS). Analyst, 2007. 132(9): p. 842-864.

20. Wu, L. and F.G. Vogt, A review of recent advances in mass spectrometric methods for gas-phase chiral analysis of pharmaceutical and biological compounds. Journal of Pharmaceutical and Biomedical Analysis, 2012. 69(0): p. 133-147.

21. Nanotech, O., FAIMS White Paper. New York, NY, 2006.

22. Guevremont, R. and R.W. Purves, Atmospheric pressure ion focusing in a high-field asymmetric waveform ion mobility spectrometer. Review of Scientific Instruments, 1999. 70(2): p. 1370-1383.

23. Guevremont, R. and R.W. Purves, High field asymmetric waveform ion mobility spectrometrymass spectrometry: an investigation of leucine enkephalin ions produced by electrospray ionization. Journal of the American Society for Mass Spectrometry, 1999. 10(6): p. 492-501.

24. Guevremont, R., et al., Calculation of ion mobilities from electrospray ionization high-field asymmetric waveform ion mobility spectrometry mass spectrometry. The Journal of Chemical Physics, 2001. 114: p. 10270.

25. Du, J., et al. Wavelet Transform and Bagging Predictor Approaches to Cancer Identification from Mass Spectrometry-Based Proteomic Data. in Bioinformatics and Biomedical Engineering , 2009. ICBBE 2009. 3rd International Conference on. 2009.

26. Andrade, L. and E.S. Manolakos, Signal Background Estimation and Baseline Correction Algorithms for Accurate DNA Sequencing. The Journal of VLSI Signal Processing, 2003. 35(3): p. 229-243.

27. Monchamp, P., et al., Signal Processing Methods for Mass Spectrometry. Systems Bioinformatics: An Engineering Case-Based Approach, Artech House Publishers, 2007.

28. Gardner, J. W., McIntosh, J., Ouaret, N., Gold, P., Nwokolo, C., Bardhan, K., Covington, J. Classification Of Field Asymmetric Ion Mobility Spectrometry Data For Detection Of Bowel Bacteria.

29. Arasaradnam, R. P., Ouaret, N., Thomas, M. G., Gold, P., Quraishi, M. N., Nwokolo, C. U. (2012). Evaluation of gut bacterial populations using an electronic e-nose and field asymmetric ion mobility spectrometry:

further insights into'fermentonomics'. Journal of Medical Engineering and Technology, 36(7), 333-337.

30. Jurs, P. C., Bakken, G. A., McClelland, H. E. (2000). Computational methods for the analysis of chemical sensor array data from volatile analytes. Chemical Reviews, 100(7), 2649-2678.

Chapter 6

Exploration of de-synchronisation of coupled chaotic systems for usage in signal processing and measurements

6.1 Chapter Overview

The objectives of this chapter is three-fold: **first**, the features and characteristics of synchronisation in chaotic dynamical systems particularly Lorenz's chaotic equations will be discussed leading to the master-slave synchronisation of multiple, identical, chaotic systems. **Second**, the addition of external bias as well as parameters mismatch between master and slave systems will be presented, exploring the departure from synchronous regime, thats when the

systems de-synchronise. **Third**, the chapter closes by presenting two potential application in Nano-electromechanical Systems (NEMS) which will benefit from such chaotic de-synchronisation platform. This study is the first to present the synchronisation of multiple Nano-mechanical Duffing Resonators using the open-plus-close-loop (OPCL) control method and demonstrate the relationship between the synchronisation error and an added bias. The application of the schema is demonstrated in the special type of sensor arrays, namely the ENs with two coupled mechanical cantilever sensors. Additionally, two identical cantilevers commonly used in Atomic Force Microscopy will be synchronised in a novel approach to enable a detection of measurement signal by calculating the error of the non-synchronised region based on the parameters mismatch.

6.2 Introduction

Mathematical modelling attempts to **a)** provide a robust and optimised method for solving problems mathematically and **b)** construct and define a model which signifies the association of two or multiple variables applicable to a given situation or problem. Such models - as an abstraction of reality - have relentlessly helped mathematicians to understand and describe the complex natural and physical phenomena magnifying their related behaviour, functional form, variables and parameters. Mathematical models can take many forms and shapes, including but not limited to Dynamical Systems (DS), statistical models, descriptive models, optimisation models or game theoretic models.

6.3 Dynamical Systems

DS - often described by couple or series of linear or nonlinear ODEs (Ordinary Differential Equations) - have been extensively used for mathematical modelling purposes due to their capabilities in building a multi-dimensional model of a complex real-world system. DS theory attempts to understand and describe the changes over time that occur in natural, physical and artificial systems which exhibit complex behaviour such as the solar system (motion of stars and planets) [1], climate change [2], stock markets [3], formation of traffic jams [4], growth of crystals [5] or simply the movement of a basic pendulum [6].

A DS may be *linear* or *nonlinear*, *autonomous* or *non-autonomous*, *conservative* or *non-conservative*, *discrete* or *continuous*, *stochastic* or *deterministic* and *one-dimensional* or *multidimensional*.

6.4 DS Stability

The property of *stability* is one of the important characteristics of motions realised in a DS, since stable regimes are observed in a majority of situations. Followings are the definitions of different stability types [7].

6.4.1 Lyapunov Stability

A solution $\bar{x}(t)$ is said to be *Lyapunov stable* if for each small $\epsilon > 0$ there exists $\delta = \delta(\epsilon, t_0) > 0$ such that $\|x(t_0) - \bar{x}(t_0)\| < \delta$ then $\|x(t_0) - \bar{x}(t_0)\| < \epsilon$ for all $t > t_0$.

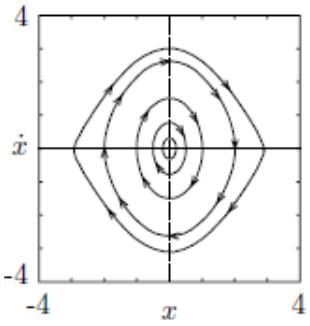

Figure 6.1: An example of 2-dimensional system, which is stable in the sense of Lyapunov

6.4.2 Asymptotic Stability

A solution $\bar{x}(t)$ is said to be *asymptotically stable* if it is Lyapunov stable and there exists δ such that $\|x(t_0) - \bar{x}(t_0)\| < \delta$ then $\|x(t) - \bar{x}(t)\| \to 0$ as $t \to \infty$.

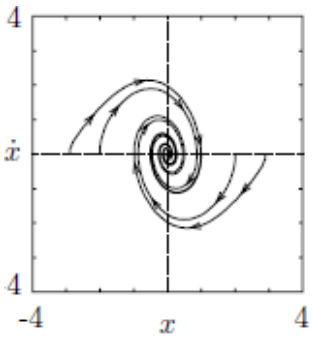

Figure 6.2: An example of 2-dimensional system, which is asymptotically stable

6.4.3 Uniform Stability

A solution $\bar{x}(t)$ is said to be *uniformly stable* if for each small $\epsilon > 0$ there exists δ, independent of t_0, such that if $\|x(t_0) - \bar{x}(t_0)\| < \delta$ for some $t_0 \in R$ then $\|x(t) - \bar{x}(t)\| < \epsilon$ for all $t > t_0$. For time-invariant DS, Lyapunov stability

implies uniform stability [8].

6.4.4 Global and Local Stability

Denitions 6.4.1 and 6.4.2 are *local* stability denitions. They describe the behaviour of a system near an equilibrium point. An equilibrium point x^* is *globally* stable if it is stable for *all* initial conditions $x_0 \in R^n$. Global stability is very desirable, but in many applications it can be difficult to achieve.

6.4.5 DS Attractors

Considering the phase space R^N of a DS, let G_1 be some finite (or infinite) region belonging to R^N and including a subregion G_0 into itself. The regions G_1 and G_0 satisfy the following conditions:

1. For any initial conditions $x_i(0)$ from the region G_1 all phase trajectories will reach sooner or later the region G_0 as $t \to \infty$.

2. The region G_0 is a minimal compact subset in the system phase space.

3. If a phase trajectory belongs to the region G_0 at the time moment $t = t_1$, then it will always belong to G_0 for any $t \geq t_1$.

If conditions 1-3 are satisfied, then the region G_0 is called the *attractor* of a DS. G_1 is called the *region* (or basin) of attraction of the attractor G_0. Attractors with a complicated geometrical structure (fractals) are known as *strange attractors* [7].

6.5 Lyapunov Exponents

Lyapunov exponents are the average rates of divergence or convergence of nearby orbits in phase space. The trajectory stability is defined by a set of N Lyapunov exponents where N is equal to the dimension of the phase space. The set of N numbers arranged in decreasing order, $\lambda_1 \geqslant \lambda_2 \geqslant \cdots \geqslant \lambda_N$, forms the so-called *Lyapunov characteristic exponents spectrum* (LCE spectrum) of phase trajectory [7]. The signs of the Lyapunov exponents provide a qualitative picture of a systems dynamics. Any system containing at least one positive Lyapunov exponent may poses chaotic behaviour [9]. Sum of all Lyapunov exponents defines the divergence of a volume in the phase space: if the sum is negative then DS is dissipative and the volume tends to zero with time goes to infinity.

6.6 Chaotic Dynamical Systems

Chaotic attractors have two fundamental properties: complex geometric structure and exponential instability of individual trajectories. It is these properties that are used as a criterion for diagnostics of the regimes of deterministic chaos. Chaotic systems also display exponentially sensitive dependence on *initial conditions* (x_0), meaning that nearby trajectories separate exponentially [7].

The Lyapunov exponents has proven [10-12] to be the most useful dynamical diagnostic for chaotic systems. The LCE spectrum of a chaotic solution always has at least one positive Lyapunov exponent ($\lambda > 0$) [13], however the sum of all exponents is negative or zero. Phase trajectories starting from

Chaotic System	Dimension	Equations	Parameters
Henon Map [15]	2D	$\begin{cases} X_{n+1} = 1 - aX_n^2 + Y_n \\ Y_{n+1} = bX_n \end{cases}$	$\begin{cases} a = 1.4 \\ b = 0.3 \end{cases}$
Rossler System [16]	3D	$\begin{cases} \dot{x} = -(y + x), \\ \dot{y} = x + ay, \\ \dot{z} = zx - cz + b. \end{cases}$	$\begin{cases} a = 0.15 \\ b = 0.20 \\ c = 10.0 \end{cases}$
Chen System [17]	3D	$\begin{cases} \dot{x} = a(y - x), \\ \dot{y} = (c - a)x + cy - xz, \\ \dot{z} = zy - bz. \end{cases}$	$\begin{cases} a = 35.0 \\ b = 3.0 \\ c = 28.0 \end{cases}$
Lorenz System [18]	3D	$\begin{cases} \dot{x} = a(y - x), \\ \dot{y} = rx - y - xz, \\ \dot{z} = xy - bz. \end{cases}$	$\begin{cases} a = 10.0 \\ r = 28.0 \\ b = 8 \div 3 \end{cases}$

Table 6.1: Examples of 2D and 3D chaotic equations

close initial points in the basin of attraction tend to the attractor but they are separated from each other on it. Finally, chaotic systems has no random or noisy inputs or parameters and the irregular behaviour arises from the systems nonlinearity rather than from noisy elements. This characterises them as a deterministic chaotic system [14].

Table 6.1 summarises four well-known chaotic equations and their parameters. Additionally, Sprott [19] proposed a collection of 19 chaotic equations that are similar but simpler than the Lorenz's and Rossler's systems.

6.7 Lorenz System

Ed Lorenz (1963) [20] derived the following three-dimensional system from a significantly simplified model of convention rolls in the atmosphere [18]:

$$\begin{cases} \dot{x} = \sigma(y - x), \\ \dot{y} = rx - y - xz, \\ \dot{z} = xy - bz. \end{cases} \tag{6.1}$$

Where $\sigma, r, b > 0$ are parameters. σ is the Prandtl number, r is the Rayleigh number and b has no universal name although in the Lorenz's problem it is related to the aspect ratio of the rolls/cylinders. Lorenz discovered that this deterministic system could have extremely erratic dynamics. Over a wide range of parameters, the solutions oscillate irregularly, never exactly repeating but always remaining in a bounded region of phase space. For some values of the parameters, Lorenz system has a positive Lyapunov exponent indicating chaos. Fig. 6.3 illustrates a plot of a solution when $r = 28$, $\sigma = 10$, and $b = 8/3$ also known as the Lorenz attractor.

Fig. 6.4 shows a projection of the phase space orbit onto the XY, XZ and YZ planes. It can be observed that the solution spirals outward from of the equilibria for some time, then switches to spiralling outward from the other equilibrium point. This pattern repeats forever with the number of circuits around an equilibrium before switching appears to change in an erratic manner.

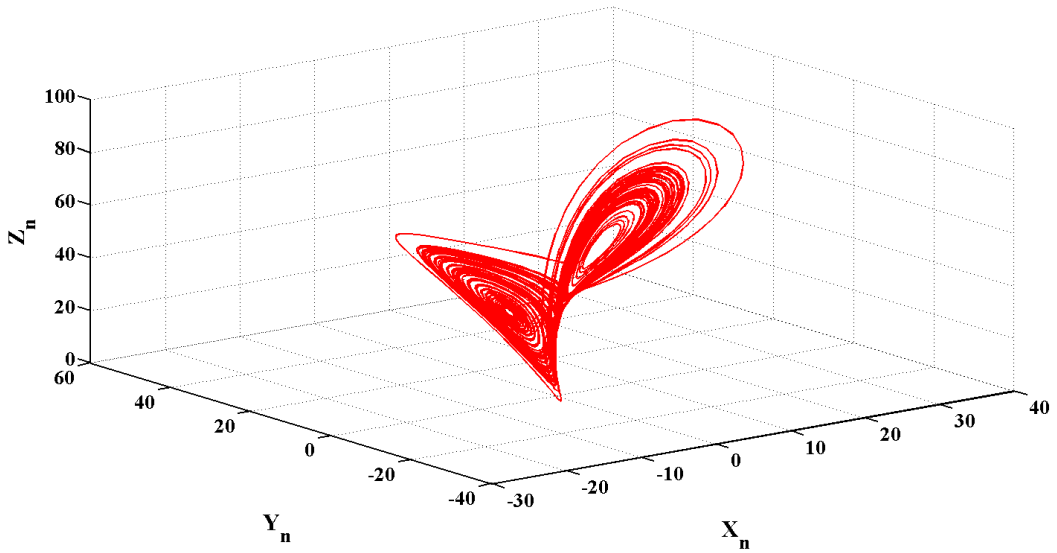

Figure 6.3: Strange attractor of Lorenz chaotic system

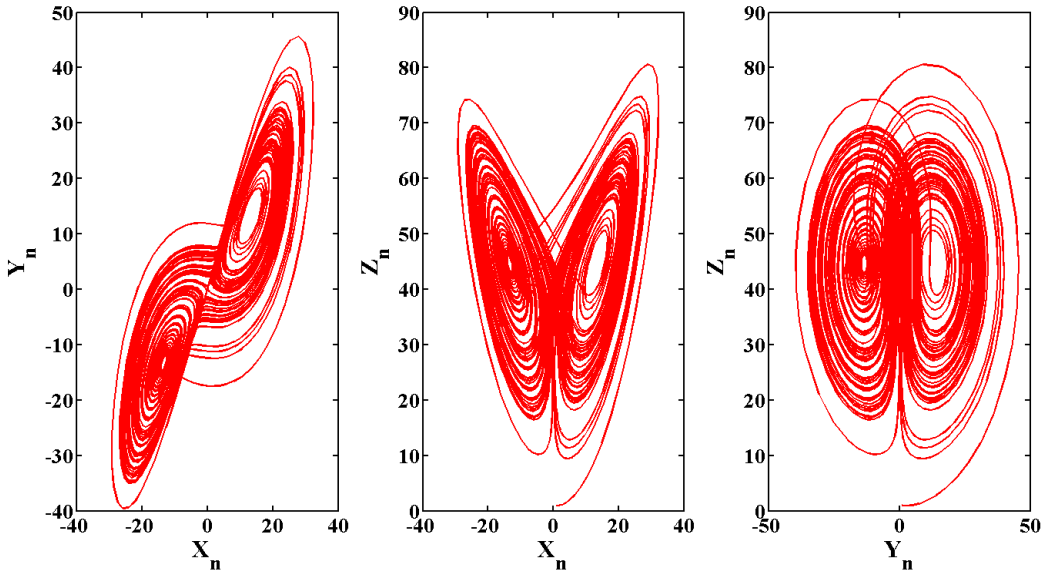

Figure 6.4: 2D illustration of the Lorenz chaotic systems representing (X, Y, Z)

Figure 6.5 shows the time series for Lorenz variables x, y and z.

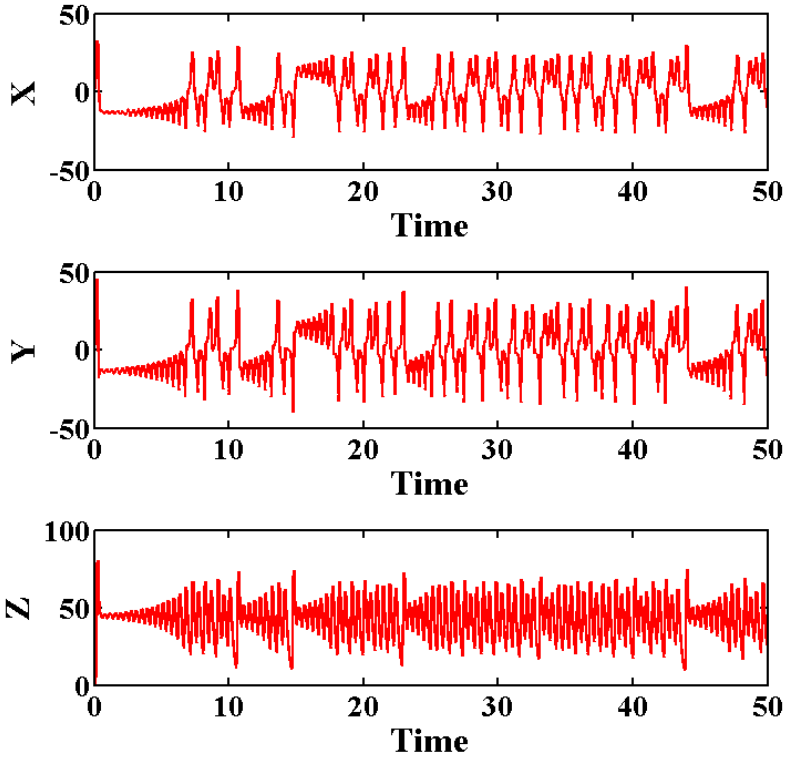

Figure 6.5: Time series of (x, y, z) vs. time evolution

6.8 Synchronisation

Christian Huygens first observed the synchronisation of two pendulum clocks in 17th century [21]. Huygens found that the coupled pendulum clocks swung at exactly the same frequency and out of phase when are within certain distance. The phenomena was resulted by the very small movements of the common frame supporting the two clocks. When he disturbed one pendulum the anti-phase state was restored within half an hour and pendulum clocks remained synchronised indefinitely if left undisturbed [22].

Originally, it was thought that chaos, in essence, is neither predictable nor controllable due to their extreme sensitivity to small uncertainties in their initial conditions. This attitude was gradually changed when Pecora [23], Ott and others [28] demonstrated systematic controllability of chaos in dynamical systems.

6.9 Synchronisation of Chaotic Systems

Fundamentally, chaotic systems defy synchronisation as even two identical systems starting from slightly different initial conditions will evolve in time in an unsynchronised manner [7]. Identical chaotic systems, run side by side, starting both at close but not exactly equal conditions, soon diverge from each other, but both retain the same attractor pattern were each is on its own attractor has no relation to where the other system is [24]. The objective of chaotic synchronisation is to force the two or multiple chaotic systems to follow the same path on the attractor [23].

Synchronisation of chaotic systems have implemented or at least experimented in several fields including communication [25-27], electronic circuits [28, 29], chemical reactions [30, 31], lasers [32, 33], robotics [34, 35], fluids [36, 37] and biological/biomechanical systems [38-40]. Chaotic synchronisation was also suggested as a platform for some security communications schemes [41-44].

6.9.1 Synchronisation Types

In regards to coupled identical systems, synchronisation appears as the equality of the state variables while evolving in time. This type of synchronisation

is known as *complete*, *full* or *identical* synchronisation. Additional types of synchronisation have appeared in literature including *phase synchronisation* [45], *lag synchronisation* [46] and *generalised synchronisation* [47].

When dealing with coupling of systems, two different options are available: **a)** *bidirectional coupling* in which both systems are connected in such a way that they mutually influence each other's behaviour and **b)** *unidirectional coupling*, in which the evolution of one of the coupled systems is remained unaltered. The resulting configuration is referred to as *drive-response* or *master-slave* synchronisation [48].

6.9.2 Master-Slave Synchronisation of Chaotic Systems

Here the master system is given by the Lorenz system such that:

$$\begin{cases} \dot{x_1} = \sigma(y_1 - x_1), \\ \dot{y_1} = rx_1 - y_1 - x_1 z_1, \\ \dot{z_1} = x_1 y_1 - b z_1. \end{cases} \tag{6.2}$$

and the slave system is the subspace containing the (x,y) variables:

$$\begin{cases} \dot{y_2} = -x_1 z_2 + r x_1 - y_2, \\ \dot{z_2} = x_1 y_2 - b z_2. \end{cases} \tag{6.3}$$

A signal is transmitted from the master to the slave system. In this case the signal is the x component of the master system. Thus, all the x component in slave system are replaced with the signal from the master system which is

called complete replacement [23].

As demonstrated in figure 6.6, Eq. (6.2) and Eq. (6.3) have the initial values of $[-10, -10, -10]$ and $[55, 55]$ respectively. As the system evolves, y_2 converges to y_1 and z_2 converges to z_1. After a period of time, the motion causes the two equalities $y_2 = y_1$ and $z_2 = z_1$. Thereafter, the y and z components of both systems stay equal to each other as the system evolves manifesting identical synchronisation [23].

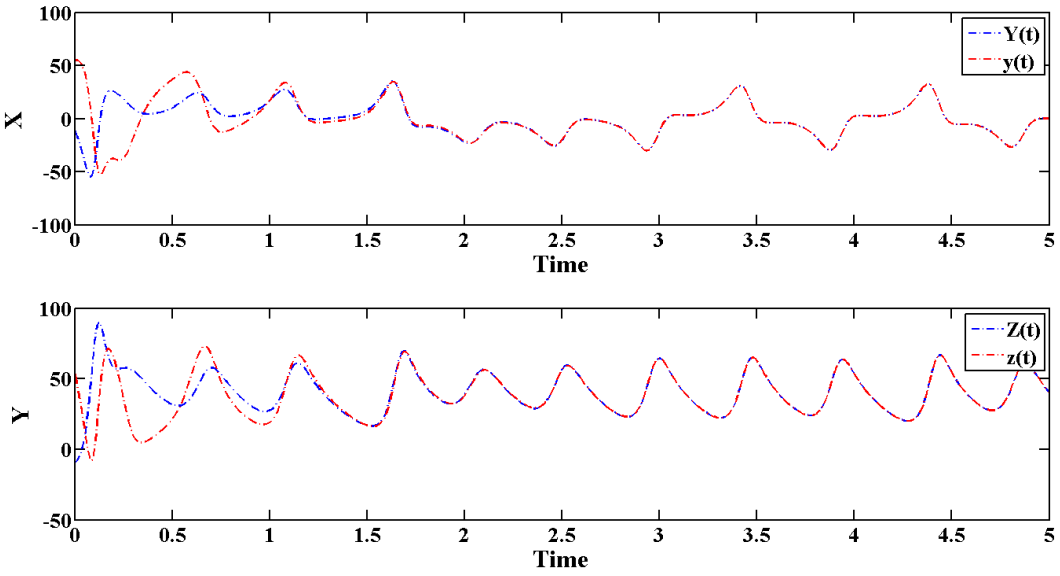

Figure 6.6: Synchronisation of Lorenz system

6.9.3 Synchronisation of Lorenz System Using OPCL

Consider a generic, multidimensional, master system:

$$\dot{X} = F(X), \quad X \in R^n \tag{6.4}$$

The open-loop designs an external excitation based on the control goal, which is a particular solution of the slave system [49]. To reach the control by open-loop alone it is required that trajectory is located in suitable regions of the state space (called convergent regions) and that master and slave systems have particular initial conditions (called the basin of entrainment) when the control is activated. To overcome these limitations the closed loop (feedback loop) is added into the scheme for forming OPCL method [49]. Thus, the slave system will have the following form:

$$\dot{x} = F(x) + S(t)(A - dF(X)/dX)(x - X) \tag{6.5}$$

assures $x(t) \to X(t)$ for any $\|x(0) - X(0)\|$ small enough. Here, A is a constant matrix with negative real part eigenvalues and $S = 0$ or 1 as a synchronisation switch. So, in principle, any two oscillators can be synchronised.

Now, let's consider two identical Lorenz systems, the master (X, Y, Z) and the slave (x, y, z). The master system is defined as follows [34]:

$$\begin{cases} \dot{X} = s(Y - X); \\ \dot{Y} = rX - Y - XZ \\ \dot{Z} = XY - bZ. \end{cases} \tag{6.6}$$

Where $s = 16, r = 45.6$ and $b = 4$. The chosen (s, r and b) values assure chaotic behaviour.

The matrix (dFX/dX) for EQ. (6.6) is:

$$\begin{pmatrix} -s & s & 0 \\ r-Z & -1 & -X \\ Y & X & -b \end{pmatrix} \tag{6.7}$$

A has to have a parameter p that can be adjusted in order that its eigenvalues have a negative real part. The parameter p is set in one position of variable terms in order to keep the number of terms to no more than four. Thus, a suitable form for A is:

$$A = \begin{pmatrix} -s & s & 0 \\ r+p & -1 & 0 \\ 0 & 0 & -b \end{pmatrix} \tag{6.8}$$

and the driven slave system is:

$$\begin{cases} \dot{x} = s(y-x), \\ \dot{y} = rx - y - xz + S[X(z-Z) + (Z+p)(x-X)], \\ \dot{z} = xy - bz + S[-X(y-Y) - Y(x-X)]. \end{cases} \tag{6.9}$$

where p is a parameter that has to be determined in order to have $(x, y, z) \rightarrow (X, Y, Z)$. The matrix (6.8) has eigenvalues with a negative real part if [49]:

$$p < 1 - r \tag{6.10}$$

The system in the form of $u = (u_1, u_2, u_3) = (x - X, y - Y, z - Z)$ has fixed points at $(0, 0, 0)$, which corresponds to a synchronised regime, and is identified as:

$$\begin{cases} \dot{u_1} = s(u_2 - u_1), \\ \dot{u_2} = (r + p)u_1 - u_2 - u_1 u_3, \\ \dot{u_3} = -bu_3 + u_1 u_2. \end{cases} \tag{6.11}$$

Figure 6.7 illustrates the result of the numerical simulation in which the Root Mean Square Error (RMSE) of the synchronisation is observed in relation to the value of the p parameter using the following equations:

$$RMSE = \sqrt{\langle (x - X)^2 + (y - Y)^2 + (z - Z)^2 \rangle} \tag{6.12}$$

Here, the brackets $\langle\rangle$ denote time averaging. As it is seen the system remains synchronised when $p < 1 - r$ as predicted by (6.10). Once the condition is violated the system loses the synchronisation and the RMSE monotonically increases with the growth of p.

Figure 6.8 demonstrates the synchronisation of master and slave systems using $p = -60$, with the initial conditions of $(X = Y = Z = 5)$ and $(x = y = z = -5)$. The time step is 0.001 and the S value is initially 0 but then changed to 1 after 1850 time steps. The two systems are synchronised after 2000 time steps even though their initial states were set to different values. There are no limitations on the dimensions of the systems.

Differential equations (6.9) and (6.11) were solved using medium order solver (ODE45) in MATLAB. Note, that other numerical schemes give similar re-

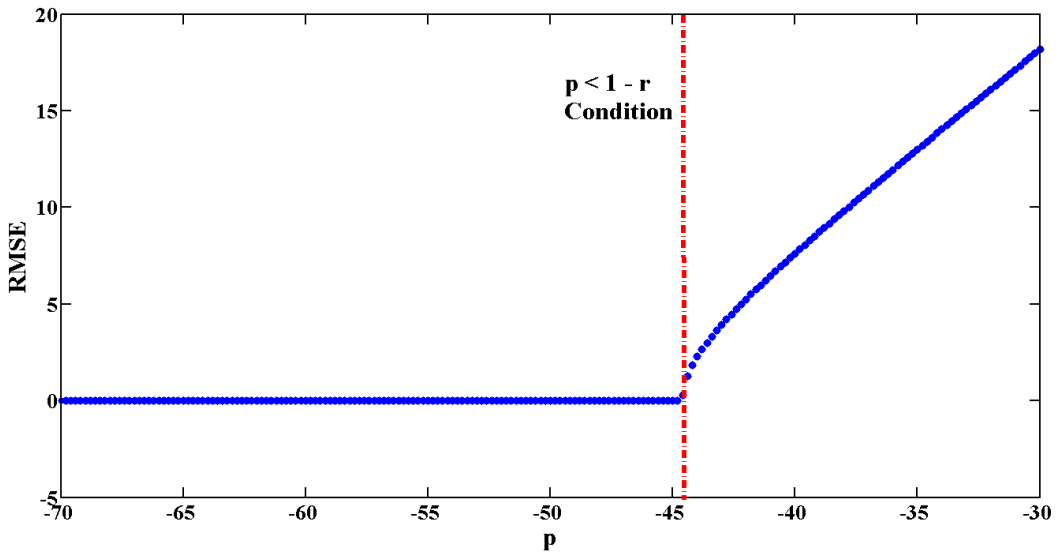

Figure 6.7: RMSE vs. the value of p parameter. The error increases when the condition $p < 1 - r$ is violated

sults. The author would also like to acknowledge the *shadowing lemma* in numerical computation of dynamical systems. Since numbers are represented in computers with finite precision, there will typically be a small difference between the true solution and how it is registered on a computer [60]. Numerical simulation of ordinary differential equations inevitably introduces errors to solutions via round-off errors of computer operations and truncations errors of numerical schemes [61, 62]. Therefore, any numerical solution would have a noisy (stochastic) component and properties of this component will depend on numerical scheme in use. As a result, trajectories of differential equation will be different for even the slightly different parameters of the same numerical scheme in the case of chaotic system. However, the statistical properties of the solution would remain the same. The last statement is based on the current development of the theory of chaotic dynamical system in the form of a conjecture of Palis [63] that a typical chaotic attractor is a union of a finite

number of hyperbolic sets and the property of the shadowing of trajectories. It was shown [63-65] that the hyperbolic attractor is robust with respect to noise, i.e. a noisy trajectory is the "shadow" of a "true" trajectory: perturbations slightly change some characteristics of the attractor, e.g. the invariant measure, Lyapunov exponents, and correlations.

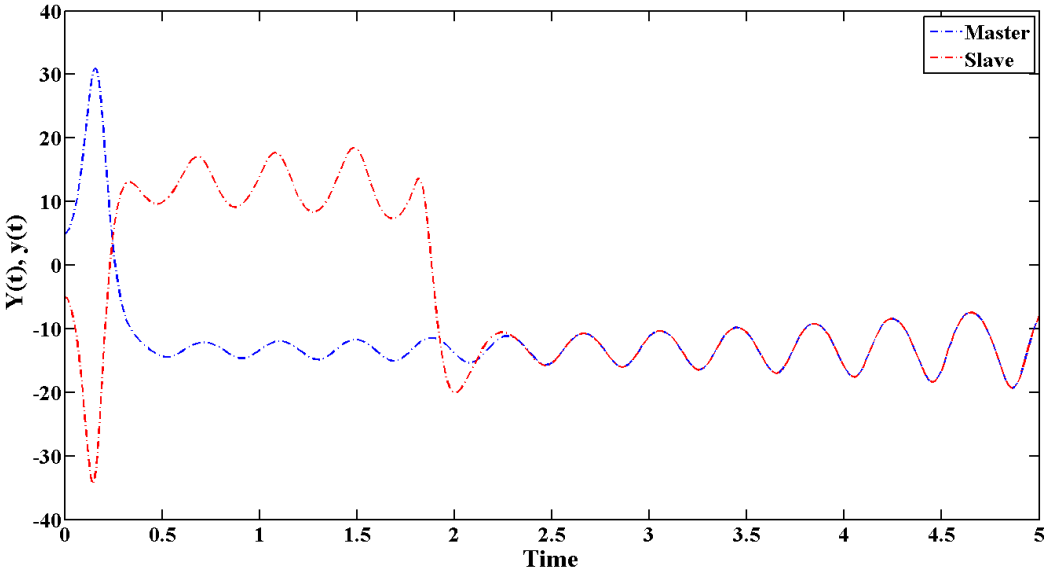

Figure 6.8: Synchronisation of two identical Lorenz systems (X, Y, Z) and (x, y, z) as described in the text

6.9.4 Generic Model

The following slave system is the model which may be used to synchronise a single master and multiple number of slave systems. If the master system has (X, Y, Z) and slave i has $(x_{i+1}, y_{i+1}, z_{i+1})$, the differential equations for slave i

will be:

$$\begin{cases} \frac{dx_{(i+1)1}}{dt} = s(x_{(i+1)2} - x_{(i+1)1}), \\ \\ \frac{dx_{(i+1)2}}{dt} = rx_{(i+1)1} - x_{(i+1)2} - x_{(i+1)1} * x_{(i+1)3} + \\ S[x_{1,1} * (x_{(i+1)3} - x_{1,3}) + (x_{13} + p) * (x_{(i+1)1} - x_{11})], \\ \\ \frac{dx_{(i+1)3}}{dt} = x_{(i+1)1}x_{(i+1)2} - bx_{(i+1)3} + \\ S[-x_{1,1}(x_{(i+1)2} - x_{1,2}) - x_{1,2}(x_{(i+1)1} - x_{1,1})]. \end{cases} \tag{6.13}$$

Figure 6.9 demonstrates the synchronisation of one master and four slave systems with different initial state (x_0). Here, the initial state for $(X, Y, Z) = 10, (x_1, y_2, z_3) = 5, (x_4, y_5, z_6) = 1$ and $(x_7, y_8, z_9) = -5$ and finally $(x_{10}, y_{11}, z_{12}) = -10$. All the three systems are synchronised after 2000 time steps.

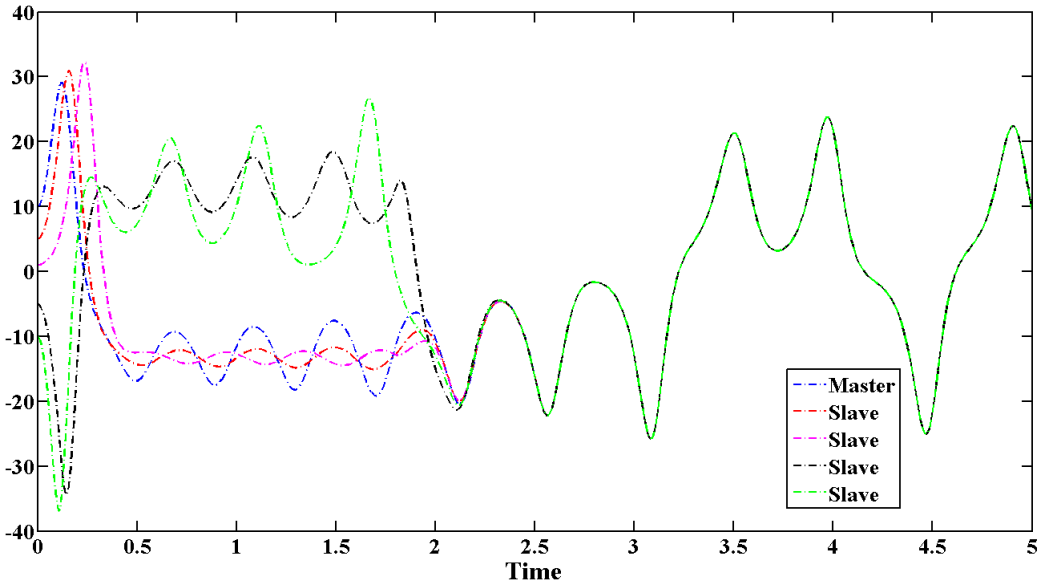

Figure 6.9: Synchronisation of four identical Lorenz systems master, slave 1, slave 2, slave 3 and slave 4

6.10 Addition of Bias

The OPCL technique discussed in the previous section is implemented to synchronise two or more identical chaotic systems. Here, the aim is to consider the influence of the addition of a bias (B) to the slave system. It is expected that the presence of the bias B will lead to de-synchronisation of the coupled systems. Subsequently, by calculating the error of synchronisation, one can estimate a value of the bias B, that can be used in measurements strategies as discussed below. The process involves the following steps:

1. Configure two identical chaotic systems: Master (X, Y, Z) and Slave (x, y, z).

2. Set the initial conditions to different values. Potentially, the initial conditions of both master and slave systems can be identical ensuring that both systems are synchronised from the starting point which eliminates the initial chaotic transient time.

$$X(0) = Y(0) = Z(0) = x(0) = y(0) = z(0) = 1 \tag{6.14}$$

3. Allow the two systems to synchronised so $(x, y, z) \rightarrow (X, Y, Z)$.

4. Once the transient synchronisation time in chaotic region is passed, add the bias (B_1, B_2, B_3) to the slave system.

$$\begin{cases} \dot{x} = s(y - x) + B_1, \\ \dot{y} = rx - y - xz + S[X(z - Z) + (Z + p)(x - X)] + B_2, \\ \dot{z} = xy - bz + S[-X(y - Y) - Y(x - X)] + B_3. \end{cases} \tag{6.15}$$

5. The addition of bias (B_1, B_2, B_3) forces the two systems to desynchronise and therefore the error of synchronisation $(e_{x-X}, e_{y-Y}, e_{z-Z})$ can be computed at every time step t_i:

$$\begin{aligned} \Delta e_{x,i} &= (x - X)^2 \\ \Delta e_{y,i} &= (y - Y)^2 \\ \Delta e_{z,i} &= (z - Z)^2 \end{aligned} \tag{6.16}$$

6. Finally, an overall error may be calculated in the form of RMSE as follow:

$$RMSE = \sqrt{\langle (x - X)^2 + (y - Y)^2 + (z - Z)^2 \rangle} \tag{6.17}$$

Figure 6.10 demonstrates the three regions of system dynamics of the process. The first phase is dedicated to the transient time needed for the synchronisation in which the systems have unstable characteristics (if initial conditions are not identical). In the second phase, both systems are fully synchronised and therefore the error approaches zero. In the third region the bias value is added thus the systems departs from the synchronised regime and enters the de-synchronised region. Evidently, in this phase the error variance can be computed.

Calculating the RMSE (eq. 6.17) will give the overall error of synchronisation based on the added bias. Figure 6.11 illustrates the change of RMSE during the synchronisations in respect to the added bias. The RMSE was observed when a single bias B_1 or B_2 or B_3 is added to the single equation in the slave system through the synchronisation process as described in eq. 6.15.

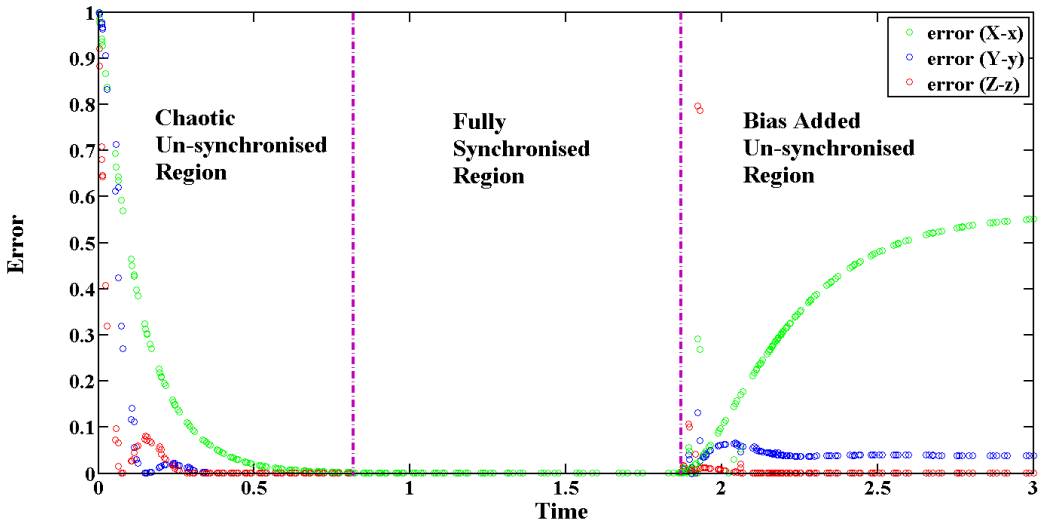

Figure 6.10: Three regions of system dynamics: chaotic un-synchronised region, fully synchronised region and unsynchronised region due to the added bias

It also demonstrates the variation of RMSE with respect to the addition of multiple biases (B_1 and B_2 and B_3). The RMSE and bias demonstrate a linear relationship when all three biases are added to the synchronisation procedure.

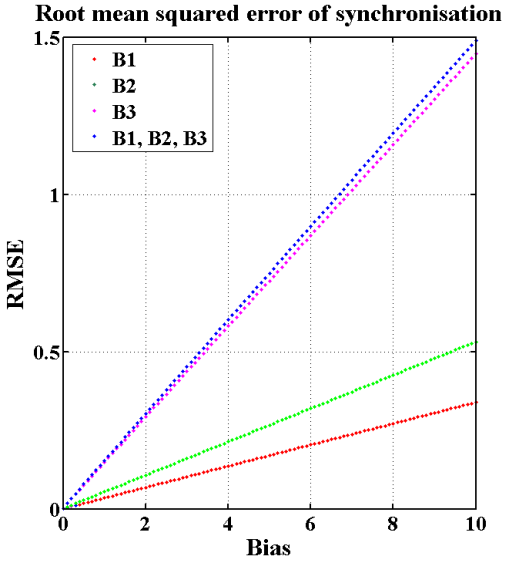

Figure 6.11: RMSE vs. the value of the added bias

As it was shown above even a small bias acting on the slave system results in an error of synchronisation. Let us assume that the bias (or a system parameter) corresponds to a measured weak signal produced by a measuring system which demonstrates chaotic behaviour (this is typical for Atomic Force Microscope [52], section 6.11.3). Then the output of such measurement is chaotic and extraction of a signal may be problematic. A precise method is needed to extract information from the complex system as such extraction may not be possible by standard (e.g. frequency filtering) signal processing tools.

Now, let us add an additional identical measuring system coupled with the original via the considered master-slave scheme, and measure the error between the outputs of master (measuring) and slave (additional) systems. Since this error is proportional to the bias (as it was shown above) then one is able to conduct measurements of a signal even for chaotic measurement instrument. The concept is illustrated by the example below.

6.11 Application in Signal Processing

Recently, chaotic measurement devices and control of chaos in signal processing have received a substantial research attention [25-27]. The analysis in previous sections demonstrated that the synchronisation error in the de-synchronised region is proportional to the bias added to the slave system (Fig. 6.11). This fact may be used in signal processing where a signal needs to be detected or measured.

In this section, the use of synchronisation with addition of bias in a Nano-mechanical Duffing Resonator is demonstrated.

6.11.1 Nano-electromechanical Systems (NEMS)

Fabrication, detection and control of microelectromechanical and nanoelectromechanical systems (MEMS and NEMS) have received significant attention in the past 10 years [53-56]. Nanoelectromechanical systems concern with the mechanical and electromechanical behaviour of nanometre-scale objects, that is, objects for which at least one dimension is significantly less than $1\mu m$ [57]. NEMS systems are constantly developed for a series of nanotechnological applications including but not limited to: highly sensitive mass [58-60], spin [61], charge detectors [62] and Atomic Force Microscopy [63-65]. Nonlinear and chaotic behaviour is readily observed in nanoscale devices [66-69] such as nanomechanical resonators that are characterised by extremely high frequencies and relatively weak dissipation [70-72].

For the purpose of this study a Nano-mechanical Duffing Resonator with linear and nonlinear damping is considered. Nano-mechanical Duffing Resonator has shown chaotic behaviour in several studies [73, 74] and hence control of such behaviour is of great importance [75]. The equation of motion for a single nanomechanical Duffing resonator is described by Lifshitz et al. [76] as:

$$m\frac{d^2x}{dt^2} + \Gamma\frac{dx}{dt} + m\omega_0^2 x + \alpha x^3 + \eta x^2\frac{dx}{dt} = Gcos\omega t \tag{6.18}$$

Where m is its effective mass, $k = m\omega_0^2$ is its effective spring constant, α is the

cubic spring constant or Duffing parameter, Γ is the linear damping rate, and η is the coefficient of nonlinear damping which is the damping that increases with the amplitude of oscillation. In this case, the parameters are set with the following values [77]: $\eta = 0, \alpha = 100, m = 1, \Gamma = 0.01$.

Here, the objective is to synchronise two identical Nano-mechanical Duffing Resonators using the OPCL Master-Slave synchronisation method described above (eq. 6.5). Lets consider the Master system based on the Nano-mechanical Duffing Resonators (eq. 6.18):

$$\begin{cases} \dot{Z}_1 = Z_2 \\ \\ \dot{Z}_2 = -\Gamma Z_2 - Z_1 - \alpha Z_1^3 + Gcos(\omega t) \end{cases} \tag{6.19}$$

In this case:

$$\frac{dF(z)}{dz} = \begin{bmatrix} 0 & 1 \\ -1 - 3\alpha z_1^2 & -\Gamma \end{bmatrix} \tag{6.20}$$

A is an arbitrary constant matrix and is choose as:

$$A = \begin{bmatrix} 0 & 1 \\ -1 & -\Gamma \end{bmatrix} \tag{6.21}$$

By using the OPCL principle the driving term D is (eq. 6.5):

$$D = (A - \frac{dF(Z)}{dZ})(z - Z) \tag{6.22}$$

Therefore, the derived slave system is:

$$\begin{cases} \dot{z_1} = z_2 \\ \\ \dot{z_2} = -\Gamma z_2 - z_1 - \alpha z_1^3 + Gcos(\omega t) + D \end{cases} \tag{6.23}$$

Finally, replacing the driving term D, constructs the slave system:

$$\begin{cases} \dot{z_3} = z_2 \\ \\ \dot{z_4} = -\Gamma z_2 - z_1 - \alpha z_1^3 + Gcos(\omega t) - S(3\alpha z_1^2(z_2 - Z_2)) \end{cases} \tag{6.24}$$

Where $S = 0$ or 1 as a switch. Figure 6.12 illustrates the chaotic behaviour of the master system in the phase space with initial conditions $Z_1 = Z_2 = 0$.

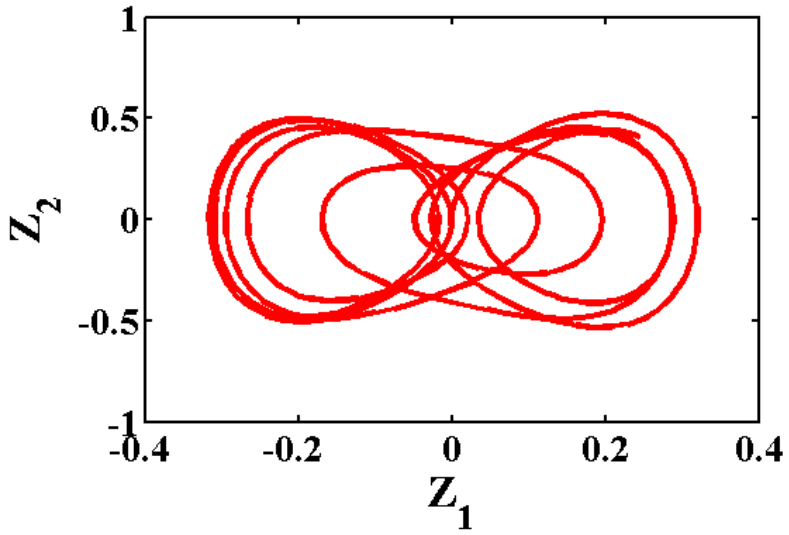

Figure 6.12: Chaotic behaviour of nano-mechanical duffing resonator with initial conditions set to 0

Using the procedure explained above the two systems starting from different initial conditions $Z_1 = Z_2 = 0$ and $z_1 = z_2 = 0.25$ are fully synchronised. The synchronisation switch S is set to 1 when $t = 15$.

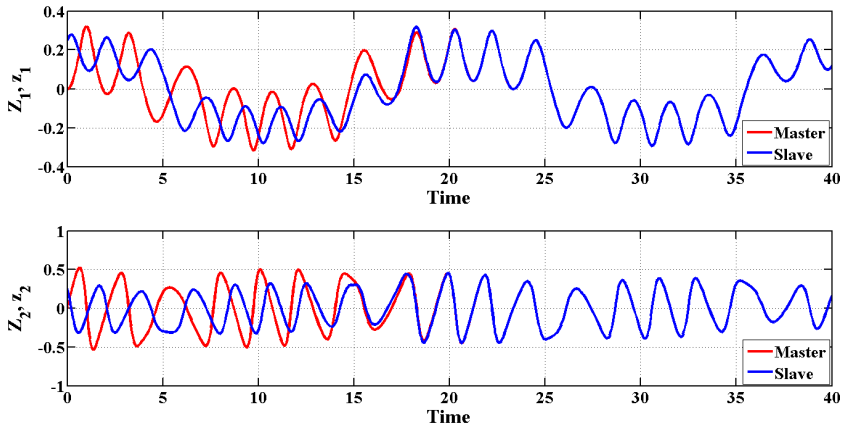

Figure 6.13: Synchronisation of two nano-mechanical resonators

Now the bias (U_1, U_2) is added to the slave system as described in (eq. 6.15):

$$\begin{cases} \dot{z_1} = z_2 + U_1 \\ \\ \dot{z_2} = -\Gamma z_2 - z_1 - \alpha z_1^3 + Gcos(\omega t) - S(3\alpha z_1^2(z_4 - Z_2)) + U_2 \end{cases} \tag{6.25}$$

The bias can potentially be the signal of week measurement coming from the

measurement device [79]. In this case the nanoscale (10^{-9}) measurement is added as a bias to the synchronisation procedure. Even such small bias cause the systems to leave the synchronised region and produce an error. The overall RMSE (explained in eq. 6.17) of desynchonisation is calculated. The following figure (Fig 6.14) demonstrates the relationship between the added bias and the RMSE.

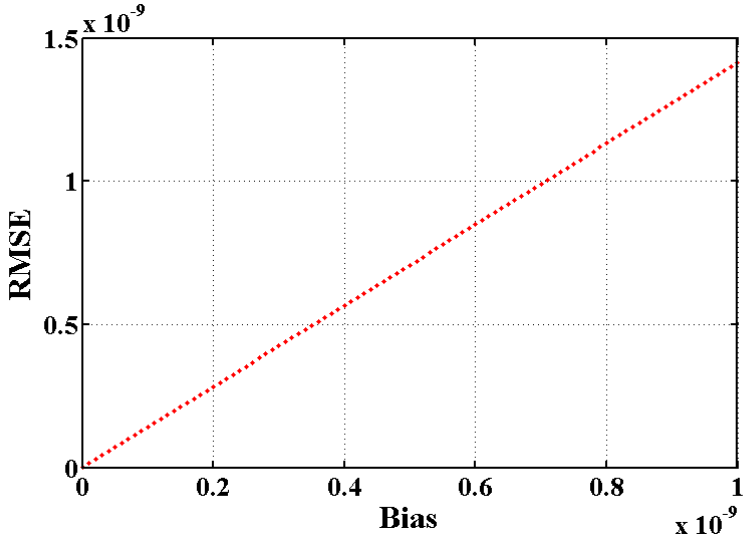

Figure 6.14: RMSE vs. the value of the added bias

The linear correlation between the RMSE and the bias is observed. Subsequently, the error produced by two synchronised chaotic resonators based on the added bias can be used as a detection or measurement signal. Note, that the RMSE corresponds to a position of resonator and this position can be measured with a high precision by either using optical technique or by measuring voltage in AFM.

As described earlier (section 6.9.4), the proposed method can be used to syn-

chronise multiple identical resonators which means large number of bias measurements can be injected to an array of synchronised nanoscale resonators. The ability to fabricate arrays of thousands of synchronised resonators opens new possibilities in the study of nonlinear dynamics much larger than one can study in macroscopic experiments [76].

6.11.2 Synchornisation of ENs with Cantilever Sensors

As described in chapter four, gas sensor arrays (Electronic Noses) are manufactured with various sensors and sensitivity levels. Different types of sensors which poses distinct behaviour have already been built into the ENs. Optical sensors [78], thermal sensors [79], chemiresistive sensors [80], metal oxide semiconducting sensors [81] and conducting polymer sensors [82] have all been widely used in commercial sensor arrays and electronic noses [83]. Furthermore, sensor arrays are also built that are operated based on NEMS cantilevers [84]. NEMS concepts have previously been acknowledged in literature and successfully developed and implemented in ulta-sensitive gas sensor arrays [88]. A chemical sensor technology based on resonant NEMS sensor arrays for mass detectors provides the speed, sensitivity, specificity, and size required by the microscale ENs [51]. Different types of nano-scale mechanical cantilevers are used for distinct applications [85]. Many of which have a sharp tip at the cantilever apex (refer to section 6.11.3) [86]. However, for the use of cantilever in a gas sensor array, neither a sharp tip nor a sample surface is required. The cantilever surfaces serve as sensor surfaces and allow the processes taking place on the surface of the beam to be monitored and detected with unprecedented

accuracy, in particular the adsorption of gaseous molecules [87]. Fundamentally, the formation of molecule layers on the cantilever surface will generate surface stress, eventually resulting in a bending of the cantilever, provided the adsorption preferentially occurs on one surface of the cantilever. Adsorption is controlled by coating the upper surface of a cantilever with a thin layer of a material that exhibits affinity to molecules on the sensor surface [88]. The following image illustrates the cantilever when exposed to the molecules and therefore reacts (resonates).

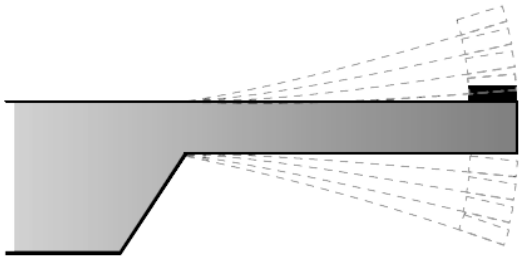

Figure 6.15: Basic cantilever dynamic operation mode [51]

If NEMS is used for measurements in EN it will change the cantilever's overall mass $(m_c + m_1)$ where m_c is the mass of cantilever and m_1 is the mass of the analyte detected. The phenomena is fully described in [50]. Consequently, the equation of motion for the master cantilever based on (eq. 6.18) will be:

$$\begin{cases} \dot{Z}_1 = Z_2 \\ \\ \dot{Z}_2 = (-\Gamma Z_2 - Z_1 - \alpha Z_1^3 + G cos(\omega t))/(m_c) \end{cases} \tag{6.26}$$

By using the OPCL principle the slave system will be in the following form:

$$\begin{cases} \dot{z_1} = z_2 \\ \\ \dot{z_2} = (-\Gamma z_2 - z_1 - \alpha z_1^3 + Gcos(\omega t) - S(3\alpha z_1^2(z_2 - Z_2)))/(m_c + m_1) \end{cases} \tag{6.27}$$

For the purpose of demonstration, the typical parameters of NEMS (described in section 6.11.1) are selected as follow: $\Gamma = 0.01$, $\alpha = 100$, $G = 2$, $\omega = 0.35$, $m_c = 1$ and $m_1 = 0, \ldots, 0.01$. The system with the named parameters is considered as the application of NEMS for a cantilever sensor in EN.

In conventional approach [50] NEMS is commonly used in a linear regime, for the selected parameters this regime is observed when the amplitude is relatively small. The sensor of EN is aimed to detect change in a cantilever mass m_c. In linear regime [50], it is required to measure the frequency response for $m_1 = 0$ and $m_1 = constant$ and therefore determine the change in the location of resonance frequency, that is frequency when the response to harmonic force is maximal. Hence, the analyte can be detected by EN based on it's mass characteristics. If the mass change of 1% which is equivalent to $m_1 = 0.01$ is introduced to the surface of the cantilever (mass of the cantilever m_c), the change in the location of the cantilever is hardly determined and ideally requires a high precision frequency measurements.

Here, the scheme based on the de-synchronisation could be applicable. In this scheme the amplitude G can be significantly larger and, consequently, easily measured (i.e. $G = 2$). At the next stage, two identical NEMS cantilever systems are synchronised. Fig. 6.16 shows the error rapidly approaching zero

indicating robust synchronisation (eq 6.26-6.27).

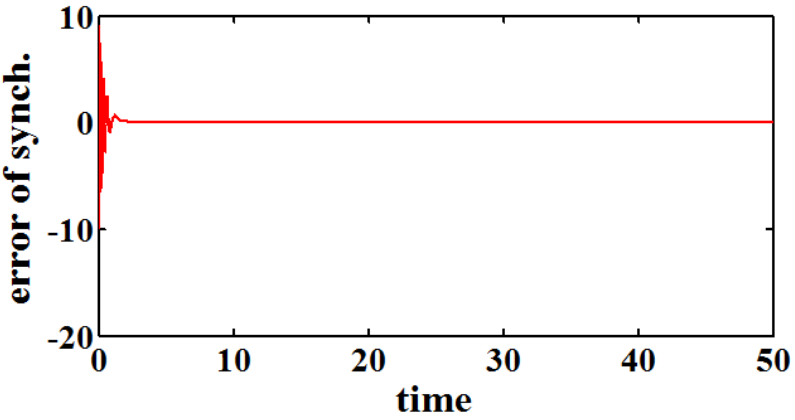

Figure 6.16: Observation of error of synchronisation

The value of m_1 is changed during the process, that is when a molecule detected on the surface, causing the systems to depart the synchronised region. The RMSE of synchronisation is then calculated (eq. 6.17) as illustrated in the following figure.

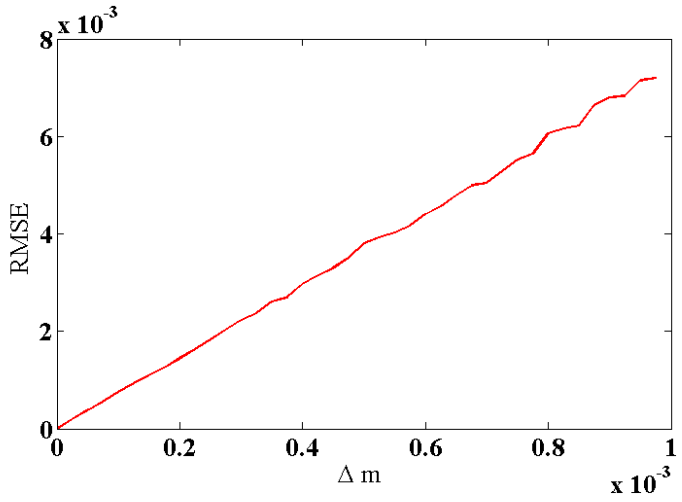

Figure 6.17: Observation of error in relation to Δm

The change in the mass of cantilever has caused the coupled systems to instantly de-synchronised. The result indicates the monotonic dependence of the error on m_1 (Δ m). Thus, the change in mass can be estimated by the error of synchronisation. Finally, since the synchronisation error corresponds to electric signal it can be additionally amplified for improved accuracy. The schema introduced here may potentially be used for synchronising a reference and measurement sensors typically found in the ENs.

6.11.3 Synchronisation of Cantilevers in AFMs

Atomic Force Microscopy (AFM) consists of a vibrating cantilever with a Nano-scale tip that interacts with a sample surface. As described earlier, cantilevers, in general, possess several distinct dynamical behaviours resulting in the tip-sample interaction forces to be highly nonlinear. They often vibrate in an unanticipated and chaotic ways making their dynamics challenging to control [80]. The nonlinear response of AFM cantilevers tapping on a sample has already attracted extensive research interest [81-83] and have been discussed through theoretical [84], computational [85], and experimental analysis [86-88]. Unlike the cantilever demonstrated for EN applications, the cantilever used in AFMs contains a tip at its apex. Figure 6.18 demonstrates a cantilever tip commonly used in AFMs.

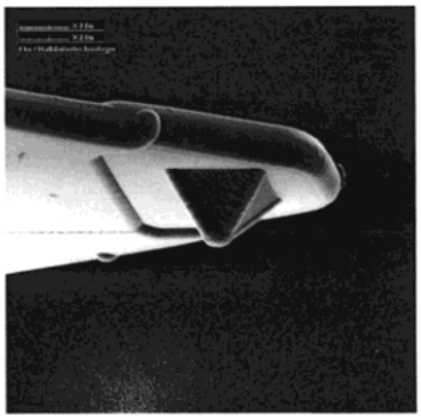

Figure 6.18: Typical nano-scale cantilever tip [89]

The cantilever-sample interaction can be modelled as a single spring-mass system. The cantilever interacts with the sample via a tip that is mounted on the cantilever (fig. 6.18). Basso et al. [84] described the cantilever-sample interaction with the following dynamical system:

$$\begin{cases} \dot{z_1} = z_2 \\ \\ \dot{z_2} = -\Delta z_2 - z_1 - \frac{d}{(\alpha+z_1)^2} + \frac{\sigma^6 d}{30(\alpha+z_1)^8} + \Gamma cos(\Omega t) \end{cases} \tag{6.28}$$

Where $\Delta, \Gamma, \Omega, \alpha, \sigma$ and d are the damping factor, the amplitude, the frequency of the forcing term, the distance, the molecular diameter and coefficient of interaction, respectively. The coefficient of interaction reflects the properties of the studied surface and, effectively, it corresponds to a parameter to be determined by AFM. However, the strong nonlinear interaction results in complex dynamics of AFM as it has complicated the inference of d. To overcome the problem, AFM is turned to a regular (non-chaotic) regime, when the interaction is weak, but sensitivity of AFM, and consequently, accuracy of measure-

ments of d, is reduced dramatically.

Below a different approach is suggested. The approach is based on the idea of measuring the synchronisation error for estimating d. It is to employ one controllable master AFM with known properties. A slave system is then introduced for taking the measurements. The objective is to measure an interaction between the tip and the sample surface using the synchronisation of the master and slave cantilevers. Let us introduce a parameter $k = d \times c$ in the slave system which corresponds to parameter d (coefficient of interaction) in the master system. The constant c defines a mistmatch between known d in the master system and k, which is an object of measurements. Thus, the slave system derived by the OPCL schema (eq. 4-12) is given by:

$$\begin{cases} \dot{z_1} = z_2 \\ \\ \dot{z_2} = -\Delta z_2 - z_1 - \frac{k}{(\alpha+z_1)^2} + \frac{\sigma^6 k}{30(\alpha+z_1)^8} + \Gamma cos(\Omega t) - S(p(Z_1 - z_1)) \end{cases} \tag{6.29}$$

where $S = 0$ or 1 is a synchronisation switch and $p > 0$ is the OPCL control parameter.

Figure 6.19 demonstrates trajectories in the phase space of identical master and slave systems representing two identical cantilever (eq. 6.28-6.29) with parameters $(\Delta, \Gamma, \Omega, \alpha, \sigma, d, c, p = 0.4, 20, 1, 1.2, 0.3, 4/27, 1, 1.5)$. The initial conditions for master and slave systems are $(Z_1, Z_2 = 0)$ and $(z_1, z_2 = 0.1)$ respectively. A chaotic behaviour of both systems is clearly seen.

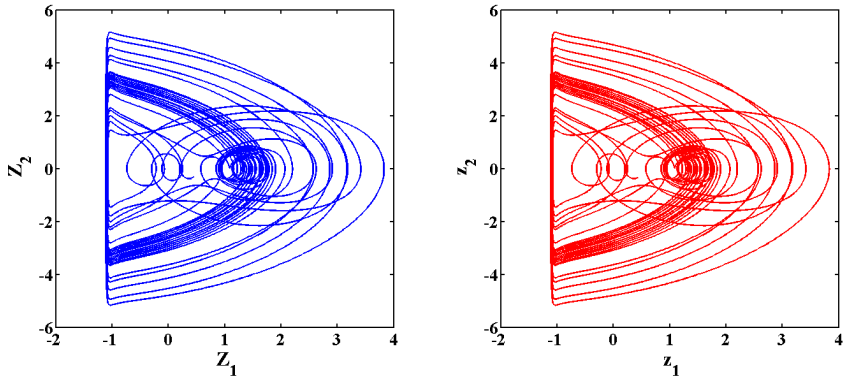

Figure 6.19: Chaotic behaviour of cantilever's tip-sample interaction, left: master system with initial conditions set to $(0, 0)$, Right: slave system with initial conditions set to $(0.1, 0.1)$

Figure 6.20 (left) demonstrates the de-synchronised trajectories of the master and slave cantilever systems when the synchronisation switch S is set to 0. Although, the two cantilever systems are identical and have equal parameters, they are not synchronised and hence the arbitrary synchronisation error (fig. 20-left) is produced.

Using the OPCL procedure and control parameter $p = 1.5$ the two cantilever systems starting from different initial conditions $Z_1 = Z_2 = 0$ and $z_1 = z_2 = 0.25$ are fully synchronised. The synchronisation switch S is set to 1 when $t = 150$. For demonstration purposes, the trajectories and synchronisation error is illustrated in Fig. 6.20 (right) for $300 < t < 800$ where the synchronisation error visibly approaches zero indicating robust synchronisation.

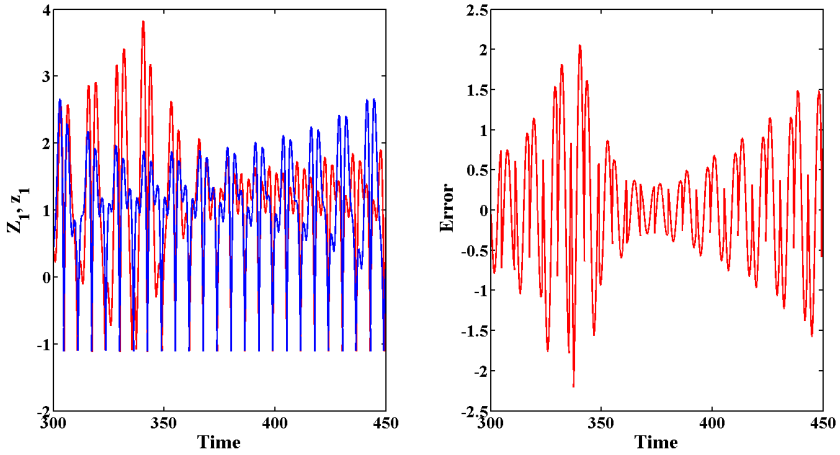

Figure 6.20: Left: systems in non-synchronised region (de-synchronisation), right: error of de-synchronisation

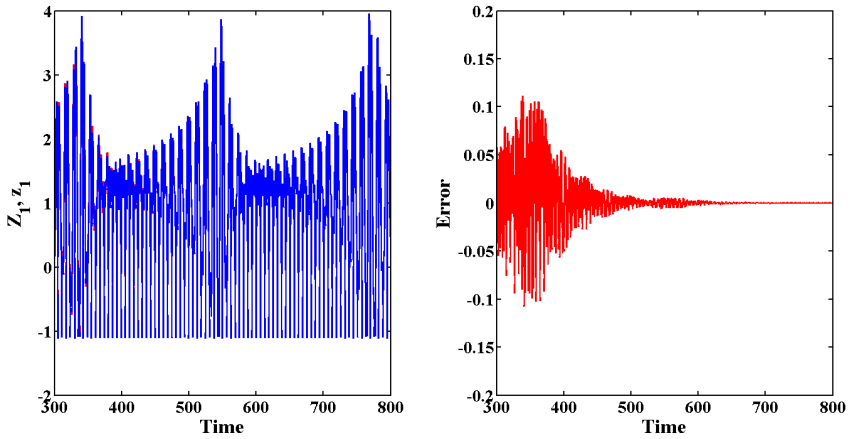

Figure 6.21: Left: Systems in synchronised region, right: error of synchronisation approaches 0

The next step, is to consider synchronisation for different values of k in the slave system by altering c. Figure 6.21 (right) was produced with parameter $c = 1(k = d)$ which results in full synchronisation. Figure 6.22 illustrates the absence of synchronisation with the c value increased to 1.2 indicating the presence of a difference between measured signal from the slave system and the master system. Noticeably, despite the strength of OPCL scheme, the mismatch in the model parameters has caused the system to leave the

synchronisation region and produce error. The construction of error caused by the incrimination of c and subsequently k values, is shown in fig. 6.22-right.

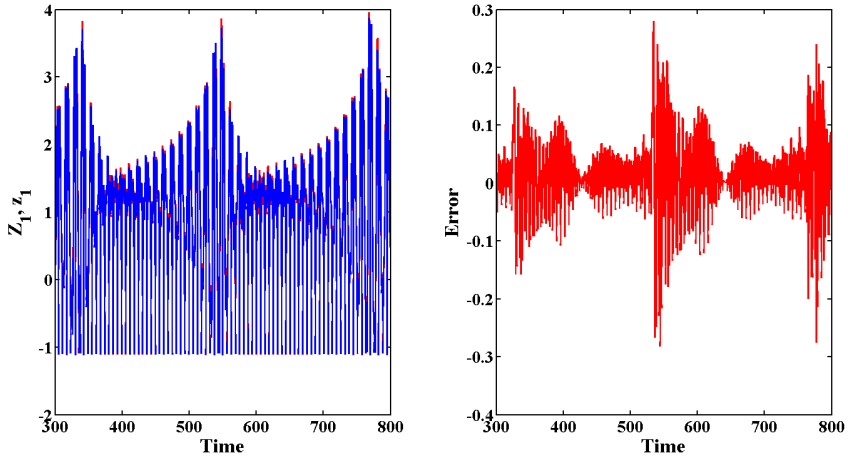

Figure 6.22: Left: systems in non-synchronised region (de-synchronisation), right: error of synchronisation due to K value (parameters mismatch)

Therefore the change in coefficient of interaction (k) has produced a synchronisation error between the two systems. The principle described earlier in the chapter is employed here to assess whether the change in the c value of the slave cantilever has any correlation to the overall RMSE produced. Figure 6.23 demonstrates the change of RMSE based on the change in the interaction coefficient (k).

The monotonic relationship between the RMSE and the coefficient of interaction ($c = k/d$) is observed as expected. The error produced by two desynchronised chaotic cantilevers based on the change in k/d can be used as a detection of measurement signal. The newly-proposed method enables the precise synchronisation of multiple identical cantilevers which will lead to high precision measurement of a signal produced by cantilevers vibration.

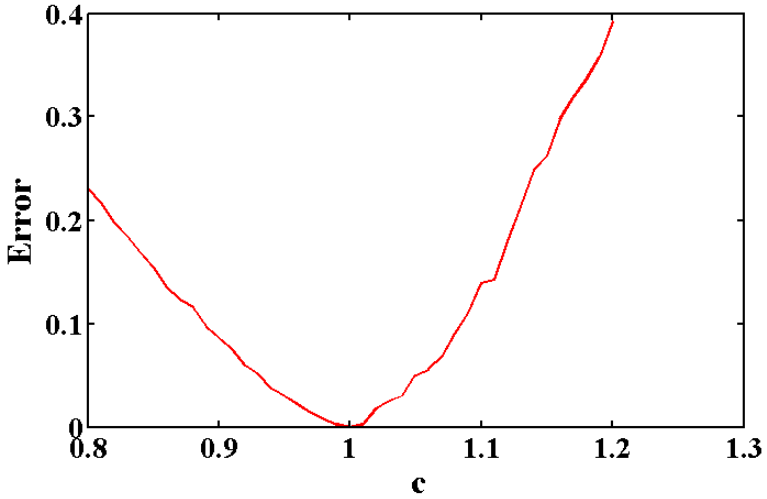

Figure 6.23: Observation of error in relation to c = k/d (parameters mismatch)

The schema described by the aid of few examples in this chapter could be extended and employed in applications in which sensitive sensory data or signal are being acquired through instrumentations as described in a recent publication by the author, Ghaffari et al. [90]. Finally, the author would like to acknowledge that the method presented in this chapter is still at the very early stage of the development and inevitably begs for more study and research as outlined in the "Future Work" section of this thesis.

6.12 Summary

In this chapter the features and characteristics of chaotic dynamical systems particularly Lorenz's chaotic equations was discussed. The ability of OPCL synchronisation was evaluated when a bias was added to the process (or in the case of parameters mismatch). It was shown that the overall synchro-

nisation error is representative of the initial bias added to the slave system. The application of bias and computed synchronisation error in signal processing and NEMS was presented. However, the principle may be applied in other applications where sensitive measurements need to be captured or transmitted.

The next chapter concludes the thesis by discussing the overall results obtained in each chapter, indicating limitations and further work as well as producing a series of recommendations.

6.13 References

1. Laskar, J., The chaotic motion of the solar system: A numerical estimate of the size of the chaotic zones. Icarus, 1990. 88(2): p. 266-291.

2. Saltzman, B., Dynamical paleoclimatology: generalized theory of global climate change. Vol. 80. 2001: Access Online via Elsevier.

3. McKenzie, M.D., Chaotic behavior in national stock market indices: New evidence from the close returns test. Global Finance Journal, 2001. 12(1): p. 35-53.

4. Nagel, K. and H.J. Herrmann, Deterministic models for traffic jams. Physica A: Statistical Mechanics and its Applications, 1993. 199(2): p. 254-269.

5. Heslot, F. and A. Libchaber, Unidirectional crystal growth and crystal anisotropy. Physica Scripta, 1985. 1985(T9): p. 126.

6. Irwin, M.C., Smooth dynamical systems. Vol. 94. 1980: Academic Press.

7. Anishchenko, V.S., V. Astakhov, and T. Vadivasova, Nonlinear dynamics of chaotic and stochastic systems: tutorial and modern developments. 2007: Springer.

8. Murray, R.M., et al., A Mathematical Introduction to Robotic Manipulation. 1994: CRC Press.

9. Wolf, A., et al., Determining Lyapunov exponents from a time series. Physica D: Nonlinear Phenomena, 1985. 16(3): p. 285-317.

10. Sano, M. and Y. Sawada, Measurement of the Lyapunov Spectrum from a Chaotic Time Series. Physical Review Letters, 1985. 55(10): p. 1082-1085.

11. Abarbanel, H.D.I., R. Brown, and M.B. Kennel, Lyapunov Exponents In Chaotic Systems: Their Importance And Their Evaluation Using Observed Data. International Journal of Modern Physics B, 1991. 05(09): p. 1347-1375.

12. Rosenstein, M.T., J.J. Collins, and C.J. De Luca, A practical method for calculating largest Lyapunov exponents from small data sets. Physica D: Nonlinear Phenomena, 1993. 65(12): p. 117-134.

13. Ott, E., Chaos in Dynamical Systems. 2002: Cambridge University Press.

14. Strogatz, S.H., Nonlinear Dynamics and Chaos: With Applications to Physics, Biology, Chemistry, and Engineering. 2008: Westview Press.

15. Hnon, M., A two-dimensional mapping with a strange attractor. Communications in Mathematical Physics, 1976. 50(1): p. 69-77.

16. Rssler, O.E., An equation for continuous chaos. Physics Letters A, 1976. 57(5): p. 397-398.

17. Qi, G., et al., Analysis of a new chaotic system. Physica A: Statistical Mechanics and its Applications, 2005. 352(2): p. 295-308.

18. Lorenz, E.N., Deterministic nonperiodic flow. Journal of the atmospheric sciences, 1963. 20(2): p. 130-141.

19. Sprott, J., Some simple chaotic flows. Physical Review-Section E-Statistical Physics Plasma Fluids Related Interdiscpl Topics, 1994. 50(2): p. R647.

20. Lorenz, E.N., The essence of chaos. 1995: University of Washington Press.

21. Huygens, C., 1673. Horologium oscillatorium.

22. Kane, D.M. and K.A. Shore, Unlocking Dynamical Diversity: Optical Feedback Effects on Semiconductor Lasers. 2005: Wiley.

23. Pecora, L.M., et al., Fundamentals of synchronization in chaotic systems, concepts, and applications. Chaos: An Interdisciplinary Journal of Nonlinear Science, 1997. 7(4): p. 520-543.

24. Boccaletti, S., et al., The control of chaos: theory and applications. Physics reports, 2000. 329(3): p. 103-197.

25. Cuomo, K.M. and A.V. Oppenheim, Circuit implementation of synchronized chaos with applications to communications. Physical Review Letters, 1993. 71(1): p. 65-68.

26. Kocarev, L. and U. Parlitz, General approach for chaotic synchronization with applications to communication. Physical Review Letters, 1995. 74(25): p. 5028.

27. Wu, C.W. and L.O. Chua, A simple way to synchronize chaotic systems with applications to secure communication systems. International Journal of Bifurcation and Chaos, 1993. 3(06): p. 1619-1627.

28. Chua, L.O., et al., Experimental chaos synchronization in Chua's circuit. International Journal of Bifurcation and Chaos, 1992. 2(03): p. 705-708.

29. Carroll, T.L. and L.M. Pecora, Synchronizing chaotic circuits. Circuits and Systems, IEEE Transactions on, 1991. 38(4): p. 453-456.

30. Peng, B., V. Petrov, and K. Showalter, Controlling chemical chaos. Journal of Physical Chemistry, 1991. 95(13): p. 4957-4959.

31. Li, Y.-N., et al., Experimental study of chaos synchronization in the BelousovZhabotinsky chemical system. Chaos, Solitons and Fractals, 2004. 22(4): p. 767-771.

32. Mirasso, C.R., P. Colet, and P. Garca-Fernndez, Synchronization of chaotic semiconductor lasers: Application to encoded communications. Photonics Technology Letters, IEEE, 1996. 8(2): p. 299-301.

33. Roy, R. and K.S. Thornburg Jr, Experimental synchronization of chaotic lasers. Physical Review Letters, 1994. 72: p. 2009-2012.

34. Nakamura, Y., K. Kishi, and H. Kawakami. Heartbeat synchronization for robotic cardiac surgery. in Robotics and Automation, 2001. Proceedings 2001 ICRA. IEEE International Conference on. 2001. IEEE.

35. Zhu, A. and H. Leung. Cooperation random mobile robots based on chaos synchronization. in Mechatronics, ICM2007 4th IEEE International Conference on. 2007. IEEE.

36. Duane, G.S. and J.J. Tribbia, Synchronized chaos in geophysical fluid dynamics. Physical Review Letters, 2001. 86(19): p. 4298.

37. Singer, J. and H.H. Bau, Active control of convection. Physics of Fluids A, 1991. 3(12): p. 2859-2865.

38. Garfinkel, A., et al., Controlling cardiac chaos. Science, 1992. 257(5074): p. 1230-1235.

39. Elson, R.C., et al., Synchronous behavior of two coupled biological neurons. Physical Review Letters, 1998. 81(25): p. 5692.

40. Glass, L., Synchronization and rhythmic processes in physiology. Nature, 2001. 410(6825): p. 277-284.

41. Parlitz, U., et al., Experimental Demonstration Of Secure Communications Via Chaotic Synchronization. International Journal of Bifurcation and Chaos, 1992. 02(03): p. 709-713.

42. Chua, L.O. and C.W. WU, Simple Way to Synchronize Chaotic Systems With Applications To Secure Communication Systems. International Journal of Bifurcation and Chaos, 1993. 03(06): p. 1619-1627.

43. Moskalenko, O.I., A.A. Koronovskii, and A.E. Hramov, Generalized synchronization of chaos for secure communication: Remarkable stability to noise. Physics Letters A, 2010. 374(29): p. 2925-2931.

44. Grzybowski, J.M.V., M. Rafikov, and J.M. Balthazar, Synchronization of the unified chaotic system and application in secure communication. Communications in Nonlinear Science and Numerical Simulation, 2009. 14(6): p. 2793-2806.

45. Rosenblum, M.G., A.S. Pikovsky, and J. Kurths, Phase Synchronization of Chaotic Oscillators. Physical Review Letters, 1996. 76(11): p. 1804-1807.

46. Rosenblum, M.G., A.S. Pikovsky, and J. Kurths, From phase to lag synchronization in coupled chaotic oscillators. Physical Review Letters, 1997. 78(22): p. 4193.

47. Rulkov, N.F., et al., Generalized synchronization of chaos in directionally coupled chaotic systems. Physical Review E, 1995. 51(2): p. 980.

48. Boccaletti, S., et al., The synchronization of chaotic systems. Physics Reports, 2002. 366(12): p. 1-101.

49. Liu, Y. and L. Chen, Control of Chaotic Attitude Motion, in Chaos in Attitude Dynamics of Spacecraft. 2013, Springer Berlin Heidelberg. p. 131-163.

50. Grosu, I., Robust synchronization. Physical Review E, 1997. 56(3): p. 3709-3712.

51. Grosu, I., et al., Designing Coupling for Synchronization and Amplification of Chaos. Physical Review Letters, 2008. 100(23): p. 234102.

52. Jackson, E.A. and I. Grosu, An open-plus-closed-loop (OPCL) control of complex dynamic systems. Physica D: Nonlinear Phenomena, 1995. 85(12): p. 1-9.

53. Hammel, S.M., J.A. Yorke, and C. Grebogi, Do numerical orbits of chaotic dynamical processes represent true orbits? Journal of Complexity, 1987. 3(2): p. 136-145.

54. Kiusalaas, J. (2005). Numerical Methods in Engineering with MATLAB, The Pennsylvania State University.

55. Corless, R. M. (1994). What good are numerical simulations of chaotic dynamical systems?. Computers and Mathematics with Applications, 28(10), 107-121.

56. Palis, J. (2005, August). A global perspective for non-conservative dynamics. In Annales de l'Institut Henri Poincare (C) Non Linear Analysis (Vol. 22, No. 4, pp. 485-507). Elsevier Masson.

57. Blank, M. L. V. (1989). Small perturbations of chaotic dynamical systems. Russian Mathematical Surveys, 44(6), 1-33.

58. Kifer, Y. (1988). Random perturbations of dynamical systems. Boston: Birkhuser.

59. Ruelle, D. (1996). Positivity of entropy production in nonequilibrium statistical mechanics. Journal of Statistical Physics, 85(1-2), 1-23.

60. Binnig, G., C.F. Quate, and C. Gerber, Atomic force microscope. Physical review letters, 1986. 56(9): p. 930.

61. Craighead, H.G., Nanoelectromechanical systems. Science, 2000. 290(5496): p. 1532-1535.

62. Ekinci, K. and M. Roukes, Nanoelectromechanical systems. Review of scientific instruments, 2005. 76(6): p. 061101-061101-12.

63. Roukes, M., Nanoelectromechanical systems face the future. Phys. World, 2001. 14(2): p. 25-31.

64. Roukes, M., Plenty of room, indeed. Scientific American, 2001. 285(3): p. 42-9.

65. Cleland, A.N., Foundations of nanomechanics: from solid-state theory to device applications. 2003: Springer.

66. Ekinci, K., X. Huang, and M. Roukes, Ultrasensitive nanoelectromechanical mass detection. Applied Physics Letters, 2004. 84(22): p. 4469-4471.

67. Ilic, B., et al., Attogram detection using nanoelectromechanical oscillators. Journal of Applied Physics, 2004. 95(7): p. 3694-3703.

68. Yang, Y.T., et al., Zeptogram-scale nanomechanical mass sensing. Nano letters, 2006. 6(4): p. 583-586.

69. Rugar, D., et al., Single spin detection by magnetic resonance force microscopy. Nature, 2004. 430(6997): p. 329-332.

70. Cleland, A.N. and M.L. Roukes, A nanometre-scale mechanical electrometer. Nature, 1998. 392(6672): p. 160-162.

71. Liu, H. and B. Bhushan, Nanotribological characterization of molecularly thick lubricant films for applications to MEMS/NEMS by AFM. Ultramicroscopy, 2003. 97(1): p. 321-340.

72. Palacio, M. and B. Bhushan, Ultrathin Wear Resistant Ionic Liquid Films for Novel MEMS/NEMS Applications. Advanced Materials, 2008. 20(6): p. 1194-1198.

73. Bhushan, B., Nanotribology and nanomechanics of MEMS/NEMS and BioMEMS BioNEMS materials and devices. Microelectronic Engineering, 2007. 84(3): p. 387-412.

74. Aldridge, J. and A. Cleland, Noise-enabled precision measurements of a Duffing nanomechanical resonator. Physical review letters, 2005. 94(15): p. 156403.

75. Almog, R., et al., High intermodulation gain in a micromechanical duffing resonator. Applied physics letters, 2006. 88(21): p. 213509-213509-3.

76. Buks, E. and M.L. Roukes, Metastability and the Casimir effect in micromechanical systems. EPL (Europhysics Letters), 2001. 54(2): p. 220.

77. Carr, D.W., et al., Parametric amplification in a torsional microresonator. Applied Physics Letters, 2000. 77(10): p. 1545-1547.

78. Cleland, A.N. and M.R. Geller, Superconducting qubit storage and entanglement with nanomechanical resonators. Physical review letters, 2004. 93(7): p. 070501.

79. Huang, X.M.H., et al., Nanoelectromechanical systems: Nanodevice motion at microwave frequencies. Nature, 2003. 421(6922): p. 496-496.

80. Peng, H., et al., Ultrahigh frequency nanotube resonators. Phys. Rev. Lett, 2006. 97(087203): p. 470.

81. Wei, X., et al., Nonlinear dynamics of a periodically driven Duffing resonator coupled to a Van der Pol oscillator. Mathematical Problems in Engineering, 2010. 2011.

82. Kenig, E., Y.A. Tsarin, and R. Lifshitz, Homoclinic orbits and chaos in a pair of parametrically driven coupled nonlinear resonators. Physical Review E, 2011. 84(1): p. 016212.

83. Karabalin, R., M. Cross, and M. Roukes, Nonlinear dynamics and chaos in two coupled nanomechanical resonators. arXiv preprint arXiv:0811.0870, 2008.

84. Lifshitz, R. and M. Cross, Nonlinear Dynamics of Nanomechanical Resonators. Nonlinear Dynamics of Nanosystems, 2010: p. 221-266.

85. Chen, Q., L. Huang, and Y.-C. Lai, Chaos-induced intrinsic localized modes in coupled microcantilever arrays. Applied Physics Letters, 2008. 92(24): p. 241914-241914-3.

86. Lerescu, A., et al., Collection of masterslave synchronized chaotic systems. Chaos, Solitons and Fractals, 2004. 22(3): p. 599-604.

87. You, H.X., et al., Atomic force microscopy imaging of living cells: a preliminary study of the disruptive effect of the cantilever tip on cell morphology. Ultramicroscopy, 2000. 82(1): p. 297-305.

88. Walt, D. R., Dickinson, T., White, J., Kauer, J., Johnson, S., Engelhardt, H., Jurs, P. (1998). Optical sensor arrays for odor recognition. Biosensors and Bioelectronics, 13(6), 697-699.

89. James, D., Scott, S. M., Ali, Z., Ohare, W. T. (2005). Chemical sensors for electronic nose systems. Microchimica Acta, 149(1-2), 1-17.

90. De Wit, M., Vanneste, E., Geise, H. J., Nagels, L. J. (1998). Chemiresistive sensors of electrically conducting poly (2, 5-thienylene vinylene) and copolymers: their responses to nine organic vapours. Sensors and Actuators B: Chemical, 50(2), 164-172.

91. Sysoev, V. V., Button, B. K., Wepsiec, K., Dmitriev, S., Kolmakov, A. (2006). Toward the nanoscopic electronic nose: hydrogen vs carbon monoxide discrimination with an array of individual metal oxide nano-and mesowire sensors. Nano letters, 6(8), 1584-1588.

92. Hatfield, J. V., Neaves, P., Hicks, P. J., Persaud, K., Travers, P. (1994). Towards an integrated electronic nose using conducting polymer sensors. Sensors and Actuators B: Chemical, 18(1), 221-228.

93. Lang, H. P., Hegner, M., Gerber, C. (2005). Cantilever array sensors. Materials today, 8(4), 30-36.

94. Baller, M. K., Lang, H. P., Fritz, J., Gerber, C., Gimzewski, J. K., Drechsler, U., Gntherodt, H. J. (2000). A cantilever array-based artificial nose. Ultramicroscopy, 82(1), 1-9.

95. Li, M., Myers, E. B., Tang, H. X., Aldridge, S. J., McCaig, H. C., Whiting, J. J., Roukes, M. L. (2010). Nanoelectromechanical resonator arrays for ultrafast, gas-phase chromatographic chemical analysis. Nano letters, 10(10), 3899-3903.

96. Yinon, J. (2003). Peer reviewed: detection of explosives by electronic noses. Analytical Chemistry, 75(5), 98-A.

97. Lang, H., Hegner, M., Gerber, C. (2007). Nanomechanical cantilever array sensors. Springer Handbook of Nanotechnology, ISBN 978-3-540-29855-7. Springer-Verlag Berlin Heidelberg, 2007, p. 443, 1, 443.

98. You, H.X., et al., Atomic force microscopy imaging of living cells: a preliminary study of the disruptive effect of the cantilever tip on cell morphology. Ultramicroscopy, 2000. 82(1): p. 297-305.

99. Raman, A., J. Melcher, and R. Tung, Cantilever dynamics in atomic force microscopy. Nano Today, 2008. 3(1): p. 20-27.

100. Hu, S. and A. Raman, Chaos in atomic force microscopy. Physical review letters, 2006. 96(3): p. 036107.

101. Jamitzky, F., et al., Chaos in dynamic atomic force microscopy. Nanotechnology, 2006. 17(7): p. S213.

102. Pishkenari, H.N., M. Behzad, and A. Meghdari, Nonlinear dynamic analysis of atomic force microscopy under deterministic and random excitation.

Chaos, Solitons and Fractals, 2008. 37(3): p. 748-762.

103. Basso, M., et al. Numerical analysis of complex dynamics in atomic force microscopes. IEEE.

104. Ashhab, M., et al., Melnikov-based dynamical analysis of microcantilevers in scanning probe microscopy. Nonlinear Dynamics, 1999. 20(3): p. 197-220.

105. Lee, S., et al., Nonlinear dynamics of microcantilevers in tapping mode atomic force microscopy: A comparison between theory and experiment. Physical Review B, 2002. 66(11): p. 115409.

106. Landman, U., W.D. Luedtke, and A. Nitzan, Dynamics of tip-substrate interactions in atomic force microscopy. Surface Science Letters, 1989. 210(3): p. L177-L184.

107. Magonov, S.N. and M.-H. Whangbo, Surface analysis with STM and AFM: experimental and theoretical aspects of image analysis. 2008: Wiley. com.

108. Kranz, C., et al., Integrating an Ultramicroelectrode in an AFM Cantilever: Combined Technology for Enhanced Information. Analytical Chemistry, 2001. 73(11): p. 2491-2500.

109. Ghaffari, R., et al., Dimensionality Reduction for Sensory Datasets Based On MasterSlave Synchronization Of Lorenz System. International Journal of Bifurcation and Chaos, 2013. 23(05): p. 1330013.

Chapter 7

Conclusion and Future Work

7.1 Chapter Overview

This chapter is divided into two major sections each discussing the two core objectives of this thesis outlined in section 1.5. The first part will present the outcome of the experiments conducted at the School of Engineering, University of Warwick and summarises the main findings of the research presented in chapters 3-5. A brief conclusion will be provided which discusses the overall results. The subsequent section discusses the findings of chapter 6 which is concerned with synchronisation of chaotic dynamical systems. Finally, the chapter closes by outlining a framework for further research as well and recommending potential enhancement.

7.2 Overview of Main Research Results

7.2.1 Non-Destructive Plant Disease Detection

Two major experiments where constructed and conducted by the author at School of Engineering, University of Warwick. The experimental design and setup for full-scale plant and for the specific sensors discussed in this thesis remains unique to the best of author's knowledge. The data acquired from these experiments have been analysed and presented throughout the thesis. Following is the summary of the findings:

7.2.1.1 EN and Plants Disease Detection

The aim of this experiment was to evaluate the EN and FAIMS technologies in detecting powdery mildew-infected and spider mite-infested tomato plants by scanning their VOC profiles. The requirements of the investigation clearly indicated that the proposed method needs to be fast, reliable, robust and non-destructive. Additionally, the experimental methods and procedures (i.e. sample collection and preparation) should be easy enough for non-expert users to conduct without any scientific or IT background knowledge.

Firstly, EN as a portable and cost effective tool was investigated. Two distinct and separate experiments were conducted using the EN device. The EN proved to be proficient in detecting the VOC fingerprints within a controlled environment. Both clustering and classification methods managed to discriminate between healthy and infected samples when the EN generated dataset were appropriately processed. Support Vector Machine proved to be

a capable tool for discriminating the samples both from accuracy and speed perspective. The results indicated that the average discrimination accuracy of 86%, 90% and 91% could be achieved with LDA, FFNN and SVM respectively.

However, EN poses some drawbacks: **a)** EN is extremely sensitive to environmental factors such as humidity and temperature. Although these parameters were constantly monitored and controlled during the experiment, doing so in real life situation may be challenging. **b)** ENs sensors degrade as time passes. This means that sensors need to be replaced on regular basis. Additionally, systematic changes in the sensors sensitivity means that the training network constructed initially to analyse the dataset needs to be retrained. Such drawback creates the motives to investigate alternative devices which offer the robustness of the EN as well as reliability and consistency in measurements.

7.2.1.2 FAIMS and Plants Disease Detection

Although EN produced the desirable result in terms of discriminating between healthy and infected plants, the drawback in the previous section creates the motives to investigate an alternative device.

The FAIMS technology was deployed to sample the VOC profiles emitted from the tomato plants in the identical experimental procedures as it offers efficiency with fast analysis, portability with a compact footprint and more importantly, high sensitivity. The results indicated that:
a) The FAIMS technology is able to detect the ion mobility fingerprints of the VOCs that are emitted by tomato plants.
b) A pattern of disease development from healthy state to heavily infected

state could be emerged by sampling the VOCs on daily basis.

c) A set of pre-processing tasks need to be conducted to minimise any undesired data sections.

d) LDA have produced an apparent classification performance of 88% between the powdery mildew-infected and healthy plant respectively.

Biological based non-destructive testing for humans has travelled a long way in the last 5 decades. Technologies such as magnetic resonance imaging, radiographic and ultrasonic testing are now matured and have significantly improved the life expectancy of millions of people around the world. Conversely, the non-destructive testing in agricultural and horticultural settings is still very much remained at the research level. Many of the available technologies are concerned with the environmental stress of the plants and therefore monitor the environmental factors such as water, temperature, humidity and CO2 levels, thus do not perceive the deficiencies due to the bacterial or viral diseases. Prominent results presented in this thesis could be considered as an extra step forward towards the integration of various other gas sensors techniques in agricultural and horticultural settings, contriving a plant monitoring tool to reduce crop waste and chemical/biochemical treatments.

7.2.2 Synchronisation of Chaotic DS with Bias

Control and synchronisation of dynamical systems have received a substantial amount of interest from both mathematical/physical theoretician and engineers since they have realised the potential for exploitation of the schema in applications such as secure communication. Grasping the phenomenon in its

most fundamental form in a view to seek for the innovative and pragmatic applications is considered to be imperative.

In chapter 6, the master-slave synchronisation of identical chaotic dynamical systems were presented using the OPCL control. The primary idea was to add an external bias to the slave system or create parameters mismatch and let the two (or multiple) systems to synchronise. Inevitably, the addition of the bias or mismatch of the parameters compel the systems to leave the synchronous region and therefore produce an error. The chapter, with the aid of two novel applications, presented the relation between the added bias and the overall error produced by the two systems. The principle was evaluated using three systems: Lorenz's chaotic systems, chaotic Nano-mechanical Duffing Resonator and chaotic cantilevers in AFMs.

7.2.2.1 Synchronisation of Nano-mechanical Resonator

The motion equation of a Nano-mechanical Duffing Resonator was obtained from the literature. The master and slave systems were identified based on the motion equation and were set to be synchronised. The change in synchronisation regime based on the addition of external bias was observed. It was detected that such addition cause the systems to leave the synchronous state (de-synchronised) and generate an error which eventually proved that the value of bias can be estimated by the composed error of de-synchronisation. The NEMS concept was considered in a special type of EN which employ cantilever sensors. By the aid of an example it was demonstrated that the schema can be used to detect signal when two NEMS EN sensors are synchronised. This is particularly useful when an array of resonators or oscillators need to

be employed in a system. The measurement signal can be detected from an array of synchronised resonator once one of them produce a bias and cause an overall error.

7.2.2.2 Synchronisation of Cantilevers in AFMs

As the second application two micro-cantilever used in AFMs were synchronised. The approach were based on the idea of measuring the synchronisation error for estimating the coefficient of interaction. One controllable master AFM with known properties was synchronised with an identical slave system for taking the measurements. The two synchronised systems produced no error until a change was occurred in the tip-sample interaction parameter of the slave system (parameters mismatch). Such nominal change caused the systems to desynchronised instantly and produce error. The computational simulation proved that such small change in the synchronisation fabricated an error which is proportional to the coefficient of interaction in the slave system. The proposed regime could be used to synchronise multiple measurement cantilevers in a single or multiple AFMs. It can also be employed in a systems were precise weak signal needs to be generated.

7.3 Future Work and Recommendations

With regards to plants non-destructive disease detection, the following further work have been identified and hence recommended by the author: **a)** the more extensive experiments in which more samples is examined in a larger enclosures may be beneficial, **b)** using different species of plants in the experiments will widen the understanding of VOCs emitted by different plant when

infected, **c)** an online agent may be implemented in which the data analysis algorithms as well as the sensors are embedded in a single system allowing a seamless integration in an agricultural settings, **d)** it is of interest to consider the environmental factors (i.e. humidity and temperature) as a new parameter to balance the inconsistencies in environmental parameters and **e)** it is beneficial to know which sensors of EN are likely to re-act the most to the organic compounds found in greenhouses. In other words, feature selection or correlation analysis can potentially reveal which sensors are not active or less active compared to others when presented with plants VOCs. Such analysis may lead us to manufacture application dependent ENs with specific sensors in order to reduce cost and enhance effectiveness.

In terms of the study presented in chapter 6 (de-synchronisation state of chaotic systems) three directions of future research are of interest.

First, it is worthwhile to explore the efficient implementation of the technique in a physical setup or instrumentation to evaluate the real-life performance of the proposed schema. Potentially, this can be achieved by synchronising two physical NEMS or MEMS oscillators and observe the change in the live synchronisation when the parameters/bias are modified. Therefore, the author recommends an experimental approach for further assessment of the proposed schema.

Second, the schema may be employed to synchronise other supplementary systems that have chaotic behaviour in a view to not only control the chaos but also enhance the precision of coupled systems which conduct the identical

task or collect similar measurements. The example of such systems would be in the field of secured communication or precision tools.

Third, it would be of interest to study how the technique behave when used for synchronisation of non-identical chaotic systems. Complete synchronisation between non-identical systems with different styles/parameters is in general more difficult to achieve [32]. This involves the optimisation of the control technique as well as the schema by which the bias is added. Such studies can ultimately lead to the full interaction of distinct collaborative systems that poses chaotic behaviour.

The End

Reza Ghaffari

November 2013

This page is intentionally left blank.